Subcontractor Report

Leaching of Alkalis in Biomass Using Banagrass as a Prototype Herbaceous Species

Final Report, February 1997

S. Turn, C. Kinoshita, D. Ishimura, B. Jenkins, and J. Zhou
Hawaii Natural Energy Institute
University of Hawaii at Manoa

NREL

National Renewable Energy Laboratory

Leaching of Alkalis in Biomass Using Banagrass as a Prototype Herbaceous Species

Final Report, February 1997

S. Turn, C. Kinoshita, D. Ishimura, B. Jenkins, and J. Zhou
Hawaii Natural Energy Institute
University of Hawaii at Manoa

NREL

National Renewable Energy Laboratory

NOTICE

Available electronically at http://www.osti.gov/bridge

Available for a processing fee to U.S. Department of Energy
and its contractors, in paper, from:

> U.S. Department of Energy
> Office of Scientific and Technical Information
> P.O. Box 62
> Oak Ridge, TN 37831-0062
> phone: 865.576.8401
> fax: 865.576.5728
> email: reports@adonis.osti.gov

Available for sale to the public, in paper, from:
> U.S. Department of Commerce
> National Technical Information Service
> 5285 Port Royal Road
> Springfield, VA 22161
> phone: 800.553.6847
> fax: 703.605.6900
> email: orders@ntis.fedworld.gov
> online ordering: http://www.ntis.gov/ordering.htm

Printed on paper containing at least 50% wastepaper, including 20% postconsumer waste

Final Report

Leaching of Alkalis in Biomass Using Banagrass as a Prototype Herbaceous Species

Final Report

Leaching of Alkalis in Biomass
Using Banagrass as a Prototype
Herbaceous Species

The body of this report is comprised of three individual sections, each a self contained document. Each section presents the findings of one of the three subtasks included in the project. They are, in order of appearance:

(1) "Removal of Alkali from Banagrass Using Mechanical Dewatering and Leaching Processes," prepared by the Hawaii Natural Energy Institute.

(2) "Combustion Characteristics of High Alkali Biomass: Laboratory Characterization of the Combustion Properties of Bagasse and Banagrass," prepared by Dr. Bryan Jenkins and coworkers at the Department of Biological and Agricultural Engineering at the University of California, Davis in cooperation with Dr. Larry Baxter at Sandia National Laboratories.

(3) "Gasification Characteristics of High Alkali Biomass Subjected to Mechanical Dewatering and Leaching Processes," prepared by the Hawaii Natural Energy Institute.

Removal of Alkali from Banagrass Using Mechanical Dewatering and Leaching Processes

Scott Turn
Charles Kinoshita
Darren Ishimura

February 1997

Abstract

Inorganic constituents of ash in biomass fuels are responsible for equipment failure and operating difficulties in thermochemical energy conversion facilities. Alkali metals, in the presence of chlorine and sulfur, are the leading contributors to this problem. Banagrass, an herbaceous species being considered for use as a dedicated energy crop, contains high levels of potassium and chlorine. Some inorganic elements are water soluble and the opportunity exists to remove them by mechanical dewatering and leaching as part of the feedstock preparation process. Laboratory-scale equipment, representative of processes employed in the commercial extraction of sugar from cane, was used to prepare banagrass fuel treatments that included two degrees of comminution (coarse and fine) and two dewatering schemes (mechanical dewatering only, and a multi-step process consisting of initial mechanical dewatering followed by a water rinse and second dewatering). The treatment that included fine comminution and multi-step dewatering resulted in a fuel with substantial reductions in ash (45%), K (90%), Cl (98%), S (55%), Na (68%), P (72%) and Mg (68%). The coarse comminution and multi-step dewatering scheme also resulted in reductions, but generally with 10 to 20% more of the initial constituent mass retained in the fuel. These two treatments produced fuels containing 0.11 and 0.23 kg (Na_2O+K_2O) GJ^{-1}, respectively, with corresponding ash fusion temperature estimates of 1250 and 1075°C. By comparison, bagasse, the fibrous byproduct of sugarcane, contains 0.06 kg (Na_2O+K_2O) GJ^{-1} and has an estimated ash fusion temperature of roughly 1500°C. Banagrass subjected to the most severe treatment, fine comminution with multi-step dewatering, should produce a boiler fuel with characteristics similar to those of bagasse.

2

Introduction

Alkali metals, principally potassium and to a lesser extent sodium, naturally exist in biomass. Although present at minor levels, alkali and alkaline earth elements react with other inorganic constituents, silica, sulfur and chlorine, resulting in unwanted deposits and corrosion in energy conversion facilities utilizing biomass fuels. In combustion systems, alkali compounds foul heat transfer surfaces, participate in slag formation in grate-fired units and contribute to the formation of fluidized bed agglomerates. The result is increased operating costs and reduced efficiency and availability of the energy conversion facility. In the case of proposed biomass integrated gasification combined cycle systems, alkali vapor deposition onto combustion turbine working surfaces and subsequent hot corrosion are of concern.

Recent research efforts have sought to address problems associated with the presence of alkali compounds in biomass fuels. Alkali deposition in biomass boilers, and its dependency on boiler design, operating conditions, fuel type, fuel properties and fuel chemistry have been studied by a number of investigators [1-4]. Deposits were determined to be composed of potassium and calcium in the form of silicates, chlorides, sulfates, hydroxides and carbonates. The release of potassium and sodium from peat in oxidizing and reducing environments was the focus of theoretical and experimental investigations to assess compatibility of the resulting gas streams with requirements of gas turbines [5,6]. Levels were found to be in excess of those recommended by turbine manufacturers.

Removal of inorganic constituents from biomass materials by water leaching has been studied with the objective of nutrient recycling [7] and more recently, for the purposes of controlling deleterious effects in biomass boilers and improving fuel combustion characteristics [8]. In the latter case, straw fuels, primarily rice and wheat, received the most attention. Laboratory leaching tests were performed on straw samples with water applied as spray, by flushing and in a submerged soak. Samples of rice straw which had been exposed to natural precipitation were also collected. Alkali metals and chlorine were effectively removed from the straw by the leaching process.

Alkali compounds are largely water soluble [3] and can be removed by a combination of mechanical compression and leaching of the plant material as demonstrated in the processing of sugar cane and the relatively trouble-free use of bagasse as a boiler fuel [10]. A moisture content of ~70% wet basis is typical of fresh herbaceous crops and mechanical dewatering can reduce the moisture content to ~50%. A cycle of rehydration and mechanical dewatering is employed in the sugar industry to obtain incremental removal of sucrose from cane; this process concurrently removes alkali species resulting in the desirable fuel qualities exhibited by bagasse.

This report summarizes the results of a study to determine the efficacy of applying sugar processing technology to the removal of alkali species from banagrass (*Pennisetum purpureum*), a fast growing tropical grass with potential for use as a dedicated feedstock for energy fuel and chemical production. The influence of fuel particle size and extraction process on the final alkali concentration in processed banagrass was investigated using four well-defined comminution and extraction treatments. Distribution of the major inorganic feedstock constituents among the process output streams was determined and elemental balances computed. Sufficient quantities of feedstock were prepared in each treatment to permit testing and characterization in laboratory-scale combustor and gasifier units.

3

Methods

Fuel Treatment

Approximately 1.2 tonnes (fresh weight) of banagrass was hand harvested from plots at Waialua Sugar Co., Inc. (WSCo) in November, 1995. One half of the material was processed using a forage chopper (John Deere, Model 34), the other half was processed using a Jeffco cutter (Jeffress Bros. Ltd. Engineers, Brisbane, Queensland, Australia). The two methods of size reduction were chosen for very specific reasons: forage chopping has been identified as the most probable harvesting technique to be employed in WSCo's dedicated feedstock supply strategy for utilizing banagrass as a power plant fuel and the Jeffco cutter was expected to provide sufficient size reduction to remove elemental transport limitations and thereby yield data which represent a practical limit for alkali removal by leaching.

The working component of the Jeffco cutter is a rotating head containing four knife edges moving over the surface of a screen plate with 9.5 mm holes. The cutter head is driven by a 10 hp electric motor and rotates at 3450 rpm. The primary difference between the two size reduction methods was the resulting particle size distributions (Figure 1). The geometric mean particle diameter and geometric standard deviation for the Jeffco cut material was ~1 mm and 2.2 mm respectively, whereas the forage chopper produced a coarser feedstock with a geometric mean particle diameter and geometric standard deviation of ~3.9 mm and 1.9 mm, respectively. For comparison, bagasse

Figure 1. Particle size distribution of feedstock treatments as determined by sieve analysis.

obtained from WSCo was found to have a geometric mean particle diameter of 2.2 mm and a geometric standard deviation of 3.1 mm. This indicates that the particle size distributions of the Jeffco cut and forage chopped banagrass bracket that which results from particle size reduction practices commonly employed in sugar factories. After comminution, all material was stored and refrigerated in plastic bags until leaching treatments were performed over two subsequent days. The prepared banagrass feedstocks were subjected to a total of four treatments summarized in Table 1. Treatment identification labels denote forage chopped, unpressed (FC-UP); forage

4

chopped, pressed (FC-P); forage chopped, pressed-rinsed-pressed (FC-PRP); and Jeffco cut, pressed-rinsed-pressed (JC-PRP).

Table 1. Summary of banagrass treatment processing steps.

Fuel	Treatment Identification	Size Reduction Method	Initial Dewatering Press	Water Rinse with Secondary Dewatering Press	Ambient Temperature Forced-Air Drying
Banagrass	FC-UP	Forage Chopper			x
Banagrass	FC-P	Forage Chopper	x		x
Banagrass	FC-PRP	Forage Chopper	x	x	x
Banagrass	JC-PRP	Jeffco Cutter	x	x	x

Each of the treatments, FC-P, FC-PRP and JC-PRP, was processed in four replicates, with each replicate initially containing 18.2 kg of material (fresh weight). Dewatering was performed with a 91 tonne press equipped with two opposed, double-acting hydraulic cylinders, each with a 33 cm stroke (Model IPE-10060, Enerpac, Butler, Wisconsin). The upper cylinder acts on a plunger working surface of 30.3 cm diameter; the lower cylinder is fitted with a larger baseplate. After obtaining a sample for analysis, the feedstock charge was loaded into a cylindrical cage with a 30.5 cm internal diameter, a wall thickness of 2.2 cm and height of 30.5 cm. The cage, open at both ends, was oriented vertically and rested in a pan on the baseplate of the lower hydraulic cylinder, with the pan serving to collect the liquids as they were expressed through the cage openings. The two cylinders were extended until the upper plunger entered the cage and contacted the sample. The control system for the unit was then switched to automatic and hydraulic pressure was increased gradually over the course of ~2 minutes with 10 second pressure plateaus at 1.4, 2.2, 4.0 and 7.4 MPa reaching a maximum pressure of 10.3 MPa, corresponding to 68 tonne force. Maximum force was held for ~20 seconds, relaxed to 49 tonne for ~10 seconds, then returned to maximum force. This cycle was repeated 5 times. Due to the limited cage volume, each replicate was dewatered as four separate charges, with approximately 4.5 kg of material per charge. The liquids expressed from the four charges were mixed and a single sample of the mixture taken for analysis. Samples were taken as each charge was removed from the press and combined into a single feedstock sample representing the replicate. Total mass of expressed liquids and pressed feedstock were recorded for each replicate.

The FC-P treatment was completed after the initial dewatering press. The feedstock for treatments FC-PRP and JC-PRP was subjected to a water rinse following the initial dewatering press. The entire quantity of material for a replicate was transferred to an expanded metal basket lined with stainless steel screen with an opening size of 0.177 mm. The basket was dimensioned to fit inside a 208 L polyethylene barrel. Approximately 52 L of tap water were placed in the barrel and the basket containing the feedstock was lowered into the water. This represented an 8.3 average ratio, by weight, of applied water to dry matter for all replicates. The feedstock was agitated by hand for approximately 3 minutes assuring that all material was subjected to thorough contact with the leach water. Following the rinse, the basket was raised out of the water and suspended from the barrel rim, allowing the leach water to drain freely from the feedstock back into the barrel. After draining for 5 to 10 minutes, the mass of the free leachate was recorded and a sample taken for analysis. The feedstock was subjected to a second dewatering press. Weights of the liquid and solid streams were recorded and samples were obtained for analysis. Tap water samples were collected prior to the rinsing step.

All of the treated feedstock was dried over the course of several days using an ambient temperature forced air dryer. Upon reaching nominal conditions of equilibrium moisture content, the treated feedstock was stored in plastic bags.

Bagasse was obtained from WSCo's processing plant shortly after the banagrass feedstock preparation. At random intervals, bagasse was sampled from the conveyors transporting material from the end of the milling tandem to the bagasse storage facility. As with the other treatments, the bagasse was air dried, then stored in plastic bags.

Analytical

All solid samples obtained during feedstock processing were oven dried to constant weight at 105 °C for moisture content determination, then milled to a particle size of <1.68 mm. Electrical conductivity (EC) of each of the liquid samples was measured using a FisherBrand conductivity meter (Model 09-326-2). Samples of the tap water used for leaching, and solid and liquid samples from two replicates of treatments FC-PRP and JC-PRP were sent for analytical analyses to Hazen Research, Inc., Golden, Colorado. Analyses performed were:

Biomass Analyses:	Proximate, Ultimate (C,H,O,N,S), Chlorine, Heating Value
Biomass Ash Analyses:	Ash Analysis for Si, Al, Ti, Fe, Ca, Mg, Na, K, P, S, Cl, CO_2
Liquid Analyses:	K, Na, Cl, Ca, Si, Al, Fe, Mg, P, S
Tap Water Analyses:	K, Na, Cl, Ca, Si, Al, Fe, Mg, P, S

Liquid samples from the first and second pressings and the free leachate were also analyzed for sugar monomers. Samples were first applied to a "clean-up column" prepared from 0.2 mL of H^+ form resin (Bio-Rad AG 50W-X8, 100-200 mesh) and 0.4 mL of CO_3^{-2} form resin (Bio-Rad AG IX-8, 100-200 mesh). The column was rinsed with 0.5 ml of distilled water. Following clean up, samples were analyzed by HPLC using a Bio-Rad HPX-87H column; mobile phase 0.01 M H_2SO_4 at 0.6 mL min^{-1} at 50°C with detection by refractive index.

Results

Figure 2 presents the distribution of the major inorganic elements found in the ash of untreated banagrass. The five major constituents, present at levels greater than 0.1% of dry matter, are K, Si, Cl, Ca and Mg, in order of decreasing abundance. Results of the analyses of the fuel samples generated from the banagrass treatment processes are shown in Table 2. For comparative purposes, analyses for bagasse samples collected from the Hawaiian Commercial & Sugar Co.'s factory at Paia on Maui are presented. It should be noted that the Paia factory utilizes a diffusion process for sugar extraction rather than the more common multiple-mill tandem, and the extraction method may result in differences in the ash content and inorganic constituents of the bagasse produced. The banagrass treatments are listed in order of increasing treatment severity, from left to right in the table.

Ash content decreases with increasing treatment severity, from 3.9% in FC-UP to about 2.7% in the FC-PRP and JC-PRP treatments. This is directly attributable to the removal of inorganic components of the ash from the feedstock, primarily K, Mg, S and Cl. The reduction in ash content produces an increase in higher heating value (HHV) of the processed fuels compared to the unpressed banagrass (FC-UP), particularly evident for the two leached treatments. The three treatments which included dewatering presses (i.e. all but FC-UP) also exhibit lower ash contents than bagasse. This results in higher HHVs for the FC-PRP and JC-PRP treatment, comparable to that of bagasse. Bagasse's higher ash content may be due to the push rake method of field harvesting cane employed in Hawaii. This technique results in the incorporation of copious amounts of soil with the cane delivered to the factory. The presence of soil in the bagasse ash is

evident in the high levels of Al and Fe (crustal elements) compared to the hand harvested banagrass.

Figure 2. Elemental components of banagrass ash as percentage of dry matter.

The reduction of ash and its individual inorganic components is more evident by examining the mass retained in each treatment as a fraction of the mass present in the unprocessed banagrass (Figure 3). Si and Ca are the two most persistent elements in all treatments, with reductions of less than 15%. Fe was removed as a result of the leaching process with little difference attributable to the method of particle size reduction, suggesting that it is present on the surface of the feedstock and originates from the soil. Mg, Na, K, and Cl all show responses to leaching and particle reduction method. Removal of K increases with increasing treatment severity from 40% for FC-P to 70% with the addition of the leaching step (FC-PRP), reaching 90% as a result of the combined effects of both greater particle size reduction and feedstock leaching. Cl, which acts as a facilitator with K in fouling and slagging boilers [2,3], is substantially reduced by the initial dewatering press, exhibiting a reduction of 54% for the FC-P treatment. Leaching results in additional removal with the finer, Jeffco cut material, yielding better results than the forage chopped treatment, 98% and 87% removal, respectively. Sulfur is reduced by 44% in the FC-P treatment, and leaching and additional pressing remove an incremental 10% of the initial sulfur mass, regardless of particle reduction method. P is the only element which exhibits a strong dependence on particle size reduction, with little effect due to the leaching process. P levels in forage chopped treatments were reduced by about 10%, whereas more than 70% removal was observed for the Jeffco cut material.

7

Table 2. Summary of average fuel analyses for bagasse and banagrass fuel treatments.

Fuel	HC&S, Co. Paia Sugar Factory	|---------------------Banagrass---------------------|		
	Bagasse	FC-UP	FC-P	FC-PRP	JC-PRP
Moisture Content (% wet basis)	*	65.6	52.1	44.7	49.3
Proximate Analysis (% dry basis)					
Ash	3.61	3.94	3.05	2.69	2.66
Volatiles	84.51	80.06	81.60	82.99	84.32
Fixed Carbon	11.88	16.01	15.36	14.32	13.03
HHV (MJ/kg)	18.5	18.2	18.3	18.7	18.6
Ultimate Analysis (% dry basis)					
C	48.19	47.98	48.69	48.84	48.79
H	5.65	5.50	5.61	5.60	5.57
O (by diff)	42.35	41.31	41.84	42.33	42.62
N	0.14	0.60	0.48	0.41	0.31
S	0.08	0.10	0.06	0.05	0.05
Cl	*	0.58	0.29	0.09	0.02
Ash	3.61	3.94	3.05	2.69	2.66
Ash Analysis (% dry basis)					
SiO_2	41.87	33.99	40.53	51.60	63.02
Al_2O_3	22.25	0.74	1.03	0.86	0.73
TiO_2	3.87	0.05	0.21	0.19	0.05
Fe_2O_3	20.90	0.78	1.05	0.91	0.95
CaO	3.50	6.00	7.45	9.84	11.20
MgO	1.45	5.36	4.53	3.98	2.44
Na_2O	0.26	1.00	1.11	0.85	0.56
K_2O	2.59	31.80	25.75	15.55	7.39
P_2O_5	1.13	4.00	5.19	5.69	2.37
SO_3	0.90	2.55	1.60	1.20	0.57
Cl	*	8.54	3.90	0.95	0.10
CO_2	*	1.05	1.21	1.96	4.47
Other	1.26	4.18	6.47	6.46	6.19

* not measured
Bagasse ultimate, proximate and HHV data are averages of 6 analyses
Bagasse ash composition data are averages of 3 analyses.
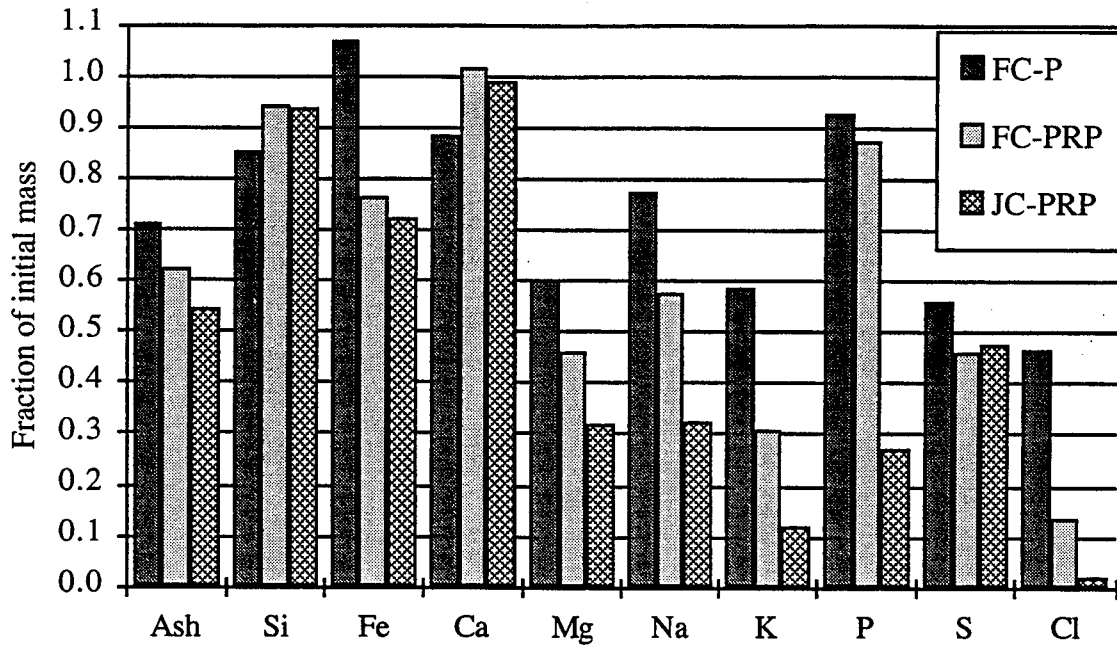Banagrass analyses are all averages of 2 analyses.

Figure 3. Fraction of initial ash and elemental mass retained in treated banagrass.

Figure 4. Fraction of inorganic element mass contributed by dewatered banagrass feedstock and tap water used in leaching, JC-PRP.

The tap water used to rinse the feedstock in the FC-PRP and JC-PRP treatments was analyzed for the elements, K, Na, Cl, Ca, Si, Al, Fe, Mg, P and S. Figure 4 presents the fractional contributions of the feedstock prior to rinsing (i.e., after the initial dewatering press) and the tap water rinse to the total input mass of each element for the JC-PRP treatment. Tap water contributes approximately 50% of the sodium and 20% of the chlorine to the total. Magnesium, calcium and silicon are also present in the tap water, accounting for 15, 6 and 2% of their total input masses, respectively.

Balances for total mass and each of the inorganic elemental masses were calculated to determine the degree to which closure could be obtained for the FC-P, FC-PRP and JC-PRP treatments. Unprocessed banagrass was the single input and the expressed liquids and resulting dewatered feedstock were outputs for the FC-P treatment. The tap water used for rinsing the fuel was included in the FC-PRP and JC-PRP elemental balances. Outputs for these two treatments were the expressed liquids from the first and second pressings, the free leachate and the solids retained after the second pressing. Total mass balances were all greater than 95%, averaging 97% closure. Results of the element balances are shown in Figures 5, 6 and 7. Potassium and chlorine balances, for all treatments, were within ±5% of full closure. Of the remaining major constituents of ash, balances for Si, Ca and Mg were generally within ±10% of full closure for all of the treatments. Sulfur balances ranged from 75 to 85%. Sodium, which was present in the tap water in an amount comparable to that found in the banagrass, exhibited poorer closure for the leached treatments than for the FC-P treatment. Closure for iron and phosphorus was within ~20%. In general, closure is better for elements present in the feedstock in higher concentrations (K, Cl, Si, Ca, Mg), elements not present in the tap water, and for those which are retained in the fuel (Fe), indicating that quantification of the liquid streams, liquid sampling methods or analytical techniques for the liquid samples are likely sources of error.

Figure 5. Distribution of initial elemental mass in output streams, FC-P.

Figure 6. Distribution of input elemental mass in output streams, FC-PRP.

Figure 7. Distribution of initial elemental mass in output stream, JC-PRP.

Measured and calculated electrical conductivities of the liquid samples are presented in Table 3. Calculated values were reconstructed from the liquid ion analyses using conductivity factors. In all cases, calculated values are less than measured values, and, with one exception (JC-PRP second

11

expressed liquid), the ratio of calculated EC to measured EC is ~0.9. Carbonate levels were not quantified in the liquid streams which may account for the disagreement.

Table 3. Average measured and calculated electrical conductivity of liquid streams.

| Liquid Stream | Treatment I.D. | EC (mS/cm) | | Ratio of |
		Measured	Calculated*	(Calculated EC):(Measured EC)
First Pressed	FC-PRP	19.1	16.7	0.88
	JC-PRP	23.8	21.4	0.90
Second Pressed	FC-PRP	3.8	3.3	0.87
	JC-PRP	3.3	2.7	0.83
Free Leachate	FC-PRP	1.6	1.4	0.89
	JC-PRP	2.5	2.2	0.90

* EC calculated from measured ion concentrations.

In addition to a fuel's alkali concentration, the propensity to produce fouling and slagging in boilers is dependent on the boiler design and operating temperature and concomitant levels of other inorganic compounds, primarily those containing sulfur and chlorine. An index of a fuel's fouling potential is the mass of total alkali compounds per unit energy, kg (K_2O+Na_2O) GJ^{-1}. Fuels with index values greater than 0.34 kg (K_2O+Na_2O) GJ^{-1} are almost certain to foul or slag, and those in the range of 0.17 to 0.34 kg (K_2O+Na_2O) GJ^{-1} are deemed probable [1], although these classifications do not account for the effect of temperature, or the presence, or absence, of other chemical species. Figure 8 presents the mass of (K_2O+Na_2O), SO_3 and Cl on a unit energy basis,

Figure 8. Concentrations of total alkali, SO_3 and Cl on a unit energy basis for fuel treatments.

12

calculated from the data in Table 2 for the four banagrass treatments and bagasse. The FC-UP, FC-P, FC-PRP, and JC-PRP fuel treatments contained 0.7, 0.45, 0.23 and 0.11 kg (K_2O+Na_2O) GJ^{-1}, respectively. Bagasse contains a total alkali concentration of 0.06 kg (K_2O+Na_2O) GJ^{-1} indicating that only the JC-PRP banagrass treatment results in a fuel roughly comparable to bagasse. FC-P and the two rinsed banagrass treatments produced lower SO_3 levels on a unit energy basis than those found in the bagasse tested. The FC-UP treatment contained slightly higher values. Chlorine concentration on a unit energy basis decreased with increasing banagrass treatment severity. Chlorine was not measured in the bagasse samples, but values reported in the literature [1] for nonfouling fuels range up to ~0.03 kg Cl GJ^{-1}, which is comparable to the concentrations found in the FC-PRP and JC-PRP treatments. Levels of chlorine present in the FC-P and FC-UP treatments, 0.16 and 0.32 kg GJ^{-1}, respectively, are associated with fuels reported in the literature to produce slagging [1].

A second indicator of slagging potential was obtained by locating the normalized percentages of SiO_2, CaO and K_2O from each fuel's ash composition on the phase diagram shown in Figure 9. Reduction of K_2O with increasing treatment severity is indicated by the horizontal progression of points from the left hand side to the right side of the diagram and higher concentrations of SiO_2. Insofar as the phase diagram can predict the behavior of ash, the fusion temperatures of the FC-UP, FC-P, FC-PRP and JC-PRP treatments are 1000, 900, 1075 and 1250 °C, respectively. Note

Figure 9. Phase diagram of the K_2O-CaO-SiO_2 system (adapted from reference 9) with locations of normalized ash compositions of fuel treatments. Label abbreviations **B**:bagasse, **F1**:FC-UP, **F2**:FC-P, **F3**:FC-PRP, **J**:JC-PRP.

that FC-P, the single dewatering press treatment serves to depress the ash fusion temperature below that of untreated banagrass. The two more severe treatments, which incorporated leaching, exhibit elevated ash melting temperatures. In comparison, the composition of bagasse ash corresponds to a fusion temperature >1500°C.

The liquid streams generated from the treatment processes were analyzed for sugar content in an effort to determine the weight fraction of the initial plant dry matter removed as soluble solids. Glucose was quantified and a second peak assumed to be fructose was identified. Figure 10 presents the results. In the first press liquid from banagrass, the combined mass of the two sugars accounted for 3.6% and 0.7% of initial dry matter for the Jeffco cut and forage chopped treatments respectively. For the treatments which included a fuel rinse and second dewatering press, combined sugar mass in the second press juice was determined to be 0.2% and <0.05% for the Jeffco cut treatments and forage chopped treatments respectively. Sugars were not detected in the free leachate resulting from the rinsing process. Total loss of initial banagrass dry matter as soluble solids measured for the FC-P, FC-PRP and JC-PRP treatments is 0.7, 0.74 and 3.8%, respectively.

Figure 10. Sugars present in the expressed liquids as percent mass of inital dry matter.

Summary and Conclusions

Analysis of freshly harvested banagrass revealed a potassium concentration of 1.1% of dry matter. Treatments consisting of two particle size reduction methods in combination with mechanical dewatering and water rinses were applied to banagrass feedstock, effectively reducing levels of ash, potassium, sodium, magnesium, sulfur and chlorine. The most severe feedstock treatment, JC-PRP, removed 90% of the initial fuel potassium, 54% of sulfur, 70% of magnesium, sodium and phosphorus, and nearly all of the chlorine. FC-PRP, an identical treatment with larger average particle size also produced substantial reduction of these elements but removal was generally 15 to 20% (absolute) less effective compared to the JC-PRP treatment.

14

Closure of balances on total mass, potassium, and chlorine was within ±5% and for other major species, Si, Ca and Mg, closure was within ±10%. Electrical conductivity values calculated from the ion analyses of liquid streams were ~90% of those determined by direct measurement.

Loss of soluble solids in the treatment processes as determined by measurement of monomers in the liquid output streams resulted in a dry matter reductions of <4% in all cases. For treatments which included forage chopped particle size reduction, losses were <1%.

Total alkali, sulfur and chlorine concentrations on a unit fuel-energy basis were computed. Based on these indices, the following conclusions are drawn: (1) JC-PRP presents fuel qualities comparable to bagasse, having low total alkali, SO_3 and Cl on a unit energy basis, (2) FC-PRP contains alkali levels falling in the lower third of the "probable slagging/fouling" range and low concentrations of both sulfur and chlorine, possibly representing acceptable boiler fuel, (3) FC-P and FC-UP contain substantial amounts of alkali, chlorine and sulfur and fall within the range of "certain fouling and slagging". Comparison of the ash fusion temperatures predicted by locating the normalized ash compositions of the fuel treatments on the phase diagram of the K_2O-$CaOSiO_2$ system generally support these conclusions. FC-UP and FC-P have predicted ash melting temperatures ≤1000°C. FC-PRP and JC-PRP produce ash with higher predicted fusion temperatures, 1075 and 1250 °C, respectively. Predicted fusion temperatures for ash from all banagrass treatments are substantially lower than that of bagasse, estimated to be 1500°C from the phase diagram.

The experimental findings contained in this report regarding abilities to leach alkalis and other inorganic components of banagrass should be substantiated using commercial size equipment .

References

1. Miles, T.R., T.R. Miles, Jr., L.L. Baxter, R.W. Bryers, B.M. Jenkins and L.L. Oden. 1995. Alkali deposits found in biomass power plants, a preliminary investigation of their extent and nature. Summary report for the National Renewable Energy Laboratory. NREL Subcontract TZ-2-11226-1.

2. Jenkins, B.M., L.L. Baxter, T.R. Miles, T.R. Miles, Jr., L.L. Oden, R.W. Bryers and E. Winther. 1994. Composition of ash deposits in biomass fueled boilers: results of full-scale experiments and laboratory simulations. Paper No. 946007. Presented at the 1994 International Summer Meeting Sponsored by ASAE, Kansas City, Kansas, June 19-24, 1994.

3. Baxter, L.L., T.R. Miles, T.R. Miles, T.R. Miles, Jr., B.M. Jenkins, G.H. Richards and L.L. Oden. 1993. Transformations and deposition of inorganic material in biomass boilers. In M.G. Carvalho (ed.) Second International Conference on Combustion Technologies for a Clean Environment. pp 9-15. Commission of the European Communities. Lisbon, Portugal.

4. Baxter, L.L. 1993. Ash deposition during biomass and coal combustion: a mechanistic approach. Biomass and Bioenergy. 42, pp. 85-102.

5. Mojtahedi, W., E. Kurkela and M. Nieminen. 1990. Release of sodium and potassium in the PFB gasification of peat. Journal of the Institute of Energy. 63(456) pp. 95-100.

6. Mojtahedi, W. and R. Backman. 1990. The fate of sodium and potassium in the pressurized fluidised-bed combustion and gasification of peat. Journal of the Institute of Energy. 62(453) pp. 189-196.

7. Garland, J.L. 1992. Characterization of the water soluble component of inedible residue from candidate CELSS crops. NASA Technical Memorandum 107557. National Aeronautics and Space Administration, John F. Kennedy Space Center.

8. Jenkins, B.M., R.R. Bakker and J.B. Wei. 1996. On the properties of washed straw. Biomass and Bioenergy. 10(4) pp. 177-200.

9. Levin, E.M., C. R. Robbins and H.F. McMurdie. 1964. Phase diagrams for ceramists. The American Ceramic Society, Columbus, Ohio.

10. Kinoshita, C.M. Cogeneration in the Hawaiian sugar industry. *Bioresource Technology.* 35, pp. 231-237. 1991.

Combustion Characteristics of High Alkali Biomass
Laboratory characterizations of the combustion properties of bagasse and banagrass

Final Report

Prepared for Hawaii Natural Energy Institute
Subcontract 96-08403V

Bryan M. Jenkins, Professor
Principal Investigator
Department of Biological and Agricultural Engineering
University of California
Davis, California 95616

December, 1996

University of California, Davis

Combustion Characteristics of High Alkali Biomass
Laboratory characterizations of the combustion properties of bagasse and banagrass

B.M. Jenkins[1], M. Sime[1], R.R. Bakker[1], R.B. Williams[1], L.L. Baxter[2],
S.Q. Turn[3], P. Thy[4], C. Lesher[4], G. Sclippa[2], and C. Kinoshita[3]

[1]Department of Biological and Agricultural Engineering, University of California, Davis
[2]Combustion Research Facility, Sandia National Laboratories, Livermore, CA
[3]Hawaii Natural Energy Institute, Honolulu, HI
[4]Department of Geology, University of California, Davis

Abstract

Fuel leaching via aqueous extraction was investigated as a potential means of controlling slagging and fouling of combustion systems burning banagrass (*Pennisetum purpureum*). Ash fusibility, high temperature volatilization of ash, and specific deposition fractions were tested in laboratory and pilot scale experiments. Coarse flyash samples and deposits collected on probes simulating boiler superheater tubes were examined for bulk elemental composition by XRF and by electron beam microprobe for microstructure and fine scale elemental distribution. Fluid temperatures of the ash were in fair correspondence with predictions from ternary phase relationships among major elements. Three different banagrass leaching treatments were tested against untreated banagrass and sugar cane bagasse for comparison. Fresh samples of forage chopped banagrass were either mechanically pressed to expel juice and air dried (FC-P), or pressed to expel juice, rinsed with water, pressed again to dewater, and air dried (FC-PRP). Another sample of fresh banagrass was comminuted through a different type of cutter producing a finer particle size, pressed to expel juice, rinsed with water, pressed again to dewater, and air dried (JC-PRP). The untreated sample of forage chopped banagrass (FC-Un) was simply air dried. Bagasse was obtained from an operating sugar mill and air dried. The FC-P treatment showed only marginal improvement over untreated banagrass in terms of ash melting temperature (1050 vs. 1000°C), with slight reduction in the fraction of ash depositing on test probes simulating boiler superheater tubes. The melting point of FC-PRP ash was elevated 150°C relative to untreated banagrass, while that for the JC-PRP treatment increased 300°C. Both treatments produced less tenacious deposits of lower sinter strength compared to untreated and FC-P banagrass. Whereas the banagrass ash was observed to be primarily of plant origin, the ash in bagasse appeared to be mostly adventitious soil material. None of the banagrass treatments achieved ash fusion temperatures as high as bagasse, with its high concentrations of aluminum and iron. An abundance of KCl crystals were observed in both the deposits and flyash from the FC-P and untreated banagrass, but were largely absent the other treatments. These two treatments also produced furnace wall deposits in the pilot combustion tests that were not observed with the other fuels. In order of decreasing fuel quality, as measured in terms of predicted fouling properties, the treatments rank as Bagasse > JC-PRP >> FC-PRP > FC-P > FC-Un.

Introduction

Fireside fouling of combustion equipment is now a widely recognized problem for biomass fuels, especially straws and grasses. These herbaceous materials typically contain large amounts of alkali and alkaline earth materials, which in combination with other elements in the fuel form undesirable deposits, slags, and in the case of fluidized beds, contribute to bed media agglomeration and defluidization. Corrosion frequently accompanies the development of deposits. The undesirable effects of fuel element transformations responsible for these phenomena motivate much of the current research and development in thermochemical conversion of biomass.

Fuel selection, and to a lesser extent furnace design, has so far served as the primary means for controlling fouling in biomass fueled boilers. Fuels with lower ash contents and superior ash compositions, such as clean wood fuels and sugar cane bagasse, are strongly preferred over other fuels, such as cereal crop straws, except where political motivations have provided adequate economic incentives for the use of poorer quality fuels. Sugar cane bagasse is widely employed for steam raising and power generation due to the improvement in fuel combustion properties accompanying the sugar extraction process. Alkali metals and chlorine in the residual cane fiber, or bagasse, are highly depleted relative to the parent sugar cane, due to leaching during processing. Recently, water leaching, including natural rain washing, has been shown to result in substantial improvements in ash fusibility and other indicators of fouling, slagging, and agglomeration for rice and wheat straw, switchgrass (*Panicum virgatum*), and other fuels [1 - 5].

This report summarizes the results of laboratory and pilot scale evaluations of the combustion properties of leached and untreated banagrass (*Pennisetum purpureum*) in comparison to sugar cane bagasse tested under the same conditions. Samples of air dry banagrass along with banagrass leached in various ways were obtained and subjected to compositional assays, tests of ash fusibility and ash volatilization upon heating, and pilot scale combustion experiments in an entrained flow furnace simulating in part the conditions experienced in typical biomass fueled furnaces. Deposit, flyash, and filter samples obtained during the pilot combustion experiments were analyzed for elemental composition by x-ray fluorescence (XRF). Deposit and flyash microstructure and composition were further analyzed via electron beam microprobe. The results suggest substantial differences among samples which may be attributed to the effects of leaching.

Fuel compositions and the influence of leaching

Two principal types of fuel were tested. Sugar cane bagasse was obtained from Waialua Sugar Co., Inc., Hawaii, by staff of the Hawaii Natural Energy Institute (HNEI). Bagasse was sampled randomly from the exit conveyors of the sugar processing plant, air dried, and stored in plastic. A sample of the bagasse weighing approximately 14 kg was shipped by HNEI to the University of California, Davis (UCD) for the testing reported here.

Banagrass samples were also obtained by HNEI from test plots at Waialua Sugar Company. Half the material was comminuted using a John Deere Model 34 forage chopper, the other half using a Jeffress Bros. Jeffco cutter. The Jeffco cutter produced a finer particle size distribution compared to the forage chopped material. Banagrass was then subjected to three different leaching treatments involving one or more of the following operations: mechanically pressing fresh material to express juice, rinsing pressed solids with tap water (aqueous extraction), and pressing rinsed solids to dewater. An untreated sample of banagrass was retained from the original sample. All samples were finally air dried and stored in plastic. Split lots weighing approximately 14 kg from each treatment were also sent by HNEI to UCD. Full details of all treatments are described in [6]. The treatments imposed on the samples are summarized in Table 1. Five treatments were ultimately used in the tests described here, as shown in the table.

Table 1. Fuel treatments.

Treatment #	Designation*	Description
1	FC-PRP	Forage chopped banagrass, pressed, rinsed, pressed again
2	JC-PRP	Jeffco cut banagrass, pressed, rinsed, pressed again
3	Bagasse	Sugar cane bagasse
4	FC-P	Forage chopped banagrass, pressed to expel juice
5	FC-Untreated	Forage chopped banagrass, untreated

*FC = forage chopped, JC = Jeffco cut, P = pressed, R = rinsed.

HNEI provided oven dry samples from all treatments to Hazen Laboratories, Golden, CO, for analyses of major elements, proximate composition, and heating value. Samples from each treatment were submitted at two separate times. Results are included in Table 2. Duplicate samples from each treatment of banagrass were submitted for analysis immediately following processing. Details of these analyses are reported in [6]. Single samples from each batch were later submitted for analysis as part of a suite of gasification experiments by HNEI, not part of this work. Average results from the first duplicate set are labeled Sample 1 in Table 2, single determinations from the second samples are labeled Sample 2.

Results in Table 2 exhibit variability among treatments as well as between samples. The second samples for each banagrass treatment yield higher ash contents than the first samples, possibly as a result of carbohydrate loss during the approximately 6 months of storage between determinations. The second sugar cane bagasse sample yields a substantially lower ash concentration (5.83% compared to 8.45% for the first sample), possibly due to inhomogeneities in the sample batch (e.g., as a result of settlement of adventitious material during storage). Nitrogen concentrations are consistently lower in the second samples of the banagrass materials.

The elemental ash analyses of the samples from JC-PRP also exhibit several discrepancies. The concentrations of Al, Ti, and Fe are substantially higher in the second sample, while the concentrations of Ca, K, and carbonate are lower. Sulfate concentrations are also higher in the second sample. The higher Al, Ti, and Fe concentrations are consistent with dilution by adventitious soil materials, which could account for the higher ash content observed in the second sample. Added dirt would proportionately reduce the concentrations of the alkali and alkaline earth metals of plant origin. Other discrepancies apparent between samples of the same treatment appear in the chloride concentrations of the FC-PRP ash and the FC-Untreated ash, and the silica concentrations of the FC-P and FC-Untreated samples. In the latter case, the undetermined fraction of the first samples is approximately equal to the discrepancy in silica between samples. Chloride concentrations also differ between the samples of bagasse ash, but the levels are low in each case and the differences may not be significant.

Proximate composition and heating value were also determined by UCD as a check against sample homogeneity. The results are given in Table 3 (the moisture contents listed in the table are approximately the as-received moistures, determined after sample preparation for the pilot scale combustion tests described later). Ash contents for FC-PRP and JC-PRP are largely consistent with the results obtained by HNEI from Hazen (Table 2). The ash concentration for bagasse is consistent with Sample 2 of the Hazen analyses, but the values for FC-P and the untreated material are higher than those reported by Hazen. The UCD values measure a consistent decline in total ash for the banagrass treatments, unlike Samples 2 of the Hazen analysis. The heating values are also roughly comparable, showing an increase with increasing leaching severity for banagrass, and a lower value for bagasse relative to banagrass. The UCD volatile matter concentrations are consistently below the Hazen results, most likely as a result of differences in analytical technique. The UCD results show a consistent increase in volatile matter with increasing leaching severity, similar to Samples 1 analyzed by Hazen. JC-PRP Sample 2 yields a lower volatile matter in the Hazen samples, possibly as a result of dirt contamination. The range in concentrations between samples within treatments indicates the extent of variation that may be expected in sampling the fuel batches, as well as reproducibility between laboratories.

Differences among banagrass treatments also exist and are indicative of changes due to leaching. Consistent declines are observed in total ash, Cl, Mg, Na, K, P, and S concentrations in the banagrass fuel as the apparent leaching severity increases from the untreated material (FC-Untreated) through FC-P (juice expression only without rinsing), FC-PRP (with a coarser particle size than the Jeffco cut material), to the JC-PRP sample that appears to be the best leached

Table 2. Fuel compositions, alkali index, and heating values.

Treatment # Fuel	1 FC-PRP		2 JC-PRP		3 Bagasse		4 FC-P		5 FC-Untreated	
	Sample 1*	Sample 2*	Sample 1*	Sample 2*	Sample 1*	Sample 2*	Sample 1*	Sample 2*	Sample 1*	Sample 2*
Proximate Analysis (% dry matter)										
Volatile	82.99	81.52	84.32	80.55	81.42	79.25	81.60	79.45	80.06	78.20
Fixed Carbon	14.32	15.48	13.02	15.70	10.13	14.92	15.35	16.48	16.00	17.33
Ash (600°C)	2.69	3.00	2.66	3.75	8.45	5.83	3.05	4.07	3.94	4.47
Higher Heating Value (MJ/kg dry basis)										
	18.70	18.68	18.60	18.54	17.74	17.86	18.30	18.51	18.20	18.33
Alkali Index (kg alkali oxide/GJ)										
	0.24	0.25	0.11	0.13	0.17	0.12	0.45	0.54	0.71	0.85
Ultimate Analysis (% dry matter)										
C	48.84	47.39	48.79	47.04	45.20	46.27	48.69	46.93	47.98	47.1
H	5.60	5.24	5.57	5.11	5.48	5.27	5.61	5.09	5.50	5.29
N	0.41	0.36	0.31	0.22	0.13	0.12	0.48	0.44	0.60	0.44
S	0.05	0.14	0.05	0.04	0.05	0.05	0.06	0.14	0.10	0.16
Cl	0.09	0.11	0.01	0.03	0.06	0.05	0.29	0.32	0.58	0.61
Ash	2.69	3.00	2.66	3.75	8.45	5.83	3.05	4.07	3.94	4.47
O**	42.32	43.76	42.61	43.81	40.63	42.41	41.82	43.01	41.30	41.93
Ash Elemental* (% dry matter)**										
SiO_2	1.388	1.713	1.676	2.309	3.601	2.503	1.236	1.948	1.339	1.687
Al_2O_3	0.023	0.024	0.019	0.308	1.957	1.386	0.031	0.040	0.029	0.042
TiO_2	0.005	0.001	0.001	0.031	0.233	0.148	0.006	0.004	0.002	0.003
Fe_2O_3	0.024	0.032	0.025	0.134	1.367	0.983	0.032	0.042	0.031	0.052
CaO	0.265	0.299	0.298	0.325	0.249	0.128	0.227	0.345	0.236	0.270
MgO	0.107	0.124	0.065	0.078	0.166	0.121	0.138	0.211	0.211	0.231
Na_2O	0.023	0.025	0.015	0.028	0.048	0.033	0.034	0.032	0.039	0.040
K_2O	0.418	0.450	0.197	0.207	0.251	0.188	0.785	0.973	1.253	1.511
P_2O_5	0.153	0.095	0.063	0.060	0.111	0.076	0.158	0.144	0.158	0.161
SO_3	0.032	0.043	0.015	0.058	0.042	0.035	0.049	0.088	0.100	0.074
Cl	0.026	0.067	0.003	0.003	0.006	<0.001	0.119	0.234	0.336	0.501
CO_2	0.053	0.015	0.119	0.034	0.055	0.023	0.037	0.011	0.041	0.013
Und.†	0.173	0.112	0.164	0.176	0.363	0.207	0.196	-0.002	0.163	-0.114
Ash Elemental (% ash, 600°C)										
SiO_2	51.60	57.11	63.02	61.56	42.62	42.93	40.53	47.87	33.99	37.73
Al_2O_3	0.86	0.81	0.73	8.20	23.16	23.77	1.03	0.98	0.74	0.93
TiO_2	0.19	0.02	0.05	0.82	2.76	2.54	0.21	0.10	0.05	0.07
Fe_2O_3	0.91	1.08	0.95	3.58	16.18	16.86	1.05	1.03	0.78	1.16
CaO	9.84	9.97	11.20	8.66	2.95	2.19	7.45	8.48	6.00	6.05
MgO	3.98	4.12	2.44	2.07	1.97	2.07	4.53	5.19	5.36	5.16
Na_2O	0.85	0.82	0.56	0.74	0.57	0.57	1.11	0.79	1.00	0.90
K_2O	15.55	15.00	7.39	5.52	2.97	3.22	25.75	23.90	31.80	33.80
P_2O_5	5.69	3.18	2.37	1.60	1.31	1.30	5.19	3.55	4.00	3.61
SO_3	1.20	1.42	0.57	1.55	0.50	0.60	1.60	2.16	2.55	1.65
Cl	0.95	2.24	0.10	0.09	0.07	<0.01	3.90	5.75	8.54	11.20
CO_2	1.96	0.50	4.47	0.91	0.65	0.40	1.21	0.26	1.05	0.30
Und.†	6.42	3.73	6.15	4.70	4.29	3.55	6.44	-0.06	4.14	-2.56

*Sample 1 collected during leaching trials and is average of 2 determinations for banagrass (single determination
 for bagasse). Sample 2 collected during gasification trials, single determination for each treatment.
**Oxygen by difference, including Cl.
***Ash elemental (% dry matter) computed from Ash elemental (% ash) and ash content from ultimate analysis.
†Undetermined.
Source: HNEI.

Table 3. Fuel proximate compositions and heating values (UCD).

Treatment # Fuel	1 FC-PRP	2 JC-PRP	3 Bagasse	4 FC-P	5 FC-Untreated
Moisture (% wet basis, as-fired)					
	11	11	8	11	12
Proximate Analysis (% dry matter)					
Volatile	73.90	75.51	75.36	70.99	67.68
Fixed Carbon	22.80	21.61	18.36	24.49	27.39
Ash (575°C)	3.30	2.88	6.28	4.52	4.93
Higher Heating Value (MJ/kg dry basis)					
	18.87	19.15	18.28	18.69	18.53

treatment. If unaffected by leaching, Si and Ca concentrations would increase with increasing treatment severity. Although there is a trend in this direction, enough variability exists in the data to suggest only that these two elements are not quantitatively removed, a result consistent with their structural roles in the plant. Of primary importance are the large removal fractions for K (85%) and Cl (83% for FC-PRP, 95% for JC-PRP). The extraction of these elements substantially improves the fuel value both from the standpoint of ash fusibility and fouling as well as corrosion. The removal of K in this manner may provide a potential mechanism for the more direct agronomic recycling of available nutrient [1]. The value of the potassium in the untreated banagrass is approximately \$4.74 Mg^{-1} dry matter based on current prices for muriate of potash (\$0.34 kg^{-1} K equivalent).

Differences among treatments were also observed in a comparison of incremental electrical conductivity (EC) of leachate acquired during laboratory leaching of the already treated samples obtained by UCD from HNEI. The results are shown in Figure 1. In each case, a 50 g sample of air dry milled material passing a 2 mm screen was sequentially leached with 500 mL units of distilled deionized water. The EC was measured in each incremental volume of leachate. The EC is an indicator of ion concentration in the leachate, and higher EC indicates greater quantities of alkali and other elements removed, although the dependence of EC on concentration is non-linear. Composition of leachate from straw along with comparative EC measurements have been reported earlier [1]. Leachate composition and EC were also determined by HNEI for the FC-PRP and JC-PRP treatments during processing, and are reported in [6].

As shown in Figure 1, the untreated banagrass generated an incremental EC above 1600 μS cm^{-1} after a total of 2 L distilled water was applied. The FC-P treatment yielded a somewhat lower peak EC at 1200 μS cm^{-1}, with FC-PRP, JC-PRP and bagasse at peak values of 450, 200, and 450 μS cm^{-1}, respectively. Total extraction is related to the area under the EC curve, showing the large amount of soluble material in the untreated and FC-P banagrass. For banagrass, the extraction appears to be complete for the method employed after a total volume of 3 L, or 60 L kg^{-1}. A shift in the location of peak EC towards higher volumes of total applied water occurs with decreasing leaching severity, indicating both greater quantities of material extracted and lower leaching rates. The initially well leached JC-PRP and bagasse treatments still yield some extractable ions, although the total quantity is greatly reduced relative to the untreated banagrass. The bagasse appears fully
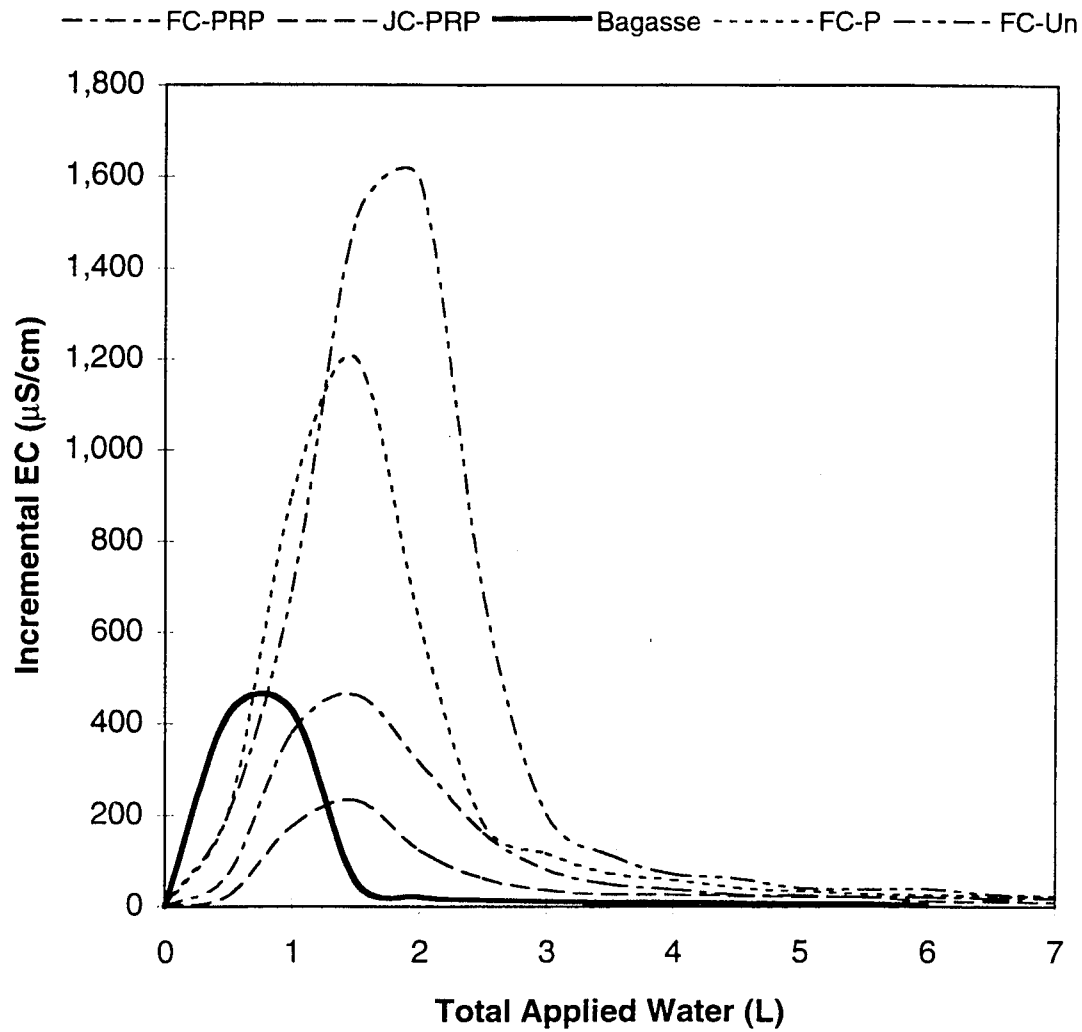
Figure 1. Incremental electrical conductivity (EC) of leachate from secondary leaching of banagrass and bagasse.

leached after 30 L kg^{-1} applied water. The peak values of EC for the forage chopped (FC) banagrass are shifted towards higher applied water volumes compared with a number of other fuels. Peak incremental EC values for rice straw, wheat straw, switchgrass, and two different wood fuel blends were identified at approximately 20 L kg^{-1} (1 L on 50 g) in [4]. Differences are believed to be due to the relative absorption rates of applied water by the biomass. Forage chopped banagrass was observed to absorb water more slowly compared to the JC-PRP material and the other fuels just mentioned. As a result, soluble compounds are extracted at a reduced rate.

Leaching has been shown to result in an increase in fuel heating value due to a reduction in total ash [1,2, 4]. A similar trend exists for the banagrass, although the changes are relatively minor as a result of the initially low ash content of this material compared to some cereal straws and other grasses. The combination of alkali depletion and heating value enhancement due to leaching results in a reduction in the alkali index (kg Na$_2$O + K$_2$O GJ^{-1}), which is sometimes used as a general indicator of fouling potential [7]. When the alkali index exceeds a value of 0.17 kg GJ^{-1}, at least moderate fouling can be anticipated. Above 0.34 kg GJ^{-1} more severe fouling is probable. Alkali concentration is not the only factor influencing fouling, and the prediction of the fouling severity depends on a fuller analysis of the fuel composition and the burning conditions. Fouling can be expected with virtually any biomass fuel. For an individual fuel type, however, changes in the alkali index are suggestive of potential changes in fouling potential. As indicated in Table 2, leaching reduces the alkali index of the untreated banagrass from above 0.7 kg GJ^{-1} to a level below the low threshold value of 0.17 kg GJ^{-1} for the JC-PRP treatment. Note also that the bagasse exhibits an alkali index at or below the lower threshold.

Predictions of ash sintering and melting behavior are better made from phase relationships among the oxide systems for the major reactive species of the fuel, although the phase behavior can be quite complex. Predictions of fusion temperatures from normalized ash compositions in the ternary CaO-K$_2$O-SiO$_2$ phase system have been shown to be largely consistent with experimental observations for straw materials [1]. Banagrass compositions have also been compared on this basis in [6], suggesting a reduction in fusion temperature for the FC-P treatment relative to the untreated material due to the limited partial removal of potassium by the single press treatment. That such reductions in melting temperatures might occur by inadequate leaching has also been predicted for straw materials [1]. Where potash glasses form the bulk of the melt this possibility is readily observed on the binary alkali oxide-silicate phase system [1, 8]. In the region between 20 and 50% K$_2$O, the melting point in the binary SiO$_2$ - K$_2$O system is quite sensitive to the composition, as shown by the liquidus in Figure 2. Within this region the melting temperature is also sensitive to the presence of calcium, which can either serve to increase or decrease the melting point. This is also shown in Figure 2. In the figure, ash compositions for the various treatments are displayed on a normalized basis using K$_2$O and SiO$_2$ only (dashed lines). Were these two elements to comprise the majority of the ash, the fusion temperatures could be predicted by the liquidus at these compositions. In this case, the FC-P treatment would realize a melting temperature similar to that of the untreated material (with a slightly poorer potassium removal realizing a substantially lower melting point), but the FC-PRP treatment (at its corresponding normalized composition) would have a melting point approximately 200°C below that of the untreated material. The presence of calcium, however, serves to increase the expected value of the melting temperature for FC-PRP, increasing it 50 to 100°C above that of the untreated parent material. Below 20% K$_2$O in the binary system (above 80% SiO$_2$), the melting temperatures increase rapidly with decreasing alkali concentrations. The benefits to obtaining a well leached material are readily apparent in the behavior of the liquidus in this region and the predicted values of the melting temperatures for JC-PRP and bagasse. The presence of calcium in the system may serve to reduce the melting temperature in this range, in contrast to its effect at higher alkali concentrations.

Figure 2. Locations of the normalized ash compositions for banagrass and bagasse on the binary K_2O-SiO_2 phase system. Labels refer to treatment (see Table 1), numbers are sample numbers (see Table 2). Solid line (curve I): liquidus. Vertical dashed lines: normalized compositions for K_2O and SiO_2 only, melting temperatures at intersections with liquidus. Symbols: melting temperatures predicted from the ternary CaO-K_2O-SiO_2 phase system for comparison, ◐ banagrass, ▨ bagasse. The banagrass treatments lie roughly on the liquidus (thick solid line, curve II) for CaO varying linearly between 13% (JC-PRP) and 8% (FC-Untreated). Thin dashed line (curve III) is the liquidus for a constant 10% CaO. For curves II and III, the values are plotted against the normalized SiO_2 concentration in the K_2O-SiO_2 phase space, found as $100(SiO_2/(SiO_2+K_2O))$.

The bagasse ash composition cannot be compared directly against the banagrass compositions in the CaO-K_2O-SiO_2 phase space due to the high alumina and iron concentrations in the bagasse. These elements are not present in the parent biomass, but originate from soil contamination. The compositional position of bagasse in the Al_2O_3-FeO-SiO_2 phase space (Figure 3) predicts a fusion temperature approximately equal to that in the CaO-K_2O-SiO_2 phase space, however. The presence of alkali and alkaline earth fluxes would cause a depression in melting point relative to that predicted in the Al_2O_3-FeO-SiO_2 phase space alone. The composition of the bagasse ash is remarkably different from that of a clean sugar cane, which contains much lower concentrations of iron [9] and aluminum. Aluminum is toxic to growing plants, and its presence is generally regarded to represent contamination from adventitious materials. The composition of the bagasse ash is similar to that of a weathered or hydrothermally altered basalt with dilution from plant constituents (e.g. Si, K). For comparison, the composition of some Hawaiian lavas and soils are shown in Table 4 [10, 11] . The parent lava composition shows the higher proportion of Fe(II) ferrous iron (FeO) compared to Fe(III) ferric iron (Fe_2O_3), hence the use of the Al_2O_3-FeO-SiO_2 phase diagram in Figure 3. Analyses of soil from the cane fields supplying the source of the bagasse are pending. Aluminum and iron are present in the banagrass at concentrations more typical of clean biomass, with the exception of JC-PRP Sample 2 as noted above.

Table 4. Chemical Composition of Hawaiian Lava and Soils.

	Olivine Basalt Lava*	Alkali Olivine Basalt**	Low Humic Latosol**	Humic Latosol**
SiO_2	48.35	46.4	30.0	22.7
Al_2O_3	13.18	14.3	29.5	21.1
TiO_2	2.77	3.0	4.4	4.6
FeO	9.08			
Fe_2O_3	2.35	10.2[†]	21.8[†]	30.3[†]
CaO	10.34	10.6		
MgO	9.72	8.7		
Na_2O	2.42	3.0		
K_2O	0.58	0.8		
P_2O_5	0.34			
MnO	0.14			
H_2O			14.3	21.3

*average of 53 analyses [10].
**[11]
[†]total iron as Fe_2O_3

The compositions of the banagrass samples suggest that neither the FC-P nor FC-PRP treatments should be expected to demonstrate remarkable improvements in the slagging characteristics compared to untreated banagrass. Only the JC-PRP treatment shows significant improvement over the untreated material. These predictions follow from the assumption that the ash composition in the furnace remains close to that of the determined fuel ash composition, and is not substantially altered by volatilization of fuel elements. Such predictions are partially supported by experimental observations as discussed below, but neither slagging nor fouling can be predicted solely on the basis of the original fuel composition without regard to transformations occurring in the furnace.

Figure 3. Al2O3-FeO-SiO2 phase system showing location of normalized ash composition for bagasse, ▣ .

Ash fusibility and volatilization

Two comparative analysis techniques have recently been developed for evaluating the fusibility and potential slagging and fouling characteristics of biomass ash [1]. Ash fusibility is rated by burning compressed fuel pellets of approximately 1 g each under controlled conditions in a high temperature furnace. This differs from the standard ASTM pyrometric cone test [12] in the use of dry fuel in the pellet rather than calcined ash in the pyrometric cone. A different rating system has been developed as well, although it still describes ash behavior as a function of furnace temperature. This method is considered superior to the standard test in that the appearance of the pellet is evaluated from the start of combustion, rather than observing the pre-calcined ash cone. The standard pyrometric cone test is thought to be of questionable value in terms of predicting the fouling and slagging characteristics of many biomass fuels [7]. Attempts are currently underway to correlate the new test with the standard ASTM test where possible, but the difference in initial burning conditions is not expected to yield strong correlations overall. The fusibility test used here burns the fuel pellet under pre-set isothermal furnace conditions. A series of pellets from the same fuel are burned at increasing temperature levels, holding the pellet at temperature for a minimum of 20 min. The hold time of 20 min was found to be generally satisfactory for identifying major stages of ash fusibility in comparison against tests of much longer duration [1]. For the tests

described here, an air atmosphere was used in the furnace (no reducing conditions were tested), and fuels were milled through 20 mesh prior to pelletizing.

Whereas fusibility ratings characterize the behavior of the condensed phase, volatile species may contribute substantially to fouling. A crude descriptor of the fouling potential of a fuel due to volatilization of inorganic species can be obtained simply from the weight loss of the ash as a function of temperature. The second technique ashes the fuel in a muffle furnace at increasing temperatures to obtain these weight loss data. One to two grams of fuel is milled through 20 mesh, placed loose in an alumina crucible, and inserted into the cold furnace. The furnace is ramped up to temperature and held for 2 hours, similar to the standard ASTM method for ash analysis [13]. The sample is removed from the furnace, cooled and weighed, then reinserted for the next temperature step. An air atmosphere was also used in the tests on banagrass and bagasse described here. Temperatures utilized were 575, 750, and 900°C. The relative ash concentrations at 750 and 900°C were computed by normalizing the ash concentrations to the ash concentration at 575°C. Details of both tests are discussed in [1].

Results of the fusibility test are given in Figure 4. Shown are the fusibility ratings as a function of temperature for each fuel and each treatment. The fusibility ratings range from 1 to 6, with the following classification:

Fusibility Rating	
1	No apparent sintering of ash particles in pellet or pellet to refractory alumina support
2	Weak sintering of particles in pellet, high porosity, pellet free of refractory support
3	Pellet contracted to spherical shape with rough surface texture, particles strongly sintered, low porosity surface, slagged to refractory support
4	Pellet contracted to smooth closed spherical shape, slagged to refractory support
5	Ash fully molten with flat shape and thickness less than approximately 2 mm
6	Ash vaporized or absorbed by refractory support with no measurable thickness

The sixth, most severe rating, has been observed with certain fuels at very high temperatures [1]. All of the tests reported here were stopped after achieving a fully molten state represented by a rating of 5, so that the rating level of 6 is not used.

The ash from the untreated banagrass achieves a fully molten state by 1000°C. The untreated material and the treatments FC-P and FC-PRP exhibit weak sintering of particles (stage 2) by 800°C. The FC-P and FC-PRP treatments are more refractory compared with untreated banagrass. The melting point of FC-P is delayed to 1050°C, and for FC-PRP to 1150°C. However, substantial liquid has formed in the intervals below these temperatures, as can be determined from the phase systems discussed above. The extent to which the JC-PRP treatment has been modified by leaching is clearly apparent from Figure 4, with stage 2 delayed to 850°C, and the melting point (stage 5) to 1300°C. By comparison, bagasse achieves stage 2 at 1000°C (equal to the melting point of the untreated banagrass), and stage 5 between 1400 and 1450°C, some 100-150°C higher than the well leached JC-PRP treatment. The melts formed from banagrass and bagasse are substantially different in appearance. Whereas at stage 5 the banagrass exhibits a glassy lustre, the bagasse has a dull surface making it difficult to determine if a fully molten state has been obtained.

The trends in fusion temperatures are largely consistent with the predicted trends from the phase relationships discussed above. The melting temperature of the untreated banagrass was anticipated to be in the vicinity of 1000°C (Figure 2), the same temperature at which this material achieves stage 5 in the fusibility test. The predicted fusion point of the FC-P treatment in the $CaO-K_2O-SiO_2$ system is at a lower temperature compared to the untreated banagrass (FC-Un), although the

Fusibility rating □1 ▨2 □3 □4 ■5

Figure 4. Fusibility ratings for bagasse and banagrass.

liquidus in the $K_2O\text{-}SiO_2$ system suggests a temperature either above or below based on the actual composition of the sample. Figure 4 shows the FC-P treatment to reach the fluid point at 1050°C, about 50 K higher than the untreated material. The influence of Ca is apparent in the melting characteristics of the FC-PRP ash, where the predicted fusion point in the $CaO\text{-}K_2O\text{-}SiO_2$ system corresponds to that observed experimentally. The observed fusion temperature for the JC-PRP treatment corresponds to the predicted temperature of Sample 1 for this treatment. The apparent melting point of bagasse ash is in rough correspondence with that predicted from Figure 3, although the presence of the fluxes again suggest a decrease in fusion point in a manner similar to that observed (noting that the bagasse may not have been fully molten at the highest temperature tested).

Results from the ash volatilization tests are included in Table 5 and Figure 5. For every treatment, the ash content is observed to decline as the furnace temperature is increased above 575°C. However, the rate of decline varies among treatments, as shown by Figure 5. The bagasse is the most refractory sample, losing only 7% of weight by 900°C. The volatile loss increases as the severity of leaching decreases, with FC-Untreated > FC-P > FC-PRP > JC-PRP > bagasse. The untreated banagrass ash loses 20% of its weight between 575 and 900°C. What elements are volatilized has not been determined, as the samples have not yet been analyzed.

Table 5 also includes observations of color and sintering behavior of the ash in the crucibles at each temperature. At the lowest temperature, 575°C, well leached materials are generally observed to produce a white ash, free of residual carbon [1]. The JC-PRP treatment comes closest to this condition, revealing only a slight gray cast to the ash. The untreated banagrass and the FC-P treatment yield a darker ash. The color of the FC-PRP treatment is intermediate to the Untreated/FC-P and JC-PRP treatments. Of some interest is the red color of the bagasse ash. The high iron concentration is evident in the color of this ash. The gray cast of the less well leached

banagrass samples is retained up to 900°C, the red color of the bagasse ash browns slightly, likely as a result of oxidation, or possibly as a result of changes in the mineral state. Iron as hematite appears red, while brown to yellow colors are often associated with limonite or goethite. The crucible samples exhibit some sintering and slagging at the higher temperatures in accordance with the results of the fusibility tests employing pelleted fuel. Sintering in some samples at lower temperatures than observed in the pellet tests may be due to the longer residence time at elevated temperature.

Table 5.   Ash characteristics, muffle furnace.

| | Furnace Temperature | | |
	575°C	750°C	900°C
	Ash content (% dry matter)		
FC-PRP	3.30	3.05	2.91
JC-PRP	2.88	2.65	2.64
Bagasse	6.28	6.29	6.25
FC-P	4.52	3.92	3.73
FC-Un	4.93	4.28	3.89
	Color of ash		
FC-PRP	Medium gray-milky white	Medium gray	Medium gray
JC-PRP	Light gray-milky white	Light gray	Light gray-white
Bagasse	Dark red	Dark red	Dark red-brown
FC-P	Dark gray	Medium gray	Light gray
FC-Un	Dark gray	Medium-light gray	Light gray
	Fusibility		
FC-PRP	None	None	Heavy sintering, little slagging
JC-PRP	None	None	Light sintering, no slagging
Bagasse	None	None	None
FC-P	None	Sintering	Heavy sintering and slagging
FC-Un	None	Light sintering	Heavy sintering and slagging

During the fusibility tests using pelleted fuel, observations were made of the duration of luminous flaming (volatile burning) and the duration of char incandescence. The results are plotted in Figures 6 and 7. Because the fuel mass, pellet density, and fuel moisture were kept roughly constant for all samples, the duration of flaming and incandescence may serve as qualitative indicators of other influences the fuel composition has on burning behavior. Although the results are quite variable, the flame duration of the JC-PRP treatment was consistently longer than for the other treatments. At 850°C, the volatile burnout was 62% (21 s) longer than the shortest burnout (FC-PRP), and 17% (9 s) longer than the burnout for the untreated banagrass. To some extent this may reflect the higher volatile matter content with increased leaching, but the extraction of alkali metals may also be involved. Alkali metals serve to catalyze the pyrolysis reactions leading to volatile emission, and the effective leaching of the alkali metals may serve to retard the rate of pyrolysis and extend the volatile burning period. This effect has also been observed with straw fuels [4]. A competitive effect arises from the presence of halogens, especially Cl, which serve as flame retardants. The more poorly leached materials may be subject to some amount of flame suppression due to the higher concentrations of Cl compared to the well leached materials. This effect is also thought to pertain to straw fuels [4]. The two effects, combined with uncontrolled

Figure 5. Residual ash fraction after heating above 575°C in air.

effects in the test conditions, may contribute to the variability observed. The consistently longer volatile burnout for the JC-PRP treatment is at least noteworthy, however. The duration of char incandesence is also extended at the lower furnace temperatures for the JC-PRP treatment, although the trend is not as clear as in the case of the flame duration.

Pilot combustion tests

Pilot combustion experiments utilizing bagasse and banagrass were conducted in the Multi-Fuel Combustor (MFC) at Sandia National Laboratories, Livermore, CA. These tests were intended to directly evaluate deposition rates as well as deposit structure and composition using simulated boiler furnace conditions. All five treatments of Table 1 were tested.

The MFC is an electrically heated vertical tube furnace approximately 4 m long as shown schematically in Figure 8. The furnace consists of six 0.6 m long independently controlled heater sections followed at the bottom by an unheated but insulated sampling stage. For these tests, fuel was injected pneumatically through a water-cooled fuel lance into the furnace near the top. Combustion air was introduced as transport air through the fuel lance as well as primary air through the top of the furnace. A natural gas burner located at the top of the furnace for supplying a vitiated air stream was not used; instead fresh air alone entered through the top. The furnace flow discharges across an open space at the bottom of the unheated section into an exhaust inlet drawing both furnace flow and laboratory air. Deposit probes were located in the open space as described below.

Figure 6. Duration of flaming combustion following ignition.

Figure 7. Duration of char incandescence following ignition.

Air dry materials received from HNEI were milled and sieved through 16 mesh (1 mm) prior to firing. The eductor used to entrain the fuel in the transport air of the fuel lance requires fuel particles of this size or smaller. The residence time of fuel particles in the MFC (maximum for these tests approximately 4 s) also requires a fairly small size.

Natural gas
Combustion air

Preheat Burner
Flow straightener
Fuel lance

Pneumatic fuel transport

15 cm

Heater element
Insulation
Liner

Instrument port

Heater Module

0.6 m

Gas sample probe

Open test section {

Upper deposit probe
Lower deposit probes
Instrument table

To exhaust blower

Figure 8. Multifuel Combustor (MFC).

Furnace conditions were set at 900°C (1650°F) wall temperature, 10 ft^3 min^{-1} (283 L min^{-1}) primary combustion air flow rate, and 5.4 ft^3 min^{-1} (153 L min^{-1}) transport air flow rate. Gas temperatures at the bottom of furnace just prior to the open sampling zone were approximately 670°C (1240°F) when firing biomass.

Tests were conducted in the order shown in Table 1. The leached fuels were burned first so as to reduce the potential for furnace wall slagging and fouling. The deposit probes were stainless steel tubes approximately 19 mm outside diameter. The probes were held stationary in the furnace exit flow. Only two probes were used in the first test, later a third probe was inserted into the flow above the other two probes to evaluate the effect of increased surface temperature. The two lower probes were installed across the flow from either side, and aligned end to end at the center. The upper probe was inserted just off center, out of line with the lower probes. Probe temperatures were monitored via optical pyrometry, and by intermittent thermometry. The lower probes, situated 125 mm below the furnace exit, had surface temperatures of approximately 400°C during biomass firing. The upper probe, located 50 mm below the furnace exit, was at 450°C. After completing a test, probes were removed and photographed. The deposit end of one probe was cast in epoxy resin to preserve the deposit for later microscopy and microprobe analysis. Deposits from the other two probes were removed from the probes, weighed, and retained for later analysis.

Fuel was loaded onto a flat belt feeder and fed at a controlled uniform rate into the eductor of the pneumatic transport line and fuel lance. The fuel rate was set to maintain O_2 concentration in the furnace exit gas at approximately 5% by volume. Fuel rate was measured gravimetrically over the course of the test, and intermittently by observing the travel speed of the fuel feed belt. With the exception of the first test (FC-PRP), the fuels were burned in sequential duplicate runs to check for consistency. Fuel samples were collected at the feeder and analyzed for moisture content (by air oven method).

Furnace exit gas composition was monitored via on-line gas analysis for O_2, CO_2, CO, NO_x (as NO_2), SO_2, and total hydrocarbons (HC, as CH_4). Data were automatically collected at 1 Hz, subsampled at 1/3 Hz, and stored on disk. In three of the duplicates, data logging was inadvertently stopped, and gas composition was not recorded. Gas composition for both duplicates is therefore available only for JC-PRP, although in general gas composition remained nearly constant due to the constant furnace conditions and steady fuel feed. Gas data were used to check for consistency in flow rate measurements via carbon balance, and to determine emission factors and fuel element conversions.

Larger fly ash representing primarily charred fuel particles was collected in a stainless steel beaker below the probes at the entrance to the MFC exhaust. A rapid quench flyash sampling system was available but not fully instrumented and was not used. Fly ash samples were bottled for later analysis. Three other flyash samples (bagasse, FC-P, and FC-PRP) were collected on the upstream cartridge filters of the on-line gas analyzer sampling train. These filters were situated approximately 1 m downstream of the sampling nozzle in the furnace, and stayed above the dew point temperature throughout each run.

Deposit, flyash, and cartridge filter samples were submitted to Hazen Laboratories, Golden, CO, for bulk analysis by x-ray fluorescence (XRF). Specimens were sectioned from the probe deposits cast in epoxy, polished in kerosene (to avoid loss of water soluble elements), and analyzed for microstructure and composition using the Cameca SX-50 electron beam microprobe operated by the Department of Geology, University of California, Davis.

Results

Firing conditions for each fuel type and each test are summarized in Table 6. The table includes air flow rates (both primary air through the top of the furnace and transport air through the fuel lance), fuel moistures, weight of fuel consumed, test duration, and overall fuel feed rate. Also listed are the gas compositions where available. For these tests, the excess air, exit gas velocity, bulk Reynolds number of the flow, and flow residence time were computed. The measurements were checked against carbon element balances for all tests having complete gas analyses. The net carbon yields were consistently high by 30 to 45%, indicating, most likely, errors in either the fuel feed rate, air flow rate, or both. Table 6 shows the results of closing the carbon balances under each of two conditions: 1) adjusting the fuel feed rate without adjusting the measured air flow rate, and 2) adjusting the air flow rate without adjusting the measured fuel flow rate. The first case requires the moist fuel rate to be increased by an average of 41% in order to balance the carbon in the system.

The second yields a necessary average reduction of 29% in air flow rate. The gravimetric measurements of fuel rate agreed well with volumetric measurements made from feed belt travel. The air flow rate is therefore believed to be in error, biasing the carbon balance by about 30% high. The values for fuel or air flow rate, excess air, exit gas velocity, bulk Reynolds number, and flow residence time computed by closing the carbon balance under the two adjustments are listed in Table 6. Element balances were also computed for hydrogen, nitrogen, sulfur, and oxygen. Full details of these results, along with element conversion ratios and emission factors are contained in Tables A1a-f through A5a-f of the appendix. Each set of tables (six tables for each treatment) includes the full results for the measured conditions as well as the two adjustments leading to closure of the carbon balance mentioned above.

Banagrass was fired at a moisture content of 11 to 12% wet basis. The bagasse was slightly drier at 8%. Assuming an error in the measured air flow rate as discussed above, and utilizing the adjusted air flow rate obtained by closing the carbon balance, excess air was kept at approximately 40% for an exit O_2 concentration of 4.5 - 5% by volume. The exit gas velocity of approximately 1 m s^{-1} yields a flow Reynolds number in the vicinity of 1000, and a furnace residence time of 4 s.

Results from the deposit probes are listed in Table 7. Included are deposit masses from the lower and upper probes (not including the second lower probe used for casting). For the purpose of comparison, deposit masses were normalized to total fuel, as well as to total ash, fired to the furnace. Banagrass deposit fractions were then normalized to the bagasse deposit fractions for the respective upper and lower probes (except for FC-PRP with no upper probe). Increases in deposit accumulation on the upper probes for the lightly treated (FC-P) and untreated (FC-Untreated) banagrass are apparent. The lower probe accumulated a substantially higher deposit fraction with untreated banagrass compared to bagasse (0.3% compared to 0.08% of ash). No major differences in fuel deposit fraction were observed among the FC-PRP, JC-PRP, and bagasse treatments, but all banagrass treatments yielded higher deposit fractions compared to bagasse based on the amount of ash fired to the furnace. Relative to the fuel and ash fired to the furnace, the FC-PRP treatment yielded a higher deposit fraction on the lower probe than did the FC-P treatment. To some extent this may be the result of the smaller quantity of fuel fired during the FC-PRP test.

When installed, the upper probe generally collected a larger total mass of deposit due to its higher temperature, in addition to its greater exposure to furnace flow. The exit flow contracts as it leaves the furnace due to entrainment of laboratory air under the suction of the exhaust blower. The flow contraction results in a shorter deposition length for probes located farther away from the furnace exit (the lower probes). In terms of average deposit fraction normalized to total fuel consumption for both upper and lower probes, the treatments rank as JC-PRP < Bagasse < FC-PRP < FC-P < FC-Untreated. Relative to the total ash fired to the furnace, the treatments rank as Bagasse < JC-PRP < FC-PRP = FC-P < FC-Untreated.

Table 6. Summary results, firing conditions, MFC.

Fuel Treatment* Test Number	Banagrass FC-PRP 1	Banagrass JC-PRP 2a	 2b	Sugar Cane Bagasse 3a	 3b	Banagrass FC-P 4a	 4b	Banagrass FC-Un 5a	 5b
Moisture as-fired (% w.b.)	11	11	11	8	8	11	11	12	12
Weight of fuel fired (kg w.b.)	4.10	3.15	1.97	3.12	2.29	4.04	2.38	3.81	1.41
Duration (min)	81	65	37	60	39	78	45	67	25
Measured fuel feed rate (g/s w.b.)	0.84	0.81	0.89	0.87	0.98	0.86	0.88	0.95	0.94
Measured Air Flowrate (L/min)									
Primary	283	283	283	283	283	283	283	283	283
Transport	153	153	153	153	153	153	153	153	153
Total	436	436	436	436	436	436	436	436	436
Measured Air Mass Flow rate (g/s)									
Primary	5.57	5.57	5.57	5.57	5.57	5.57	5.57	5.57	5.57
Transport	3.01	3.01	3.01	3.01	3.01	3.01	3.01	3.01	3.01
Total	8.58	8.58	8.58	8.58	8.58	8.58	8.58	8.58	8.58
Furnace exit gas temperature (°C)	670	670	670	670	670	670	670	670	670
Exit gas composition†									
O_2 (% dry basis)	4.5	5.1	4.6		4.6	4.6			4.6
CO_2 (% dry basis)	15.2	14.5	15.0		15.2	15.0			15.0
N_2** (% dry basis)	80.2	80.3	80.3		80.2	80.3			80.3
CO (ppm)	430	401	389		63	389			864
HC (ppm)	11	30	69		10	9			55
NO_x (ppm)	478	427	415		362	426			384
SO_2 (ppm)	1	2	9		26	4			11
Excess air (%)	101	110	91		90	97			85
Exit gas velocity (m/s)	1.37	1.36	1.38		1.38	1.37			1.38
Flow Reynolds Number	1,318	1,316	1,328		1,327	1,322			1,336
Residence time (s)	2.93	2.93	2.91		2.91	2.92			2.89
Results of Carbon Balance (Adjusted Fuel Feed Rate, Unadjusted Air Flow Rate)									
Fuel feed rate (g/s w.b.)	1.25	1.19	1.23		1.31	1.24			1.27
Difference relative to measured (%)	48	48	39		34	43			36
Excess air (%)	36	42	37		42	37			36
Exit gas velocity (m/s)	1.44	1.44	1.44		1.43	1.44			1.45
Flow Reynolds Number	1,392	1,386	1,391		1,383	1,391			1,396
Residence time (s)	2.77	2.78	2.77		2.79	2.77			2.76
Results of Carbon Balance (Measured Fuel Feed Rate, Adjusted Air Flow Rate)									
Air flow rate (L/min)	293	296	315		325	304			322
Difference relative to measured (%)	-33	-32	-28		-25	-30			-26
Excess air (%)	36	42	37		42	37			36
Exit gas velocity (m/s)	0.97	0.98	1.04		1.07	1.00			1.07
Flow Reynolds Number	937	941	1,003		1,031	968			1,030
Residence time (s)	4.12	4.10	3.85		3.74	3.98			3.75

*FC=Forage chopped. JC=Jeffco Cut. P=pressed. R=rinsed.
**by difference
†Blank indicates not recorded

To eliminate comparative differences due to possible differences in exposure and deposit area, the deposit fractions were further normalized to deposit area, giving the specific deposition (m^{-2}). All deposits covered roughly two-thirds of the probe surface exposed to the furnace flow, and a constant two-thirds of probe circumference was used in computing the specific depositions. The under side of each probe extending from the 4 to 8 o'clock positions collected little if any deposit in these tests. Comparing specific depositions, the trend towards higher fouling with the untreated fuel is again apparent. Based on fuel fraction, the better leached banagrass treatments yielded lower specific depositions compared to the bagasse, although insufficient data exist to determine if these differences are significant. Results from the FC-P treatment are again mixed, with greater accumulation on the upper probe, and smaller amounts on the lower probe. The relatively high specific deposition on the lower probe for FC-Untreated suggests significant fouling problems with untreated banagrass.

In appearance, the deposits formed from banagrass all started as uniform white layers on the upper surfaces of the probes. With the better leached fuels, the deposits on the lower probes grew at very slow rates, and only a very loosely structured crown deposit developed. The crown deposits were easily removed by simply overturning the probes, indicating that little attachment strength had developed. These crown deposits were also friable with little inter-particle sinter strength. Both the lower and upper probe deposits from FC-Untreated and the upper probe deposit from FC-P exhibited greater sinter strength and tenacity compared to the other treatments. Crown deposits for these probes were heavier and were not removed by overturning the probes, although they were removed by light brushing. The finer textured initial deposit layer had to be removed by brushing in all cases.

The bagasse deposits differed substantially in color from the banagrass deposits. These deposits started and remained brown in color in marked contrast to the white deposits of banagrass. The high iron content of the bagasse is likely responsible.

Bulk compositions of deposits, flyash, and filter samples

Bulk compositions of deposit, flyash, and cartridge filter samples were analyzed by XRF for elements sodium (atomic number 11) through uranium (92). Full results are included in Tables B1 through B14 in the appendix. Summary results appear in Tables 8 - 10 for major elements. These XRF analyses are considered to be semi-quantitative only, and concentrations for sodium and magnesium may be unreliable. Iron in the deposit samples is subject to contamination from the probe metal, and is not necessarily representative of the bulk deposit composition. Deposit samples from the upper probes were analyzed where available. Samples from both the upper and lower probes were analyzed in the case of FC-Untreated due to the larger sample masses available.

Major elements of the banagrass deposit compositions are Si, Ca, K, and Cl, the latter principally being found in the FC treatments. The bagasse deposit is rich in Fe, Si, and Al, with K at about half the concentration found in JC-PRP. To a large extent, the deposit compositions mirror the fuel compositions for the better leached materials. The untreated banagrass and the FC treatments show enrichment in K and Cl relative to fuel composition. The concentrations of the five major elements Si, Fe, Ca, K, and Cl are graphically depicted in Figure 9.

Tables 8-10 also report a loss-on-ignition (LOI) which is used by Hazen to correct the raw oxide concentrations. The LOI is obtained by heating the sample in an air atmosphere at 1000°C to correct for elements, such as carbon in carbonates, not determined by XRF. This is done following the analysis of the original sample by XRF. The LOI in Tables 8-10 is the total loss. The oxide and element concentrations are corrected by the LOI less S, Cl, Br, Hg, and I, which are

Table 7. Deposit accumulations and comparative deposit fractions.

Test #	Fuel*	Deposit Probe	Deposit Mass (g)	Total Fuel Fired to Furnace (kg, d.b.)	Total Ash Fired to Furnace (g)	Deposit Fraction (%) Fuel	Ash	Relative Deposit Fraction** (--) Fuel	Ash	Deposit Area (mm^2)	Specific Deposition† (1/m^2) Fuel	Ash	Relative Deposition** (--) Fuel	Ash
1	FC-PRP	Lower	0.0583	3.7	98.4	0.0016	0.0593	1.10	3.45	2,032	0.008	0.29	0.96	3.02
2	JC-PRP	Lower	0.0563	4.6	121.2	0.0012	0.0464	0.85	2.71	1,778	0.007	0.26	0.85	2.71
		Upper	0.2420	4.6	121.2	0.0053	0.1996	0.79	2.51	3,048	0.017	0.65	0.79	2.51
3	Bagasse	Lower	0.0725	5.0	422.5	0.0015	0.0172	1.00	1.00	1,778	0.008	0.10	1.00	1.00
		Upper	0.3355	5.0	422.5	0.0067	0.0794	1.00	1.00	3,048	0.022	0.26	1.00	1.00
4	FC-P	Lower	0.0724	5.7	174.6	0.0013	0.0415	0.87	2.42	2,540	0.005	0.16	0.61	1.69
		Upper	0.6558	5.7	174.6	0.0115	0.3756	1.71	4.73	4,064	0.028	0.92	1.28	3.55
5	FC-untreated	Lower	0.2200	4.6	181.2	0.0048	0.1214	3.30	7.08	2,540	0.019	0.48	2.31	4.95
		Upper	0.5490	4.6	181.2	0.0119	0.3031	1.78	3.82	4,064	0.029	0.75	1.33	2.86

*FC=Forage chopped. JC=Jeffco Cut. P=pressed. R=rinsed.
**Relative to bagasse, lower and upper probes respectively.
†Deposit fraction (fuel or ash)/Deposit area

volatile but detected by XRF. The correction does not account for alkali and other semi-volatile elements which are also detected by XRF. The deposit samples yield LOI in inverse proportion to the extent of leaching, that is, higher LOI with the FC-P and untreated samples. Much of this is likely unreacted carbon, but may also include volatile alkali. Unclear is whether the LOI values of the different treatments reflect substantially different concentrations of carbon, either as fixed carbon or as carbonates, or whether they indicate the presence of volatile elements in the original sample which are also detected by XRF.

Bulk compositions of the coarse flyash are listed in Table 9. The trends are in many respects similar to those observed for the deposits. An exception is the loss-on-ignition, which is higher for the FC-PRP and JC-PRP samples than for the less well leached FC-P and the untreated banagrass. Contrary to the deposit samples, the LOI of the banagrass flyash are in direct proportion to the extent of leaching. The LOI for bagasse is again quite low.

The bulk compositions of the cartridge filters for bagasse, FC-P and FC-Untreated are listed in Table 10. The bagasse filter composition bears a resemblance to the fuel composition. This sample also exhibited a brown coloration, similar to the deposit, due to the high iron concentration. The FC-P and untreated banagrass filter samples were white in color, and were composed almost entirely of K and Cl. In both cases, the K to K+Cl ratio is 0.65, somewhat above the mass stoichiometric ratio for K in KCl of 0.52. By virtue of the compositions of these two samples, a LOI correction was not made. The composition of these two filter samples is rather interesting, in that the filter catches particles bigger than about 8 μm (nominal 90% larger than 8 μm), but the composition is markedly different from the coarse flyash. The velocity at the gas sampling nozzle (approximately 2.5 m s^{-1}) is evidently low enough to provide some size segregation. Few coarse particles (i.e., those with the composition of Table 9) were observed in these samples, and the compositions of the filter catch reflect their absence. Coarse particles are sometimes accumulated loose in the filter canister but were not observed on the filter in these tests. The presence of substantial amounts of KCl particles in the combustion gas is consistent with microprobe observations of deposits and flyash described below, and also with the initial formation of a white layer on the probes when firing banagrass, especially the untreated material and the poorly leached FC-P.

Deposit microstructure and composition

Specimens sectioned from the deposit probes cast in epoxy were examined via electron beam microprobe, as were samples of coarse flyash and a few furnace wall deposits. Backscattered electron (bse) images were acquired, along with point compositions of particles and compositional maps (element dot maps). The results are shown in Tables 11 - 15, and in image sequences 1 - 5.

1. FC-PRP

Image 1A is a bse image of the FC-PRP deposit at 50 times magnification (50X). The white area along the left margin of the image is the probe steel, the interface between the white and dark area designating the probe surface. The image is rotated 90° clockwise from the probe orientation in the furnace. The top of the probe is therefore oriented towards the right in the image. The probe surface is rough partly as a result of corrosion of the steel surface and partly as a result of the cutting process. The image reveals a fine structured deposit of filamentous particles, only weakly sintered. The deposit is thin, extending not much more than 1 mm above the probe surface. The composition of the crescent shaped particle labeled "a" in the image is listed in Table 11. The table shows the original analysis along with total reconstructed mass (iron was analyzed as FeO, then converted to Fe$_2$O$_3$ basis for comparison to bulk compositions; the actual form of the iron is unknown). Each analysis has been converted to a normalized basis in the lower part of the table by

Table 8. *Major element concentrations from XRF, deposit probes.*

Element	FC-PRP Lower Probe (%)	JC-PRP Upper Probe (%)	Bagasse Upper Probe (%)	FC-P Upper Probe (%)	FC-Untreated Upper Probe (%)	FC-Untreated Lower Probe (%)
Si	17.88	30.86	16.69	19.29	14.34	11.43
Al	<0.01	<0.01	5.81	<0.01	<0.01	<0.01
Ti	0.19	0.11	3.07	0.52	0.13	0.29
Fe	1.54	0.94	23.41	3.72	1.20	2.41
Ca	13.53	11.37	1.86	7.96	7.70	9.26
Mg*	2.07	0.96	1.47	2.46	2.58	1.73
Na*	<0.01	<0.01	1.26	<0.01	<0.01	0.10
K	15.60	6.09	3.35	14.81	20.90	23.97
P	1.58	0.50	0.48	1.25	1.37	1.29
S	1.21	0.67	0.21	1.04	0.99	0.77
Cl	3.58	0.49	<0.01	3.68	5.02	6.71
Mn	0.76	0.48	1.12	0.74	0.75	1.03
Subtotal	57.94	52.48	58.73	55.45	54.99	59.02
Total Non-oxygen	58.13	52.67	59.35	55.86	55.40	59.52
Subtotal/Total (%)	99.67	99.64	98.96	99.26	99.26	99.15
LOI**	13.70	5.66	0.27	15.90	24.00	23.30
Total Non-oxygen + LOI	71.83	58.33	59.62	71.76	79.40	82.82
Oxygen†	28.17	41.67	40.38	28.24	20.60	17.18

*not generally considered reliable.
**Loss on ignition.
†excluding oxygen in LOI.

Table 9. Major element concentrations from XRF, flyash.

Element	FC-PRP Flyash (%)	JC-PRP Flyash (%)	Bagasse Flyash (%)	FC-P Flyash (%)	FC-Untreated Flyash (%)
Si	11.27	18.61	21.14	20.09	16.82
Al	<0.01	<0.01	6.33	<0.01	<0.01
Ti	0.09	0.05	2.31	0.15	0.13
Fe	0.36	0.44	18.11	1.18	1.02
Ca	6.65	7.75	2.08	8.83	8.56
Mg*	1.01	0.59	1.31	2.26	2.92
Na*	<0.01	0.16	1.10	<0.01	0.08
K	5.15	3.80	2.28	13.16	17.80
P	0.67	0.31	0.38	1.21	1.43
S	0.14	0.15	0.07	0.39	0.38
Cl	0.07	0.07	0.01	0.45	0.55
Mn	0.30	0.35	0.86	0.70	0.79
Subtotal	25.70	32.27	55.98	48.41	50.50
Total Non-oxygen	25.74	32.44	56.56	48.69	50.80
Subtotal/Total (%)	99.84	99.49	98.98	99.43	99.40
LOI**	56.60	41.80	0.98	19.40	19.60
Total Non-oxygen + LOI	82.34	74.24	57.54	68.09	70.40
Oxygen†	17.66	25.76	42.46	31.91	29.60

*not generally considered reliable.

**Loss on ignition.

†excluding oxygen in LOI.

Table 10. Major element concentrations from XRF, gas filters.

Element	Bagasse Gas Filter (%)	FC-P Gas Filter (%)	FC-Un Gas Filter (%)
Si	20.82	1.93	0.84
Al	6.23	<0.01	<0.01
Ti	2.64	0.13	0.01
Fe	14.85	0.85	0.20
Ca	1.50	1.12	0.49
Mg*	0.93	<0.01	<0.01
Na*	1.77	<0.01	0.51
K	4.77	56.54	58.54
P	0.66	0.41	0.34
S	0.21	1.78	2.10
Cl	0.62	30.01	30.99
Mn	0.60	0.12	0.07
Subtotal	55.59	92.89	94.10
Total Non-oxygen	56.01	93.55	94.84
Subtotal/Total (%)	99.24	99.29	99.22
LOI**	3.42	ND	ND
Total Non-oxygen + LOI	59.43	93.55	94.84
Oxygen†	40.57	6.45	5.16

*not generally considered reliable.
**Loss on ignition.
ND = not determined
†excluding oxygen in LOI.

Figure 9. Element mass fractions for five major elements in deposits (-L = lower probe, -U = upper probe).

dividing each original element concentration by the total reconstructed mass. The crescent shaped particle is almost pure silica, and is almost certainly of fuel origin as opposed to adventitious matter. Many of the filamentous particles in image 1A have similar compositions, others have higher Ca and K concentrations.

Image 1B is of an area near the probe surface, enlarged 500X. The location of this area is indicated by the square outline in image 1A. Accompanying the bse is a series of element dot maps of the same region. The concentration of each element is in proportion to the black level on the map. Each map is at a different contrast level, however, and concentration magnitudes can only be roughly compared across maps. Actual compositions for a few particles are listed in Table 11.

The Fe dot map shows clearly the probe steel, and a few iron containing particles distributed throughout the deposit. Lying along the surface of the probe is a 10 μm thick layer of KCl, interrupted by potassium-silicate particles, possibly glasses. The KCl layer is consistent with the white layer observed to form on the probe shortly after introducing fuel to the furnace. It is also consistent with the role of condensation in initiating the sequence leading to deposit growth and development. The presence of the K-Si particles at the surface suggests a concurrent attachment of molten or partially molten glass, or displacement of the salt layer by the particles. However, sample handling precludes strong conclusions in this regard. This is the only sample in which a clean, mostly continuous salt layer was observed. Cutting and polishing of the specimens, although done with due regard to the delicate nature of the surface structure, may have distorted the finer detail.

Potassium appears among the siliceous particles in the bulk deposit. Of particular interest is the large particle in the lower right hand corner. The upper half of this particle is predominantly composed of silica, as shown in Table 11 (1B:a). There is a small amount of K present, although the total element recovery is fairly poor at only 88% and K or other elements may not have been fully detected. The lower half of this particle (Image 1B:b) appears to be a mixture of alkali-sulfate and alkali-chloride. The element recovery was extremely poor, however. Many particles of this type yield poor recovery due to volatilization under beam heating (even with reduced beam current), and a highly porous structure. The dot maps reveal several particles containing Ca, P, and Mg, as well as Si, which may be of plant origin. Dark areas in the Al dot map suggest the presence of soil particles. The compositions indicated from the dot maps are for the most part consistent with the perceived mechanisms of deposit formation [14], that is, formation of a condensed layer adjacent to the surface, followed by capture of impacting particles to form the bulk deposit. The presence of the K-Si material next to the probe surface suggests early capture of potentially molten glass without need of a preceding condensed layer. This has so far not been confirmed by other samples.

Image 1C is a backscattered electron image of coarse flyash at 50X. The particle labeled "a" in the image is of definite fuel origin, having the characteristic filamentous silica structure of the grasses. Its composition is listed in Table 11, and shown to be nearly pure silica. The particle appears unmelted, similar to straw particles burned under similar conditions after leaching [1], [4]. The porous particle extending perpendicular to the silica filament and labeled "b" in 1C, has a high Ca content, but the element recovery is so poor due to the high porosity that conclusions as to its origin cannot be made.

2. JC-PRP

Image 2A is a bse image of the deposit from JC-PRP taken near the top of the probe in the region of greatest deposition. The deposit extends 0.5 to 1 mm above the surface of the probe at this point. The deposit is sparse, but has a greater number of spherical particles than the deposit of FC-PRP. A region near the probe surface is shown in image 2B, accompanied by the relevant dot

Table 11. Microstructural compositions for banagrass FC-PRP.

1

Image label: (%)	Banagrass FC-PRP Fuel Ash (Bulk)	Banagrass FC-PRP Deposit (1A: a) Crescent Particle	Banagrass FC-PRP Deposit (1B:a) Particle Upper Half	Banagrass FC-PRP Flyash (1C: a) Silica Fiber
SiO2	51.60	87.76	85.55	84.66
Al2O3	0.86	0.04	0.07	0.04
TiO2	0.19	0.00	0.02	0.00
Fe2O3	0.91	0.12	0.23	0.06
CaO	9.84	0.10	0.07	0.06
MgO	3.98	0.04	0.19	0.09
Na2O	0.85	0.07	0.30	0.04
K2O	15.55	0.23	1.67	0.33
P2O5	5.69	0.00	0.18	0.00
SO3	1.20	0.09	0.09	0.07
Cl	0.95	0.02	0.02	0.04
MnO		0.03	0.00	0.00
CO2	1.96			
Total	93.58	88.51	88.41	85.40

Normalized

1

Image label: (%)	Banagrass FC-PRP Fuel Ash (Bulk)	Banagrass FC-PRP Deposit (1A: a) Crescent Particle	Banagrass FC-PRP Deposit (1B:a) Particle Upper Half	Banagrass FC-PRP Flyash (1C: a) Silica Fiber
SiO2	55.14	99.15	96.77	99.13
Al2O3	0.92	0.04	0.08	0.05
TiO2	0.20	0.00	0.02	0.00
Fe2O3	0.97	0.14	0.26	0.07
CaO	10.52	0.12	0.08	0.08
MgO	4.25	0.05	0.22	0.10
Na2O	0.91	0.08	0.34	0.05
K2O	16.62	0.26	1.89	0.38
P2O5	6.08	0.00	0.21	0.00
SO3	1.28	0.11	0.10	0.08
Cl	1.02	0.02	0.02	0.05
MnO		0.03	0.00	0.00
CO2	2.09			
Total	100.00	100.00	100.00	100.00

1A
FC-PRP Deposit
50X

328 μm

1C
FC-PRP Flyash
50X

328 μm

maps indicating the structural composition. Few soil particles are present, at least as indicated by the aluminum distribution. Remnants of a KCl layer are evident, but it is poorly maintained if, in fact, a continuous layer existed prior to sectioning of the specimen. The filamentous particles are again mostly silica, but Ca and some K is also present. These particles are evidently of plant origin. Compositions are listed in Table 12. Note the bright rectangular particle approximately 10 μm in size near the center of the image. The K and Cl dot maps reveal this to be a crystal of KCl, probably formed following combustion and captured by the probe. Such crystals are thought to comprise the bulk of the cartridge filter catch for banagrass described above. A spherical particle lying midway out from the surface is shown in image 2C, its composition given in Table 12. Another spherical particle lying near the surface is shown in image 2D (labeled "a"), again with its composition listed in Table 12. Both particles appear to be calcium-silicates, the origin unknown. The porous, rectangular particle "b" in 2D is nearly pure silica, most likely of plant origin.

Image 2E shows the structure of the coarse flyash. The appearance of this material is substantially different from the FC-PRP flyash. Although a number of filamentous particles also appear here, there are quite a few vesiculated particles of hollow spherical construction. The filamentous particles, such as "e", are nearly pure silica of fuel origin. The particle labeled "a" in the image is also composed principally of silica (Table 12), however, its shape and vesiculated structure suggest that it has been melted at some time. Unknown is whether the particle entered the furnace in this form as adventitious material, or whether it acquired this appearance in the furnace. Particle "b" has a Ca-Si-K-Mg composition. The shell "d" is of Si-Ca-K-Mg-Al composition, the interior "c" is alumina-silicate, and the plate-like structure of the interior suggests clay particles. Although the origin is indistinct for these particles, the compositions are indicative of soil material.

3. Bagasse

Image 3A shows the sparse structure of the bagasse deposit. Several particles, such as the long filament visible to the right, appear at some distance from the surface. Loose bonding of the particles in the deposit may have allowed particles to disperse in the epoxy during pouring of the cast and prior to solidification. The particle "a" in the image has an alumina-silicate composition shown in Table 13 (3A:a). Many of the smaller compact particles also have compositions indicative of soil origin, a few silica filaments of plant origin were observed.

Image 3B shows an area at the probe surface enlarged 500X. There is little indication of a condensed layer. The three particles extending away from the surface are almost certainly of soil origin, all having high aluminum concentrations. The composition of one of these particles, labeled "a" in the image, is listed in Table 13. Particles "b" and "c" have similar compositions. These compositions resemble the bulk fuel ash composition, shown in the table for comparison, and again suggest a weathered basalt (Table 4). Other particles, such as "a" in image 3C, exhibiting a porous structure, have higher silica concentrations (Table 13), but also contain large amounts of aluminum. These could be of mixed origin, although no definitive conclusions can be drawn in this regard.

Structure of the coarse bagasse flyash is shown in image 3D. The image reveals a mixture of particle types and shapes. The solid particle "a" at center is an alumina-silicate bearing smaller amounts of iron and titanium. The vesiculated particle "b" above it appears to be of felsic composition. The fine filamentous particles, such as "c", are almost pure silica, and the only particles of obvious plant origin.

Table 12. Microstructural compositions for banagrass JC-PRP.

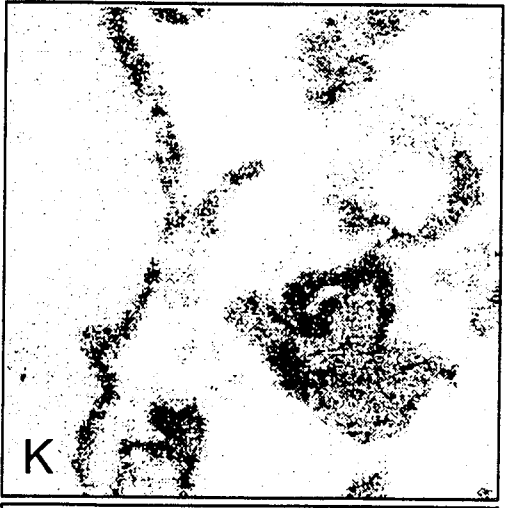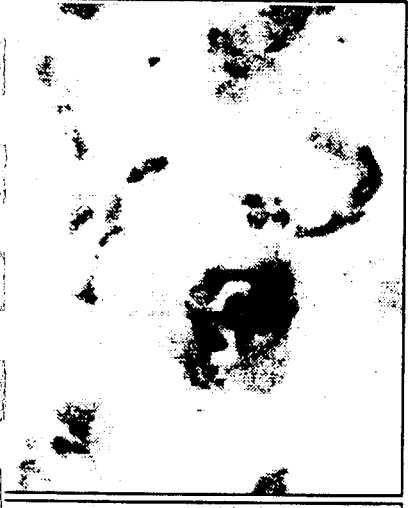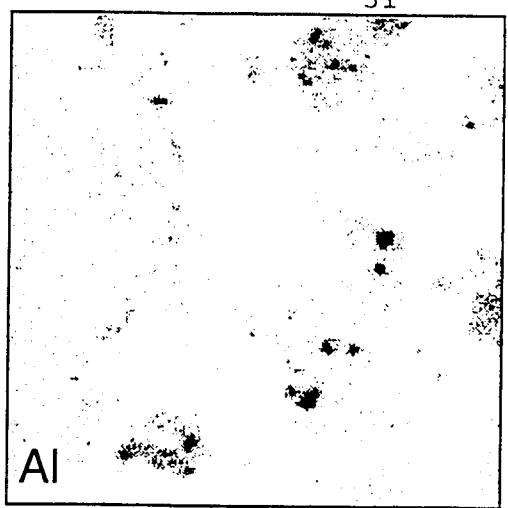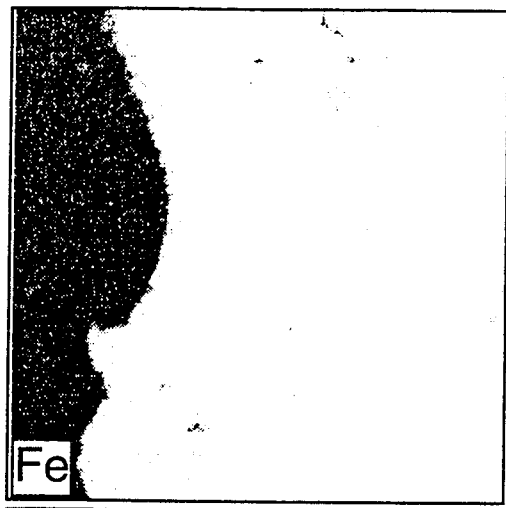| 2	Banagrass JC-PRP	Banagrass JC-PRP	Banagrass JC-PRP	Banagrass JC-PRP	Banagrass JC-PRP	Banagrass JC-PRP
Image label:	Fuel Ash (Bulk)	Deposit (2B: a) High Si particle	Deposit (2C: a) Spherical particle	Deposit (2D: a) Spherical particle	Deposit (2D: b) Rectangular particle	Flyash (2E: a) Coarse particle
(%)						
SiO_2	63.02	66.45	48.83	56.20	83.57	83.23
Al_2O_3	0.73	0.62	3.47	2.37	0.40	0.51
TiO_2	0.05	0.07	0.30	0.65	0.03	0.01
Fe_2O_3	0.95	1.87	2.77	3.05	1.21	0.24
CaO	11.20	11.15	30.99	28.63	0.13	0.88
MgO	2.44	1.48	4.71	1.15	0.10	1.92
Na_2O	0.56	0.44	0.44	0.62	0.20	0.43
K_2O	7.39	3.59	4.53	2.87	0.45	4.00
P_2O_5	2.37	0.58	1.78	0.96	0.03	0.13
SO_3	0.57	0.12	0.05	0.04	0.19	0.06
Cl	0.10	0.23	0.01	0.03	0.15	0.03
MnO		0.44	0.66	0.53	0.05	0.19
CO_2	4.47					
Total	93.85	87.04	98.54	97.10	86.50	91.62

Normalized

2	Banagrass JC-PRP	Banagrass JC-PRP	Banagrass JC-PRP	Banagrass JC-PRP	Banagrass JC-PRP	Banagrass JC-PRP
Image label:	Fuel Ash (Bulk)	Deposit (2B: a) High Si particle	Deposit (2C: a) Spherical particle	Deposit (2D: a) Spherical particle	Deposit (2D: b) Rectangular particle	Flyash (2E: a) Coarse particle
(%)						
SiO_2	67.15	76.34	49.55	57.88	96.62	90.84
Al_2O_3	0.78	0.71	3.52	2.44	0.46	0.55
TiO_2	0.05	0.08	0.31	0.67	0.04	0.01
Fe_2O_3	1.01	2.15	2.81	3.14	1.40	0.26
CaO	11.93	12.81	31.45	29.48	0.15	0.96
MgO	2.60	1.70	4.78	1.18	0.11	2.09
Na_2O	0.60	0.50	0.45	0.64	0.23	0.47
K_2O	7.87	4.13	4.60	2.95	0.52	4.36
P_2O_5	2.53	0.66	1.80	0.98	0.03	0.14
SO_3	0.61	0.14	0.05	0.04	0.22	0.06
Cl	0.11	0.26	0.01	0.03	0.17	0.03
MnO		0.50	0.67	0.54	0.06	0.21
CO_2	4.76					
Total	100.00	100.00	100.00	100.00	100.00	100.00

2B

2D

A

CPRP
0X

C

PRP
00X

a

2D

JCPRP
500X

32 µm

a

b

2E

JCPRP Flyash
50X

328 µm

c d

b

e

a

RP
X
31 μm

Fe

Al

K

Cl

Ca

Mg

P

Mn

Table 13. Microstructural compositions for bagasse.

3	Bagasse	Bagasse	Bagasse	Bagasse
Image label:	Fuel Ash (Bulk)	Deposit (3A: a) Semi-porous	Deposit (3B: a) Lower	Deposit (3C: a) Porous
(%)		particle	sphere	particle
SiO2	42.62	45.60	40.41	60.98
Al2O3	23.16	37.05	21.56	10.88
TiO2	2.76	0.00	2.38	1.14
Fe2O3	16.18	0.11	15.65	7.37
CaO	2.95	0.01	3.21	2.92
MgO	1.97	0.01	2.66	3.24
Na2O	0.57	0.04	0.53	0.76
K2O	2.97	0.00	2.66	2.96
P2O5	1.31	0.05	2.19	2.35
SO3	0.50	0.02	0.21	0.08
Cl	0.07	0.03	0.01	0.02
MnO		0.00	0.63	1.34
CO2	0.65			
Total	95.71	82.94	92.09	94.05

Normalized

3	Bagasse	Bagasse	Bagasse	Bagasse
Image label:	Fuel Ash (Bulk)	Deposit (3A: a) Semi-porous	Deposit (3B: a) Lower	Deposit (3C: a) Porous
(%)		particle	sphere	particle
SiO2	44.53	54.99	43.88	64.84
Al2O3	24.20	44.67	23.41	11.57
TiO2	2.88	0.00	2.58	1.22
Fe2O3	16.91	0.13	16.99	7.83
CaO	3.08	0.02	3.49	3.10
MgO	2.06	0.01	2.89	3.45
Na2O	0.60	0.05	0.58	0.81
K2O	3.10	0.00	2.88	3.15
P2O5	1.37	0.06	2.38	2.50
SO3	0.52	0.03	0.23	0.08
Cl	0.07	0.04	0.01	0.03
MnO		0.00	0.68	1.42
CO2	0.68			
Total	100.00	100.00	100.00	100.00

3B

A

gasse
X

gasse
X

31 μm

C

3D
Bagasse Flyash
50X

328 μm

4. FC-P

Image 4A is a backscattered electron image of the deposit from FC-P at the deepest part near the top of the probe. The particles again show signs of having dispersed during casting, but the individual particle morphology is similar to that observed with FC-PRP--many filamentous particles evidently of plant origin. Image 4B is an enlargement of the area near the surface indicated in 4A. Accompanying 4B are the element dot maps depicting the compositional distribution. Compositions of the two major particles seen in the image are listed in Table 14. Particle "a" contains large amounts of aluminum and iron, and is likely of soil origin. The crescent shaped particle "b" is mostly silica with a small amount of potassium, and from its shape and composition appears to be of plant origin. No clear condensation layer exists at the surface, but in the crook of the probe surface defect near the bottom of the image is a region of KCl, and faint traces of potassium along the rest of the surface. Vestiges of a KCl layer at the surface are evident in the dot maps accompanying image 4C, located near the region of 4B as indicated in image 4D.

Images 4E and 4F demonstrate the presence of KCl crystals in the deposit. Both crystals are 15 - 20 μm in size. 4E also shows a spherical particle, possibly a glass, composed of Si-Ca-K-P oxides, with little aluminum, titanium, or iron (Table 14). This particle is coated on the surface with smaller irregular particles of indistinct composition. Also visible in the image are smaller rectangular crystals of KCl. A large, porous particle located in the vicinity of the surface, and visible in images 4A and 4G ("a", enlarged), resembles in composition some of the particles observed in the bagasse deposit, with the same characteristic make-up of a weathered basalt. Moving down the side of the probe, as in image 4H, the deposit takes on a different character, with more rounded particles and fewer of the filaments observed at the peak.

Coarse flyash from FC-P is a mixture of plant ash filaments and smaller compact soil particles, as shown in image 4I. The obvious plant derived particle "a" in the image has a composition very similar to that of the crescent shaped particle in image 4B--mostly silica with smaller amounts of potassium. The particle "b" directly above is almost entirely silica, with little else detected.

Images 4J - 4L display the structure of particles in a furnace wall deposit dislodged from the upper MFC furnace wall near the end of the FC-P test. Such wall deposits are frequently observed to form when firing lighter fuels like straw and grass. Typically they form immediately below the injection point in the hottest zones of the furnace, building radially inward until the drag is sufficient to dislodge them. The sinter strength of the wall deposits depends on the composition of the fuel as well as the furnace conditions. With leached rice straw, lightly sintered deposits have been observed to form, which are relatively easily dislodged from the wall by the flow [4]. Untreated rice straw forms tenacious, glassy deposits of high strength, which fully bridge the furnace and require the unit to be shut down for cleaning. The wall deposits from FC-P were lightly sintered, but the bse images show the particles to be fused and vesiculated. One of the particles is enlarged in image 4K. This reveals a smooth glass phase surrounding a number of inclusions, one of which is further enlarged in image 4L. The compositions of the glass phase and the inclusion are listed in Table 14. The smooth phase is an alkaline earth-alkali-silicate glass, the inclusion is evidently of soil origin, captured in the glass matrix and possibly reacting with it. Other phases, possibly quartz, are visible in 4L, outlined by the lighter rings in the glass. The residence time of the wall deposit was likely something over an hour (FC-P was fired for 2 h). Whether the structure and composition observed can be attributed entirely to the FC-P fuel is unknown; the furnace wall was examined for deposits but not cleaned between fuels. The light texture and bulk of the deposit suggests that it was derived primarily from FC-P, however.

Table 14. Microstructural compositions for banagrass FC-P.

4 Image label: (%)	Banagrass FC-P Fuel Ash (Bulk)	Banagrass FC-P Deposit (4B: a) Elongated particle	Banagrass FC-P Deposit (4B: b) Crescent particle	Banagrass FC-P Deposit (4E: a) Spherical particle	Banagrass FC-P Wall Deposit (4K: a) Smooth glass phase	Banagrass FC-P Wall Deposit (4L:a) Porous inclusion
SiO2	40.53	30.73	83.18	21.85	69.79	44.99
Al2O3	1.03	23.74	0.04	0.49	0.92	13.93
TiO2	0.21	2.11	0.00	0.05	0.13	1.55
Fe2O3	1.05	16.39	0.22	0.78	1.76	14.51
CaO	7.45	1.12	0.12	14.49	6.28	2.89
MgO	4.53	0.92	0.30	5.40	7.89	1.49
Na2O	1.11	1.86	0.12	1.08	0.47	0.35
K2O	25.75	10.57	1.23	13.53	5.18	17.63
P2O5	5.19	0.83	0.00	31.54	1.52	1.03
SO3	1.60	0.02	0.02	0.11	0.00	0.13
Cl	3.90	0.01	0.33	0.24	0.00	0.00
MnO		0.38	0.08	0.62	0.80	0.38
CO2	1.21					
Total	93.56	88.68	85.64	90.17	94.74	98.88

Normalized

4 Image label: (%)	Banagrass FC-P Fuel Ash (Bulk)	Banagrass FC-P Deposit (4B: a) Elongated particle	Banagrass FC-P Deposit (4B: b) Crescent particle	Banagrass FC-P Deposit (4E: a) Spherical particle	Banagrass FC-P Wall Deposit (4K: a) Smooth glass phase	Banagrass FC-P Wall Deposit (4L:a) Porous inclusion
SiO2	43.32	34.65	97.12	24.23	73.66	45.50
Al2O3	1.10	26.78	0.05	0.55	0.97	14.08
TiO2	0.22	2.38	0.00	0.05	0.13	1.56
Fe2O3	1.12	18.48	0.25	0.86	1.86	14.68
CaO	7.96	1.26	0.14	16.07	6.62	2.93
MgO	4.84	1.04	0.35	5.99	8.33	1.50
Na2O	1.19	2.10	0.15	1.20	0.49	0.36
K2O	27.52	11.92	1.43	15.00	5.46	17.83
P2O5	5.55	0.94	0.00	34.98	1.61	1.04
SO3	1.71	0.02	0.03	0.12	0.00	0.13
Cl	4.17	0.01	0.38	0.27	0.00	0.00
MnO		0.43	0.09	0.68	0.85	0.38
CO2	1.29					
Total	100.00	100.00	100.00	100.00	100.00	100.00

4G

4B

4A
FC-P
50X

4B

4C

4D FC-P
50X

CI

a

4E
FC-P
1000X

KCl

4F
FC-P
1000X

31 μm

Fe

Al

K

Cl

Ca

Mg

P

Ti

31 μm

Fe

K

Cl

Mg

4G
FC-P
250X

4H
FC-P
50X

4I
FC-P Flyash
50X

328 μm

4J
FC-P Furnace Wall Deposit
50X

4K
FC-P Furnace Wall Deposit
50X

4L
FC-P Furnace Wall Deposit
500X

5. FC-Untreated

Microstructure of the FC-Untreated deposit is shown in images 5A through 5G. Compositions of selected particles are listed in Table 15a. Image 5A is at the deepest part of the deposit under the peak of the crown, which extends 2-3 mm above the surface. The particles again show signs of having dispersed during casting. The morphology of the particles is more compact than the filamentous structures observed with the leached banagrass, but the compositions are consistent with plant origin. Image 5B, whose location is shown in 5A, is an enlargement of an area about 300 μm above the probe surface. Accompanying the image are element dot maps giving compositional distribution. The spherical particle "a" yields a high aluminum concentration, and is probably of soil origin. The other, larger particles in the image are more likely of plant origin, however, as indicated by the dot maps. Both the deposit and the flyash from the untreated banagrass are characterized by substantial numbers of KCl crystals. These are clearly evident in the bse and K and Cl dot maps of image 5B. The composition of one of these crystals is listed in Table 15a ("rectangular crystal"), which yields 97% of the detected mass as K+Cl, with a K/K+Cl mass ratio of 0.55, only slightly different from the stoichiometric mass ratio for potassium in KCl of 0.52. Their inclusion in the deposit suggests these crystals form in the furnace prior to deposition. Their abundance is substantially greater than observed with FC-P.

Image 5C (located by the square outline in image 5A) shows another particle about 30 μm in size and with a porous structure. The composition is of a potassium-silicate, again likely of plant origin. A few smaller KCl crystals are also visible. Image 5D, located to the right along the probe surface from, and overlapping image 5A, shows a spherical phosphatic particle with composition listed in Table 15a. Image 5E, taken at the probe surface, shows vestigial traces of a KCl layer lying along the surface, as well as several Ca-K-silicate particles. Image 5F, from further down the side of the probe, also reveals traces of a KCl layer at the surface of the probe, and shows quite distinctly a 25 μm KCl crystal situated above the surface, along with other, smaller crystals. A spherical particle with multiple smaller particles attached to its surface is shown in image 5G. Compositions at the center, "a", and at the edge, "b", are listed in Table 15a. The element recoveries are not especially good, but the main sphere yields an abundance of potassium and magnesium in combination with silica, while the attached particles at the edge contain large amounts of potassium, phosphorous, and magnesium. The phosporous and magnesium concentrations are greatly enriched relative to the bulk fuel ash and deposit compositions.

Images of the coarse fraction of flyash are included in 5H through 5K. 5H shows a silica filament of plant origin, with many salt crystals attached. Both of the bright particles labeled "a" and "b" in the image are salt crystals. The presence of silica in the analyses shown in Table 15b is due to the inability to separate the background of the silica filament from the composition of the crystals. Both particles yield a fair amount of sodium, whereas sodium makes up a minor fraction of the fuel ash and bulk deposit composition. The filament itself is nearly pure silica. Of some interest is the presence of clusters of salt crystals in the flyash samples. One cluster may be seen in image 5I, at center. An enlargement is shown in image 5J, and in 5K for a second cluster found in the same sample. Both images show regular crystals of predominantly KCl, similar to those observed in the deposit. These clusters are generally associated with a larger silicate particle serving as an attachment base, which may be seen in all four flyash images.

Image 5L depicts material from a furnace wall deposit captured during the test with untreated banagrass. Most of the particles visible in the image are potassium silicates, the fused and vesiculated appearance indicating a molten state in the furnace. The origin of this material is not entirely clear. Contributions from both untreated banagrass as well as the FC-P treatment are possible. The formation of such deposits with the FC-P and untreated banagrass, when they are absent from the FC-PRP, JC-PRP, and bagasse tests, is another qualitative indicator of the higher slagging and fouling potential of the untreated and poorly leached materials.

Table 15a. Microstructural compositions for untreated banagrass (deposits).

5	Banagrass FC-Un	Banagrass FC-Un	Banagrass FC-Un	Banagrass FC-Un	Banagrass FC-Un	Banagrass FC-Un	Banagrass FC-Un	Banagrass FC-Un
Image label: (%)	Fuel Ash (Bulk)	Deposit (5B: a) Spherical Particle	Deposit Rectangular Crystal	Deposit Hollow particle at deposit edge	Deposit (5C: a) Porous particle	Deposit (5D:a) Large round particle	Deposit (5G: a) Center of sphere	Deposit (5G: b) Edge of sphere
SiO2	33.99	28.61	0.12	15.66	52.98	18.39	9.66	1.90
Al2O3	0.74	8.04	0.06	0.52	0.01	0.58	0.36	0.12
TiO2	0.05	0.88	0.00	0.06	0.04	0.04	0.04	0.00
Fe2O3	0.78	8.63	0.18	0.81	0.12	0.79	0.52	0.11
CaO	6.00	11.29	0.00	7.33	0.12	5.85	4.37	1.23
MgO	5.36	11.28	0.75	11.82	0.36	12.55	8.09	17.45
Na2O	1.00	0.90	0.04	1.09	0.58	0.66	3.27	0.62
K2O	31.80	12.69	53.41	15.29	12.98	10.41	30.96	25.55
P2O5	4.00	12.73	1.33	29.02	0.24	31.96	1.07	26.28
SO3	2.55	0.11	0.26	0.02	0.02	0.04	1.11	0.19
Cl	8.54	0.11	42.95	0.47	3.67	0.51	4.27	1.78
MnO		1.15	0.14	0.93	0.01	0.36	0.36	0.13
CO2	1.05							
Total	95.86	96.42	99.24	83.02	71.14	82.14	64.09	75.36

Normalized

5	Banagrass FC-Un	Banagrass FC-Un	Banagrass FC-Un	Banagrass FC-Un	Banagrass FC-Un	Banagrass FC-Un	Banagrass FC-Un	Banagrass FC-Un
Image label: (%)	Fuel Ash (Bulk)	Deposit (5B: a) Spherical Particle	Deposit Rectangular Crystal	Deposit Hollow particle at deposit edge	Deposit (5C: a) Porous particle	Deposit (5D:a) Large round particle	Deposit (5G: a) Center of sphere	Deposit (5G: b) Edge of sphere
SiO2	35.46	29.67	0.12	18.86	74.48	22.39	15.07	2.52
Al2O3	0.77	8.34	0.06	0.62	0.02	0.70	0.56	0.15
TiO2	0.05	0.92	0.00	0.07	0.05	0.05	0.06	0.00
Fe2O3	0.81	8.95	0.18	0.98	0.17	0.96	0.81	0.14
CaO	6.26	11.71	0.00	8.83	0.17	7.12	6.82	1.63
MgO	5.59	11.70	0.76	14.24	0.51	15.28	12.63	23.16
Na2O	1.04	0.93	0.04	1.32	0.82	0.80	5.10	0.82
K2O	33.17	13.17	53.81	18.41	18.25	12.67	48.31	33.90
P2O5	4.17	13.20	1.34	34.95	0.33	38.91	1.68	34.88
SO3	2.66	0.11	0.26	0.03	0.03	0.05	1.73	0.25
Cl	8.91	0.11	43.28	0.57	5.16	0.62	6.67	2.37
MnO		1.19	0.14	1.12	0.01	0.44	0.57	0.18
CO2	1.10							
Total	100.00	100.00	100.00	100.00	100.00	100.00	100.00	100.00

Table 15b. Microstructural compositions for untreated banagrass (flyash).

5	Banagrass FC-Un	Banagrass FC-Un	Banagrass FC-Un	Banagrass FC-Un
Image label:	Flyash (5H: a)	Flyash (5H: b)	Flyash (5H: c)	Flyash (5H)
(%)	Bright particle	Bright particle	Backbone particle	Bright particle
SiO2	29.63	2.61	87.72	0.66
Al2O3	0.02	0.00	0.02	0.00
TiO2	0.01	0.00	0.00	0.00
Fe2O3	0.00	0.01	0.03	0.00
CaO	0.09	0.08	0.04	0.00
MgO	0.08	0.08	0.03	0.00
Na2O	8.52	18.29	2.30	3.46
K2O	19.49	29.20	1.19	54.97
P2O5	0.22	0.26	0.21	0.00
SO3	0.76	0.56	0.06	0.36
Cl	18.35	29.65	0.13	41.16
MnO	0.00	0.06	0.03	0.00
CO2				
Total	77.17	80.79	91.75	100.62

Normalized

5	Banagrass FC-Un	Banagrass FC-Un	Banagrass FC-Un	Banagrass FC-Un
Image label:	Flyash (5H: a)	Flyash (5H: b)	Flyash (5H: c)	Flyash (5H)
(%)	Bright particle	Bright particle	Backbone particle	Bright particle
SiO2	38.40	3.23	95.60	0.65
Al2O3	0.02	0.00	0.02	0.00
TiO2	0.01	0.00	0.00	0.00
Fe2O3	0.00	0.02	0.03	0.00
CaO	0.12	0.10	0.04	0.00
MgO	0.10	0.09	0.03	0.00
Na2O	11.04	22.64	2.50	3.43
K2O	25.26	36.14	1.29	54.63
P2O5	0.28	0.32	0.23	0.00
SO3	0.98	0.69	0.06	0.36
Cl	23.78	36.70	0.14	40.91
MnO	0.00	0.07	0.04	0.00
CO2				
Total	100.00	100.00	100.00	100.00

50

5C

5B

5A
FC-Un
X

5B
FC-Un
0X

5H
FC-Un Flyash
400X

5E
FC-Un

310 µm

FC-Un
X

5I
FC-Un Flyash
100X

5 B
FC-Un
500X
31 µm

Fe

Al

K

Cl

Ca

Mg

P

Mn

Jn
K

31 µm

Fe

Al

K

Cl

Ca

Mg

P

Mn

n

31 µm

Fe

Al

K

Cl

Ca

Mg

P

Mn

5J
FC-Un Flyash
500X

5K
FC-Un Flyash
500X

5L
FC-Un Furnace Wall Deposit
50X
|——————| 328 µm

Summary and Conclusions

Leaching of banagrass was effective in increasing the fusion temperatures of ash, reducing the high temperature volatile ash fraction, and reducing both the specific deposition fraction and the tenacity of probe deposits in pilot scale combustion tests. The results suggest that fouling and slagging from well leached banagrass should be reduced compared to untreated material when burned in full-scale commercial units.

The effectiveness of the leaching treatments is quite variable, however. All of the forage chopped (FC) treatments appear to be of inferior quality to the Jeffco cut (JC) banagrass in ash fusibility and volatile ash fraction. The FC-PRP treatment, although improved relative to the FC-P and untreated material, has a melting point approximately 150°C below that of the JC-PRP material undergoing the same leaching treatment. The smaller particle size and the different texture of the Jeffco cut material appears to lead to greater extraction of fluxing elements compared to forage chopping, at least for the amount of applied water and leaching time allowed. Secondary leaching of primary treatments yields roughly double the amount of soluble, extractable material from FC-PRP compared to JC-PRP, a result consistent with compositional analyses of the fuels. Similarly, the single press treatment (FC-P) removed insufficient amounts of fouling elements to markedly improve the combustion properties relative to untreated banagrass. The melting point of FC-P was increased only about 50°C above the 1000°C melting point of the untreated material. By comparison, the melting points for FC-PRP, JC-PRP, and bagasse ash were 1150, 1300, and 1450°C respectively. The bagasse used as control had a substantially different ash composition compared with banagrass. Bagasse has an ash which is substantially altered from the inherent sugar cane ash by inclusion of large amounts of adventitious material (soil). The ash composition exhibits similarity to a weathered basalt, which is to be expected of cane harvested in Hawaii. The ash has high aluminum and iron concentrations, not observed with banagrass, that lead to a higher melting temperature. Fusion temperatures obtained via laboratory furnace experiments were in fair correspondence with predictions from the ternary $CaO-K_2O-SiO_2$ phase system for banagrass, and from the $Al_2O_3-FeO-SiO_2$ phase system for bagasse. Predictions of the liquidus temperature for the FC-P composition show little if any improvement in slagging point relative to untreated banagrass, which is consistent with experimental observations. All three compositions, FC-Untreated, FC-P, and FC-PRP, lie in a region of relatively stable melting point. Only the JC-PRP treatment removes sufficient alkali to shift the composition into a range of rapidly increasing melting point. The marginal improvement in melting temperature resulting from reduction in alkali concentration is substantially better for the JC-PRP composition compared to the FC treatments because of the steepness of the liquidus in the vicinity of the JC-PRP composition. The fraction of liquid in ash formed below the liquidus temperature is also smaller for the JC-PRP treatment compared to the FC treatments.

Volatility of ash at elevated temperatures was reduced by leaching, with the JC-PRP treatment exhibiting a more refractory nature than the FC treatments. Between 575 and 900°C, the volatile ash loss from bagasse, JC-PRP, FC-PRP, FC-P and untreated material was 7, 8, 12, 16 and 20% respectively. Although the volatile loss of ash has not been correlated against fouling severity, an increasing volatile fraction is thought to represent a greater fouling potential based on the perceived mechanisms of fouling.

Relative deposition, defined as the mass fraction of fuel depositing on a unit area of heat exchanger surface, was measured on simulated superheater tubes during pilot combustion tests in an entrained flow combustor. The relative deposition was approximately two times higher for untreated banagrass compared to bagasse fired under the same conditions. The relative deposition for the leached banagrass treatments (FC-P, FC-PRP, and JC-PRP) were roughly comparable to that of bagasse. When defined relative to the mass fraction of fuel ash depositing per unit area, however, the relative deposition for untreated banagrass was 3 to 5 times that of bagasse. FC-P was 2 to 4

times higher, and both FC-PRP and JC-PRP were 2 to 3 times higher than bagasse. The deposits formed when burning FC-P and untreated banagrass were more tenacious and more heavily sintered than the deposits from FC-PRP and JC-PRP.

The banagrass deposits started as white layers of KCl, followed by development of crown deposits containing particles of both plant and soil origin acquired through inertial impaction. The bagasse deposits started as fine textured brown layers, with very slow growth over the duration of the test. Inspection of the deposits via electron beam microprobe identified little material of plant origin from bagasse; the majority of particles collected in the bagasse deposit appeared to be of soil origin. The banagrass deposits contained a substantially higher fraction of plant derived particles, as indicated by high silica concentrations and the absence of aluminum. Both the FC-P and untreated banagrass produced deposits containing numerous KCl crystals. Salt crystals were also observed in coarse flyash from FC-P and untreated materials. Crystals were present in abundance with untreated banagrass. Clusters of crystals attached to silica particles were observed in the flyash. The close association of the alkali flux with silica suggests a high slagging character for this fuel. The filter catch from the gas sampling system when burning FC-P and untreated banagrass was almost entirely KCl. Few or no salt crystals were observed in the deposit or flyash samples from bagasse, JC-PRP, or FC-PRP. The FC-P and untreated banagrass also produced furnace wall deposits, not observed with the other treatments. These wall deposits were composed of sintered glassy particles, and grew radially inward from the wall until dislodged by the drag of the furnace flow.

In order of decreasing fuel quality, the treatments rank as Bagasse > JC-PRP >> FC-PRP > FC-P > FC-Untreated. The untreated banagrass is likely to prove a high slagging, high fouling fuel in conventional furnaces and power boilers. Little improvement is anticipated for the FC-P treatment. The larger particle size of the FC-PRP treatment appears to reduce the effectiveness of the leaching treatment employed when compared against JC-PRP. Different treatment methods should be considered if forage chopped material is favored. The JC-PRP material is markedly improved relative to the untreated banagrass, but still slightly inferior to bagasse in terms of predicted fouling potential. The ash composition of the JC-PRP material is substantially different from that of bagasse. The banagrass ash is principally of inherent plant origin, that of Hawaiian bagasse contains a large fraction of soil. However, furnace or boiler performance on JC-PRP may be acceptable with moderate fouling anticipated. Full-scale experiments are needed to test this conclusion.

References

1. Jenkins, B.M., R.R. Bakker and J.B. Wei. 1996. On the properties of washed straw. Biomass and Bioenergy 10(4):177-200.

2. Jenkins, B.M., R.R. Bakker and J.B. Wei. 1995. Removal of inorganic elements to improve biomass combustion properties. Proceedings 2nd Biomass Conference of the Americas, NREL/CP-200-8098, DE95009230, National Renewable Energy Laboratory, Golden, CO.

3. Jenkins, B.M., L.L. Baxter, T.R. Miles, Jr. and T.R. Miles. 1996. Combustion properties of biomass. Proceedings Biomass usage for utility and industrial power, Engineering Foundation, New York, NY.

4. Jenkins, B.M., R.R. Bakker, L.L. Baxter, J.H. Gilmer and J.B. Wei. 1996. Combustion characteristics of leached biomass. In: Bridgwater, A.V. and D.G.B. Boocock (eds.), Developments in Thermochemical Biomass Conversion, Blackie Academic and Professional, London, pp. 1316-1330.

5. Bakker, R.R. and B.M. Jenkins. 1996. Feasibility of fuel leaching to reduce ash fouling in biomass combustion systems. Proceedings Ninth European Bioenergy Conference, Copenhagen, Denmark.

6. Turn, S.Q., C. Kinoshita and D. Ishimura. 1996. Removal of inorganic constituents of biomass feedstocks by mechanical dewatering and leaching. Biomass and Bioenergy (in press).

7. Miles, T.R., T.R. Miles, Jr., L.L. Baxter, R.W. Bryers, B.M. Jenkins and L.L. Oden. 1995. Alkali deposits found in biomass power plants: a preliminary investigation of their extent and nature. Summary report for the National Renewable Energy Laboratory, NREL Subcontract TZ-2-11226-1, Golden, CO.

8. Levin, E.M., H.F. McMurdie and F.P. Hall. 1956. Phase diagrams for ceramists. The American Ceramic Society, Columbus, OH.

9. Jenkins, B.M. 1995. Atmospheric pollutant emission factors from open burning of sugar cane by wind tunnel simulations. Final Report to the Hawaiian Sugar Planter's Association, Aiea, Hawaii.

10. MacDonald, G.A. and D.H. Hubbard. 1975. Volcanoes of the national parks in Hawaii. Tongg Publishing, Honolulu, HI.

11. Macdonald, G.A. and A.T. Abbott. 1970. Volcanoes in the Sea. University of Hawaii Press, Honolulu.

12. ASTM E953. 1988. Standard test method for fusibility of refuse-derived fuel (RDF) ash. American Society for Testing and Materials, Philadelphia, PA (see also ASTM D1857).

13. ASTM D1102. 1990. Standard test method for ash in wood. American Society for Testing and Materials, Philadelphia, PA.

14. Baxter, L.L. 1993. Ash deposition during biomass and coal combustion: a mechanistic approach. Biomass and Bioenergy 4(2):85-102.

Appendix

Table A1.a. Mass and element balance   1: Banagrass FC-PRP

Measured Fuel Rate
(Unadjusted Air Rate)

	Mass Flowrate (g/s)	Mass Fractions (%)	Carbon Flowrate (g/s)	Hydrogen Flowrate (g/s)	Nitrogen Flowrate (g/s)	Sulfur Flowrate (g/s)	Oxygen Flowrate (g/s)
inputs							
Natural gas	0.000	0.0	0.000	0.000			
Dry air	8.575	90.3	0.001		6.578		1.995
Humidity in air	0.085	0.9		0.010			0.076
Moist biomass (as-fired)	0.840	8.8	0.365	0.052	0.003	0.0004	0.398
Moisture in biomass	0.092	1.0		0.010			0.082
Dry biomass	0.748	7.9	0.365	0.042	0.003	0.0004	0.316
Organic biomass	0.727	7.7		0.042	0.003	0.0004	0.316
Ash	0.020	0.2					
Total inputs	9.500	100.0	0.366	0.062	6.581	0.0004	2.469
Fraction of Total (%)	(100.00)		(3.86)	(0.65)	(69.28)	(0.004)	(25.99)
outputs							
Dry exit gas	8.928	94.0	0.534	1.29E-05	6.551		1.844
Water vapor from air humidity	0.085	0.9		0.010			0.076
Water vapor from biomass moisture	0.092	1.0		0.010			0.082
Water vapor from fuel hydrogen	0.374	3.9		0.042			0.332
Total water vapor	0.551	5.8		0.062			0.490
Unreacted carbon	0.000	0.0	0.000				
Vaporized inorganics	0.000	0.0					
Condensed phase inorganics	0.020	0.2					
Total inorganics	0.020	0.2					
Total inorganics+unreacted carbon	0.020	0.2	0.000				
O2	0.420	4.4					0.420
CO2	1.950	20.5	0.532				1.418
CO	0.004	0.0	0.002				0.002
HC (as CH4)	5.14E-05	0.0	3.85E-05	1.29E-05			
NOx (as NO2)	0.006	0.1			0.002		0.004
SO2	1.87E-05	0.0				9.34E-06	9.33E-06
N2 (by difference)	6.549	68.9			6.549		
Total outputs	9.500	100.0	0.534	0.062	6.551	9.34E-06	2.333
Fraction of Total (%)	(100.00)		(5.62)	(0.65)	(68.96)	(0.000)	(24.56)
(Outputs - Inputs)	0.00E+00		1.67E-01	0.00E+00	-3.05E-02	-3.64E-04	-1.36E-01
(Outputs/Inputs)	1.00000		1.45655	1.00000	0.99536	0.02500	0.94508

Table A1.b. Element Conversions, Emission Factors, and Stoichiometry from Measured Fuel Rate (Unadjusted Air Rate) = 436.2 L/min

1: Banagrass FC-PRP

	Natural Gas Background (mol %)	Natural Gas (Stoich) (g/s)	Combustion Air (g/s)	Net Biomass (g/s)	Emission Factor (Biomass) (% dry fuel)	Biomass Element Conversion (%)	Net Natural Gas	Net Biomass	Total
CO2	0	0.005		1.945	260.182	145.389			
CO				0.004	0.470	0.412			
HC (as CH4)				0.000	0.007	0.011			
NOx (as NO2)				0.006	0.857	63.663			
SO2				1.87E-05	0.002	2.500			

O2 for Natural gas combustion (g/s)		0
Air for Natural gas combustion (g/s)		0
Air for Biomass combustion (g/s d.b.)		8.575
Air-Fuel Ratio (kg/kg, dry basis)		11.5
Stoich. Air for Biomass (g/s d.b.)		4.3
Stoich. Air-Fuel (kg/kg, dry basis)		5.7
Equivalence ratio for Biomass (d.b.)		0.496
Excess air for Biomass (% d.b.)		101
Volumetric exit gas density (kg/m^3 d.b.)		0.3958
Total volumetric exit gas flowrate (m^3/s w.b.)		0.0249
Exit gas velocity (m/s)		1.37
Reynolds Number		1,318
Approximate residence time (s)		2.93

Anticipated Gas Compositions from Measured Fuel Rate
(including major species only, dry basis)

1: Banagrass FC-PRP

	Inlet Air			Exit Gas			Measured
	Mass Flow (g/s)	Mass Fraction (%)	Mol Fraction (%)	Mass Flow (g/s)	Mass Fraction (%)	Mol Fraction (%)	Mol Fraction (%)
O2	1.992	23.229	20.946	1.003	11.238	10.563	4.50
CO2	0.005	0.053	0.035	1.342	15.038	10.278	15.20
N2	6.578	76.718	79.019	6.581	73.724	79.159	80.21
Total	8.575	100.000	100.000	8.927	100.000	100.000	99.908
Mol. Wt.		28.854			30.078		

Table A1.c. Mass and element balance   1: *Banagrass FC-PRP*

Carbon Balance

	Mass Flowrate (g/s)	Mass Fractions (%)	Carbon Flowrate (g/s)	Hydrogen Flowrate (g/s)	Nitrogen Flowrate (g/s)	Sulfur Flowrate (g/s)	Oxygen Flowrate (g/s)
inputs							
Natural gas	0.000	0.0	0.000	0.000			
Dry air	8.575	86.5	0.001		6.578		1.995
Humidity in air	0.085	0.9		0.010			0.076
Moist biomass (as-fired)	1.248	12.6	0.543	0.078	0.005	0.0006	0.592
Moisture in biomass	0.137	1.4		0.015			0.122
Dry biomass	1.111	11.2	0.543	0.062	0.005	0.0006	0.470
Organic biomass	1.081	10.9		0.062	0.005	0.0006	0.470
Ash	0.030	0.3					
Total inputs	9.908	100.0	0.544	0.087	6.583	0.0006	2.663
Fraction of Total (%)	(100.00)		(5.49)	(0.88)	(66.44)	(0.006)	(26.88)
outputs							
Dry exit gas	9.100	91.8	0.544	1.32E-05	6.677		1.879
Water vapor from air humidity	0.085	0.9		0.010			0.076
Water vapor from biomass moisture	0.137	1.4		0.015			0.122
Water vapor from fuel hydrogen	0.556	5.6		0.062			0.494
Total water vapor	0.778	7.9		0.087			0.691
Unreacted carbon	0.000	0.0	0.000				
Vaporized inorganics	0.000	0.0					
Condensed phase inorganics	0.030	0.3					
Total inorganics	0.030	0.3					
Total inorganics+unreacted carbon	0.030	0.3	0.000				
O2	0.428	4.3					0.428
CO2	1.987	20.1	0.542				1.445
CO	0.004	0.0	0.002				0.002
HC (as CH4)	5.24E-05	0.0	3.92E-05	1.32E-05			
NOx (as NO2)	0.007	0.1			0.002		0.005
SO2	0.000	0.0				9.52E-06	9.51E-06
N2 (by difference)	6.675	67.4			6.675		
Total outputs	9.908	100.0	0.544	0.087	6.677	9.52E-06	2.570
Fraction of Total (%)	(100.00)		(5.49)	(0.88)	(67.39)	(0.000)	(25.94)
(Outputs - Inputs)	-1.78E-15		0.00E+00	-1.39E-17	9.41E-02	-5.46E-04	-9.24E-02
(Outputs/Inputs)	1.00000		1.00000	1.00000	1.01429	0.01714	0.96530

Table A1.d. Element Conversions, Emission Factors, and Stoichiometry from Carbon Balance   *1: Banagrass FC-PRP*

	Natural Gas Background (mol %)	Natural Gas (Stoich) (g/s)	Air (g/s)	Net Biomass (g/s)	Emission Factor (Biomass) (% dry fuel)	Biomass Element Conversion (%)	Net Natural Gas	Net Biomass	Total
CO2		0	0.005	1.983	178.437	99.710			
CO				0.004	0.322	0.283			
HC (as CH4)				0.000	0.005	0.007			
NOx (as NO2)				0.007	0.588	43.659			
SO2				1.90E-05	0.002	1.714			
O2 for Natural gas combustion (g/s)							0		
Air for Natural gas combustion (g/s)							0		
Air for Biomass combustion (g/s d.b.)								8.575	
Biomass Air-Fuel Ratio (kg/kg, d.b.)								7.7	
Stoich. Air for Biomass (g/s d.b.)								6.3	
Stoich. Air-Fuel (kg/kg, dry basis)								5.7	
Equivalence ratio for Biomass (d.b.)								0.738	
Excess air for Biomass (% d.b.)								36	
Volumetric exit gas density (kg/m^3 d.b.)									0.3958
Total volumetric exit gas flowrate (m^3/s w.b.)									0.0263
Exit gas velocity (m/s)									1.44
Reynolds Number									1,392
Approximate residence time (s)									2.77

Anticipated Gas Compositions from Carbon Balance   *1: Banagrass FC-PRP*
(including major species only, dry basis)

	Inlet Air				Exit Gas			Measured
	Mass Flow (g/s)	Mass Fraction (%)	Mol Fraction (%)		Mass Flow (g/s)	Mass Fraction (%)	Mol Fraction (%)	Mol Fraction (%)
O2	1.992	23.229	20.946		0.522	5.742	5.505	4.50
CO2	0.005	0.053	0.035		1.993	21.905	15.268	15.20
N2	6.578	76.718	79.019		6.583	72.352	79.227	80.21
Total	8.575	100.000	100.000		9.098	100.000	100.000	99.908
Mol. Wt.		28.854				30.675		

Table A1.e. Mass and element balance   1: Banagrass FC-PRP

Measured Fuel Rate
(Adjusted Air Rate)

	Mass Flowrate (g/s)	Mass Fractions (%)	Carbon Flowrate (g/s)	Hydrogen Flowrate (g/s)	Nitrogen Flowrate (g/s)	Sulfur Flowrate (g/s)	Oxygen Flowrate (g/s)
inputs							
Natural gas	0.000	0.0	0.000	0.000			
Dry air	5.769	86.5	0.001		4.426		1.342
Humidity in air	0.057	0.9		0.006			0.051
Moist biomass (as-fired)	0.840	12.6	0.365	0.052	0.003	0.0004	0.398
Moisture in biomass	0.092	1.4		0.010			0.082
Dry biomass	0.748	11.2	0.365	0.042	0.003	0.0004	0.316
Organic biomass	0.727	10.9		0.042	0.003	0.0004	0.316
Ash	0.020	0.3					
Total inputs	6.667	100.0	0.366	0.059	4.429	0.0004	1.792
Fraction of Total (%)	(100.00)		(5.49)	(0.88)	(66.44)	(0.006)	(26.88)
outputs							
Dry exit gas	6.123	91.8	0.366	8.86E-06	4.492		1.264
Water vapor from air humidity	0.057	0.9		0.006			0.051
Water vapor from biomass moisture	0.092	1.4		0.010			0.082
Water vapor from fuel hydrogen	0.374	5.6		0.042			0.332
Total water vapor	0.524	7.9		0.059			0.465
Unreacted carbon	0.000	0.0	0.000				
Vaporized inorganics	0.000	0.0					
Condensed phase inorganics	0.020	0.3					
Total inorganics	0.020	0.3					
Total condensed phase	0.020	0.3	0.000				
O2	0.288	4.3					0.288
CO2	1.337	20.1	0.365				0.972
CO	0.002	0.0	0.001				0.001
HC (as CH4)	3.53E-05	0.0	2.64E-05	8.86E-06			
NOx (as NO2)	0.004	0.1			0.001		0.003
SO2	1.28E-05	0.0				6.41E-06	6.40E-06
N2 (by difference)	4.491	67.4			4.491		
Total outputs	6.667	100.0	0.366	0.059	4.492	6.41E-06	1.729
Fraction of Total (%)	(100.00)		(5.49)	(0.88)	(67.39)	(0.000)	(25.94)
(Outputs - Inputs)	-8.88E-16		6.11E-16	0.00E+00	6.33E-02	-3.67E-04	-6.22E-02
(Outputs/Inputs)	1.00000		1.00000	1.00000	1.01429	0.01714	0.96530

Table A1.f. Element Conversions, Emission Factors, and Stoichiometry from Measured Fuel Rate   1: Banagrass FC-PRP

(Adjusted Air Rate)   =   293.5 L/min

	Natural Gas Background (mol %)	Natural Gas (Stoich) (g/s)	Combustion Air (g/s)	Net Biomass (g/s)	Emission Factor (Biomass) (% dry fuel)	Biomass Element Conversion (%)	Net Natural Gas	Net Biomass	Total
CO2		0	0.003	1.334	178.437	99.710			
CO				0.002	0.322	0.283			
HC (as CH4)				0.000	0.005	0.007			
NOx (as NO2)				0.004	0.588	43.659			
SO2				1.28E-05	0.002	1.714			

O2 for Natural gas combustion (g/s)	0	
Air for Natural gas combustion (g/s)	0	
Air for Biomass combustion (g/s d.b.)	5.769	
Air-Fuel Ratio (kg/kg, dry basis)	7.7	
Stoich. Air for Biomass (g/s d.b.)	4.3	
Stoich. Air-Fuel (kg/kg, dry basis)	5.7	
Equivalence ratio for Biomass (d.b.)	0.738	
Excess air for Biomass (% d.b.)	36	
Volumetric exit gas density (kg/m^3 d.b.)		0.3958
Total volumetric exit gas flowrate (m^3/s w.b.)		0.0177
Exit gas velocity (m/s)		0.97
Reynolds Number		937
Approximate residence time (s)		4.12

Anticipated Gas Compositions from Measured Fuel Rate   1: Banagrass FC-PRP

(including major species only, dry basis)

	Inlet Air			Exit Gas			Measured
	Mass Flow (g/s)	Mass Fraction (%)	Mol Fraction (%)	Mass Flow (g/s)	Mass Fraction (%)	Mol Fraction (%)	Mol Fraction (%)
O2	1.340	23.229	20.946	0.352	5.742	5.505	4.50
CO2	0.003	0.053	0.035	1.341	21.905	15.268	15.20
N2	4.426	76.718	79.019	4.429	72.352	79.227	80.21
Total	5.769	100.000	100.000	6.122	100.000	100.000	99.908
Mol. Wt.		28.854			30.675		

Table A2a.a. Mass and element balance   2a: Banagrass JC-PRP

Measured Fuel Rate
(Unadjusted Air Rate)

	Mass Flowrate (g/s)	Mass Fractions (%)	Carbon Flowrate (g/s)	Hydrogen Flowrate (g/s)	Nitrogen Flowrate (g/s)	Sulfur Flowrate (g/s)	Oxygen Flowrate (g/s)
inputs							
Natural gas	0.000	0.0	0.000	0.000			
Dry air	8.575	90.5	0.001		6.578		1.995
Humidity in air	0.085	0.9		0.010			0.076
Moist biomass (as-fired)	0.810	8.6	0.352	0.050	0.002	0.0004	0.384
Moisture in biomass	0.089	0.9		0.010			0.079
Dry biomass	0.721	7.6	0.352	0.040	0.002	0.0004	0.305
Organic biomass	0.702	7.4		0.040	0.002	0.0004	0.305
Ash	0.019	0.2					
Total inputs	9.470	100.0	0.353	0.060	6.580	0.0004	2.455
Fraction of Total (%)	(100.00)		(3.73)	(0.63)	(69.49)	(0.004)	(25.92)
outputs							
Dry exit gas	8.918	94.2	0.510	3.53E-05	6.571		1.837
Water vapor from air humidity	0.085	0.9		0.010			0.076
Water vapor from biomass moisture	0.089	0.9		0.010			0.079
Water vapor from fuel hydrogen	0.359	3.8		0.040			0.318
Total water vapor	0.533	5.6		0.060			0.473
Unreacted carbon	0.000	0.0	0.000				
Vaporized inorganics	0.000	0.0					
Condensed phase inorganics	0.019	0.2					
Total inorganics	0.019	0.2					
Total condensed phase	0.019	0.2	0.000				
O2	0.476	5.0					0.476
CO2	1.863	19.7	0.508				1.355
CO	0.003	0.0	0.001				0.002
HC (as CH4)	1.41E-04	0.0	1.05E-04	3.53E-05			
NOx (as NO2)	0.006	0.1			0.002		0.004
SO2	3.74E-05	0.0				1.87E-05	1.87E-05
N2 (by difference)	6.569	69.4			6.569		
Total outputs	9.470	100.0	0.510	0.060	6.571	1.87E-05	2.310
Fraction of Total (%)	(100.00)		(5.39)	(0.63)	(69.39)	(0.000)	(24.39)
(Outputs - Inputs)	-1.78E-15		1.57E-01	-6.94E-18	-9.67E-03	-3.42E-04	-1.45E-01
(Outputs/Inputs)	1.00000		1.44488	1.00000	0.99853	0.05194	0.94107

Table A2a.b. Element Conversions, Emission Factors, and Stoichiometry from Measured Fuel Rate   **2a: Banagrass JC-PRP**

(Unadjusted Air Rate)   =   436.2 L/min

	Natural Gas Background (mol %)	Natural Gas (Stoich) (g/s)	Combustion Air (g/s)	Net Biomass (g/s)	Emission Factor (Biomass) (% dry fuel)	Biomass Element Conversion (%)	Net Natural Gas	Net Biomass	Total
CO2		0	0.005	1.859	257.819	144.216			
CO				0.003	0.455	0.400			
HC (as CH4)				0.000	0.019	0.030			
NOx (as NO2)				0.006	0.796	78.139			
SO2				3.74E-05	0.005	5.194			
O2 for Natural gas combustion (g/s)							0		
Air for Natural gas combustion (g/s)							0		
Air for Biomass combustion (g/s d.b.)								8.575	
Air-Fuel Ratio (kg/kg, dry basis)								11.9	
Stoich. Air for Biomass (g/s d.b.)								4.1	
Stoich. Air-Fuel (kg/kg, dry basis)								5.7	
Equivalence ratio for Biomass (d.b.)								0.477	
Excess air for Biomass (% d.b.)								110	
Volumetric exit gas density (kg/m^3 d.b.)									0.3947
Total volumetric exit gas flowrate (m^3/s w.b.)									0.0249
Exit gas velocity (m/s)									1.36
Reynolds Number									1,316
Approximate residence time (s)									2.93

Anticipated Gas Compositions from Measured Fuel Rate   **2a: Banagrass JC-PRP**

(including major species only, dry basis)

	Inlet Air				Exit Gas			Measured
	Mass Flow (g/s)	Mass Fraction (%)	Mol Fraction (%)		Mass Flow (g/s)	Mass Fraction (%)	Mol Fraction (%)	Mol Fraction (%)
O2	1.992	23.229	20.946		1.041	11.678	10.961	5.10
CO2	0.005	0.053	0.035		1.293	14.508	9.901	14.50
N2	6.578	76.718	79.019		6.580	73.814	79.138	80.31
Total	8.575	100.000	100.000		8.915	100.000	100.000	99.914
Mol. Wt.		28.854				30.034		

Table A2a.c. Mass and element balance 2a: Banagrass JC-PRP

Carbon Balance

	Mass Flowrate (g/s)	Mass Fractions (%)	Carbon Flowrate (g/s)	Hydrogen Flowrate (g/s)	Nitrogen Flowrate (g/s)	Sulfur Flowrate (g/s)	Oxygen Flowrate (g/s)
inputs							
Natural gas	0.000	0.0	0.000	0.000			
Dry air	8.575	87.0	0.001		6.578		1.995
Humidity in air	0.085	0.9		0.010			0.076
Moist biomass (as-fired)	1.193	12.1	0.518	0.074	0.003	0.0005	0.566
Moisture in biomass	0.131	1.3		0.015			0.117
Dry biomass	1.062	10.8	0.518	0.059	0.003	0.0005	0.449
Organic biomass	1.034	10.5		0.059	0.003	0.0005	0.449
Ash	0.028	0.3					
Total inputs	9.853	100.0	0.519	0.083	6.581	0.0005	2.636
Fraction of Total (%)	(100.00)		(5.27)	(0.85)	(66.80)	(0.005)	(26.76)
outputs							
Dry exit gas	9.080	92.2	0.519	3.60E-05	6.690		1.870
Water vapor from air humidity	0.085	0.9		0.010			0.076
Water vapor from biomass moisture	0.131	1.3		0.015			0.117
Water vapor from fuel hydrogen	0.528	5.4		0.059			0.469
Total water vapor	0.744	7.6		0.083			0.661
Unreacted carbon	0.000	0.0	0.000				
Vaporized inorganics	0.000	0.0					
Condensed phase inorganics	0.028	0.3					
Total inorganics	0.028	0.3					
Total condensed phase	0.028	0.3	0.000				
O2	0.485	4.9					0.485
CO2	1.897	19.3	0.518				1.379
CO	0.003	0.0	0.001				0.002
HC (as CH4)	1.43E-04	0.0	1.07E-04	3.60E-05			
NOx (as NO2)	0.006	0.1			0.002		0.004
SO2	3.81E-05	3.87E-04				1.91E-05	1.90E-05
N2 (by difference)	6.688	67.9			6.688		
Total outputs	9.853	100.0	0.519	0.083	6.690	1.91E-05	2.532
Fraction of Total (%)	(100.00)		(5.27)	(0.85)	(67.90)	(0.000)	(25.69)
(Outputs - Inputs)	-1.78E-15		0.00E+00	-1.39E-17	1.09E-01	-5.12E-04	-1.05E-01
(Outputs/Inputs)	1.00000		1.00000	1.00000	1.01652	0.03591	0.96024

Table A2a.d. Element Conversions, Emission Factors, and Stoichiometry from Carbon Balance   **2a: Banagrass JC-PRP**

	Natural Gas Background (mol %)	Natural Gas (Stoich) (g/s)	Air (g/s)	Net Biomass (g/s)	Emission Factor (Biomass) (% dry fuel)	Biomass Element Conversion (%)	Net Natural Gas	Net Biomass	Total
CO2		0	0.005	1.892	178.242	99.703			
CO				0.003	0.314	0.276			
HC (as CH4)				0.000	0.013	0.021			
NOx (as NO2)				0.006	0.550	54.019			
SO2				3.81E-05	0.004	3.591			
O2 for Natural gas combustion (g/s)							0		
Air for Natural gas combustion (g/s)							0		
Air for Biomass combustion (g/s d.b.)								8.575	
Biomass Air-Fuel Ratio (kg/kg, d.b.)								8.1	
Stoich. Air for Biomass (g/s d.b.)								6.0	
Stoich. Air-Fuel (kg/kg, dry basis)								5.7	
Equivalence ratio for Biomass (d.b.)								0.703	
Excess air for Biomass (% d.b.)								42	
Volumetric exit gas density (kg/m^3 d.b.)									0.3947
Total volumetric exit gas flowrate (m^3/s w.b.)									0.0262
Exit gas velocity (m/s)									1.44
Reynolds Number									1,386
Approximate residence time (s)									2.78

Anticipated Gas Compositions from Carbon Balance   **2a: Banagrass JC-PRP**
(including major species only, dry basis)

	Inlet Air			Exit Gas			Measured
	Mass Flow (g/s)	Mass Fraction (%)	Mol Fraction (%)	Mass Flow (g/s)	Mass Fraction (%)	Mol Fraction (%)	Mol Fraction (%)
O2	1.992	23.229	20.946	0.592	6.518	6.232	5.10
CO2	0.005	0.053	0.035	1.903	20.965	14.573	14.50
N2	6.578	76.718	79.019	6.581	72.517	79.195	80.31
Total	8.575	100.000	100.000	9.076	100.000	100.000	99.914
Mol. Wt.		28.854			30.593		

Table A2a.e. Mass and element balance   2a: Banagrass JC-PRP

Measured Fuel Rate
(Adjusted Air Rate)

	Mass Flowrate (g/s)	Mass Fractions (%)	Carbon Flowrate (g/s)	Hydrogen Flowrate (g/s)	Nitrogen Flowrate (g/s)	Sulfur Flowrate (g/s)	Oxygen Flowrate (g/s)
inputs							
Natural gas	0.000	0.0	0.000	0.000			
Dry air	5.822	87.0	0.001		4.466		1.355
Humidity in air	0.058	0.9		0.006			0.051
Moist biomass (as-fired)	0.810	12.1	0.352	0.050	0.002	0.0004	0.384
Moisture in biomass	0.089	1.3		0.010			0.079
Dry biomass	0.721	10.8	0.352	0.040	0.002	0.0004	0.305
Organic biomass	0.702	10.5		0.040	0.002	0.0004	0.305
Ash	0.019	0.3					
Total inputs	6.690	100.0	0.353	0.057	4.469	0.0004	1.790
Fraction of Total (%)	(100.00)		(5.27)	(0.85)	(66.80)	(0.005)	(26.76)
outputs							
Dry exit gas	6.165	92.2	0.353	2.44E-05	4.542		1.270
Water vapor from air humidity	0.058	0.9		0.006			0.051
Water vapor from biomass moisture	0.089	1.3		0.010			0.079
Water vapor from fuel hydrogen	0.359	5.4		0.040			0.318
Total water vapor	0.505	7.6		0.057			0.449
Unreacted carbon	0.000	0.0	0.000				
Vaporized inorganics	0.000	0.0					
Condensed phase inorganics	0.019	0.3					
Total inorganics	0.019	0.3					
Total condensed phase	0.019	0.3	0.000				
O2	0.329	4.9					0.329
CO2	1.288	19.3	0.352				0.937
CO	0.002	0.0	0.001				0.001
HC (as CH4)	9.71E-05	0.0	7.27E-05	2.44E-05			
NOx (as NO2)	0.004	0.1			0.001		0.003
SO2	2.59E-05	0.0				1.29E-05	1.29E-05
N2 (by difference)	4.541	67.9			4.541		
Total outputs	6.690	100.0	0.353	0.057	4.542	1.29E-05	1.719
Fraction of Total (%)	(100.00)		(5.27)	(0.85)	(67.90)	(0.000)	(25.69)
(Outputs - Inputs)	0.00E+00		-1.67E-16	6.94E-18	7.38E-02	-3.48E-04	-7.12E-02
(Outputs/Inputs)	1.00000		1.00000	1.00000	1.01652	0.03591	0.96024

Table A2a.f. Element Conversions, Emission Factors, and Stoichiometry from Measured Fuel Rate
2a: Banagrass JC-PRP

(Adjusted Air Rate)	=	296.2 L/min

	Natural Gas Background (mol %)	Natural Gas (Stoich) (g/s)	Combustion Air (g/s)	Net Biomass (g/s)	Emission Factor (Biomass) (% dry fuel)	Biomass Element Conversion (%)	Net Natural Gas	Net Biomass	Total
CO2		0	0.003	1.285	178.242	99.703			
CO				0.002	0.314	0.276			
HC (as CH4)				0.000	0.013	0.021			
NOx (as NO2)				0.004	0.550	54.019			
SO2				2.59E-05	0.004	3.591			

	Net Natural Gas	Net Biomass	Total
O2 for Natural gas combustion (g/s)	0		
Air for Natural gas combustion (g/s)	0		
Air for Biomass combustion (g/s d.b.)		5.822	
Air-Fuel Ratio (kg/kg, dry basis)		8.1	
Stoich. Air for Biomass (g/s d.b.)		4.1	
Stoich. Air-Fuel (kg/kg, dry basis)		5.7	
Equivalence ratio for Biomass (d.b.)		0.703	
Excess air for Biomass (% d.b.)		42	
Volumetric exit gas density (kg/m^3 d.b.)			0.3947
Total volumetric exit gas flowrate (m^3/s w.b.)			0.0178
Exit gas velocity (m/s)			0.98
Reynolds Number			941
Approximate residence time (s)			4.10

Anticipated Gas Compositions from Measured Fuel Rate
2a: Banagrass JC-PRP
(including major species only, dry basis)

	Inlet Air			Exit Gas			Measured
	Mass Flow (g/s)	Mass Fraction (%)	Mol Fraction (%)	Mass Flow (g/s)	Mass Fraction (%)	Mol Fraction (%)	Mol Fraction (%)
O2	1.352	23.229	20.946	0.402	6.518	6.232	5.10
CO2	0.003	0.053	0.035	1.292	20.965	14.573	14.50
N2	4.466	76.718	79.019	4.469	72.517	79.195	80.31
Total	5.822	100.000	100.000	6.162	100.000	100.000	99.914
Mol. Wt.		28.854			30.593		

Table A2b.a. Mass and element balance

Measured Fuel Rate
(Unadjusted Air Rate)

	Mass Flowrate (g/s)	Mass Fractions (%)	Carbon Flowrate (g/s)	Hydrogen Flowrate (g/s)	Nitrogen Flowrate (g/s)	Sulfur Flowrate (g/s)	Oxygen Flowrate (g/s)
inputs							
Natural gas	0.000	0.0	0.000	0.000			
Dry air	8.575	89.8	0.001		6.578		1.995
Humidity in air	0.085	0.9		0.010			0.076
Moist biomass (as-fired)	0.890	9.3	0.386	0.055	0.002	0.0004	0.422
Moisture in biomass	0.098	1.0		0.011			0.087
Dry biomass	0.792	8.3	0.386	0.044	0.002	0.0004	0.335
Organic biomass	0.771	8.1		0.044	0.002	0.0004	0.335
Ash	0.021	0.2					
Total inputs	9.550	100.0	0.388	0.065	6.581	0.0004	2.493
Fraction of Total (%)	(100.00)		(4.06)	(0.68)	(68.91)	(0.004)	(26.10)
outputs							
Dry exit gas	8.952	93.7	0.529	8.14E-05	6.583		1.840
Water vapor from air humidity	0.085	0.9		0.010			0.076
Water vapor from biomass moisture	0.098	1.0		0.011			0.087
Water vapor from fuel hydrogen	0.394	4.1		0.044			0.349
Total water vapor	0.576	6.0		0.065			0.512
Unreacted carbon	0.000	0.0	0.000				
Vaporized inorganics	0.000	0.0					
Condensed phase inorganics	0.021	0.2					
Total inorganics	0.021	0.2					
Total condensed phase	0.021	0.2	0.000				
O2	0.431	4.5					0.431
CO2	1.931	20.2	0.527				1.404
CO	0.003	0.0	0.001				0.002
HC (as CH4)	3.24E-04	0.0	2.42E-04	8.14E-05			
NOx (as NO2)	0.006	0.1			0.002		0.004
SO2	1.69E-04	0.0				8.44E-05	8.42E-05
N2 (by difference)	6.581	68.9			6.581		
Total outputs	9.550	100.0	0.529	0.065	6.583	8.44E-05	2.352
Fraction of Total (%)	(100.00)		(5.54)	(0.68)	(68.93)	(0.001)	(24.63)
(Outputs - Inputs)	0.00E+00		1.41E-01	0.00E+00	2.29E-03	-3.12E-04	-1.40E-01
(Outputs/Inputs)	1.00000		1.36346	1.00000	1.00035	0.21312	0.94371

Table A2b.b. Element Conversions, Emission Factors, and Stoichiometry from Measured Fuel Rate   **2b: Banagrass JC-PRP**
(Unadjusted Air Rate)   =   436.2 L/min

	Natural Gas Background (mol %)	Natural Gas (Stoich) (g/s)	Combustion Air (g/s)	Net Biomass (g/s)	Emission Factor (Biomass) (% dry fuel)	Biomass Element Conversion (%)	Net Natural Gas	Net Biomass	Total
CO2		0	0.005	1.927	243.214	136.047			
CO				0.003	0.402	0.354			
HC (as CH4)				0.000	0.041	0.063			
NOx (as NO2)				0.006	0.705	69.247			
SO2				1.69E-04	0.021	21.312			

O2 for Natural gas combustion (g/s)	0	
Air for Natural gas combustion (g/s)	0	
Air for Biomass combustion (g/s d.b.)	8.575	
Air-Fuel Ratio (kg/kg, dry basis)	10.8	
Stoich. Air for Biomass (g/s d.b.)	4.5	
Stoich. Air-Fuel (kg/kg, dry basis)	5.7	
Equivalence ratio for Biomass (d.b.)	0.524	
Excess air for Biomass (% d.b.)	91	
Volumetric exit gas density (kg/m^3 d.b.)		0.3955
Total volumetric exit gas flowrate (m^3/s w.b.)		0.0251
Exit gas velocity (m/s)		1.38
Reynolds Number		1,328
Approximate residence time (s)		2.91

Anticipated Gas Compositions from Measured Fuel Rate   **2b: Banagrass JC-PRP**
(including major species only, dry basis)

	Inlet Air			Exit Gas			Measured
	Mass Flow (g/s)	Mass Fraction (%)	Mol Fraction (%)	Mass Flow (g/s)	Mass Fraction (%)	Mol Fraction (%)	Mol Fraction (%)
O2	1.992	23.229	20.946	0.947	10.585	9.974	4.60
CO2	0.005	0.053	0.035	1.421	15.876	10.876	15.00
N2	6.578	76.718	79.019	6.581	73.539	79.150	80.31
Total	8.575	100.000	100.000	8.948	100.000	100.000	99.912
Mol. Wt.		28.854			30.151		

Table A2b.c. Mass and element balance   2b: Banagrass JC-PRP
Carbon Balance

	Mass Flowrate (g/s)	Mass Fractions (%)	Carbon Flowrate (g/s)	Hydrogen Flowrate (g/s)	Nitrogen Flowrate (g/s)	Sulfur Flowrate (g/s)	Oxygen Flowrate (g/s)
inputs							
Natural gas	0.000	0.0	0.000	0.000			
Dry air	8.575	86.7	0.001		6.578		1.995
Humidity in air	0.085	0.9		0.010			0.076
Moist biomass (as-fired)	1.234	12.5	0.536	0.076	0.003	0.0005	0.585
Moisture in biomass	0.136	1.4		0.015			0.121
Dry biomass	1.099	11.1	0.536	0.061	0.003	0.0005	0.465
Organic biomass	1.069	10.8		0.061	0.003	0.0005	0.465
Ash	0.029	0.3					
Total inputs	9.894	100.0	0.537	0.086	6.582	0.0005	2.656
Fraction of Total (%)	(100.00)		(5.43)	(0.87)	(66.52)	(0.006)	(26.84)
outputs							
Dry exit gas	9.098	92.0	0.537	8.27E-05	6.690		1.870
Water vapor from air humidity	0.085	0.9		0.010			0.076
Water vapor from biomass moisture	0.136	1.4		0.015			0.121
Water vapor from fuel hydrogen	0.546	5.5		0.061			0.485
Total water vapor	0.767	7.8		0.086			0.681
Unreacted carbon	0.000	0.0	0.000				
Vaporized inorganics	0.000	0.0					
Condensed phase inorganics	0.029	0.3					
Total inorganics	0.029	0.3					
Total condensed phase	0.029	0.3	0.000				
O2	0.438	4.4					0.438
CO2	1.963	19.8	0.536				1.427
CO	0.003	0.0	0.001				0.002
HC (as CH4)	3.29E-04	0.0	2.46E-04	8.27E-05			
NOx (as NO2)	0.006	0.1			0.002		0.004
SO2	1.71E-04	1.73E-03				8.58E-05	8.56E-05
N2 (by difference)	6.688	67.6			6.688		
Total outputs	9.894	100.0	0.537	0.086	6.690	8.58E-05	2.551
Fraction of Total (%)	(100.00)		(5.43)	(0.87)	(67.62)	(0.001)	(25.79)
(Outputs - Inputs)	0.00E+00		0.00E+00	0.00E+00	1.09E-01	-4.64E-04	-1.05E-01
(Outputs/Inputs)	1.00000		1.00000	1.00000	1.01649	0.15616	0.96063

Table A2b.d. Element Conversions, Emission Factors, and Stoichiometry from Carbon Balance 2b: Banagrass JC-PRP

	Natural Gas Background (mol %)	Natural Gas (Stoich) (g/s)	Air (g/s)	Net Biomass (g/s)	Emission Factor (Biomass) (% dry fuel)	Biomass Element Conversion (%)	Net Natural Gas	Net Biomass	Total
CO2		0	0.005	1.958	178.227	99.695			
CO				0.003	0.295	0.259			
HC (as CH4)				0.000	0.030	0.046			
NOx (as NO2)				0.006	0.517	50.742			
SO2				1.71E-04	0.016	15.616			
O2 for Natural gas combustion (g/s)							0		
Air for Natural gas combustion (g/s)							0		
Air for Biomass combustion (g/s d.b.)								8.575	
Biomass Air-Fuel Ratio (kg/kg, d.b.)								7.8	
Stoich. Air for Biomass (g/s d.b.)								6.2	
Stoich. Air-Fuel (kg/kg, dry basis)								5.7	
Equivalence ratio for Biomass (d.b.)								0.727	
Excess air for Biomass (% d.b.)								37	
Volumetric exit gas density (kg/m^3 d.b.)									0.3955
Total volumetric exit gas flowrate (m^3/s w.b.)									0.0263
Exit gas velocity (m/s)									1.44
Reynolds Number									1,391
Approximate residence time (s)									2.77

Anticipated Gas Compositions from Carbon Balance 2b: Banagrass JC-PRP
(including major species only, dry basis)

	Inlet Air			Exit Gas			Measured
	Mass Flow (g/s)	Mass Fraction (%)	Mol Fraction (%)	Mass Flow (g/s)	Mass Fraction (%)	Mol Fraction (%)	Mol Fraction (%)
O2	1.992	23.229	20.946	0.543	5.972	5.721	4.60
CO2	0.005	0.053	0.035	1.969	21.649	15.078	15.00
N2	6.578	76.718	79.019	6.582	72.380	79.201	80.31
Total	8.575	100.000	100.000	9.093	100.000	100.000	99.912
Mol. Wt.		28.854			30.653		

Table A2b.e. Mass and element balance

2b: Banagrass JC-PRP

Measured Fuel Rate
(Adjusted Air Rate)

	Mass Flowrate (g/s)	Mass Fractions (%)	Carbon Flowrate (g/s)	Hydrogen Flowrate (g/s)	Nitrogen Flowrate (g/s)	Sulfur Flowrate (g/s)	Oxygen Flowrate (g/s)
inputs							
Natural gas	0.000	0.0	0.000	0.000			
Dry air	6.183	86.7	0.001		4.743		1.439
Humidity in air	0.061	0.9		0.007			0.054
Moist biomass (as-fired)	0.890	12.5	0.386	0.055	0.002	0.0004	0.422
Moisture in biomass	0.098	1.4		0.011			0.087
Dry biomass	0.792	11.1	0.386	0.044	0.002	0.0004	0.335
Organic biomass	0.771	10.8		0.044	0.002	0.0004	0.335
Ash	0.021	0.3					
Total inputs	7.134	100.0	0.387	0.062	4.745	0.0004	1.915
Fraction of Total (%)	(100.00)		(5.43)	(0.87)	(66.52)	(0.006)	(26.84)
outputs							
Dry exit gas	6.560	92.0	0.387	5.96E-05	4.824		1.349
Water vapor from air humidity	0.061	0.9		0.007			0.054
Water vapor from biomass moisture	0.098	1.4		0.011			0.087
Water vapor from fuel hydrogen	0.394	5.5		0.044			0.350
Total water vapor	0.553	7.8		0.062			0.491
Unreacted carbon	0.000	0.0	0.000				
Vaporized inorganics	0.000	0.0					
Condensed phase inorganics	0.021	0.3					
Total inorganics	0.021	0.3					
Total condensed phase	0.021	0.3	0.000				
O2	0.316	4.4					0.316
CO2	1.415	19.8	0.386				1.029
CO	0.002	0.0	0.001				0.001
HC (as CH4)	2.37E-04	0.0	1.78E-04	5.96E-05			
NOx (as NO2)	0.004	0.1			0.001		0.003
SO2	1.24E-04	0.0				6.18E-05	6.17E-05
N2 (by difference)	4.823	67.6			4.823		
Total outputs	7.134	100.0	0.387	0.062	4.824	6.18E-05	1.840
Fraction of Total (%)	(100.00)		(5.43)	(0.87)	(67.62)	(0.001)	(25.79)
(Outputs - Inputs)	-8.88E-16		1.67E-16	-6.94E-18	7.83E-02	-3.34E-04	-7.54E-02
(Outputs/Inputs)	1.00000		1.00000	1.00000	1.01649	0.15616	0.96063

Table A2b.f. Element Conversions, Emission Factors, and Stoichiometry from Measured Fuel Rate

2b: Banagrass JC-PRP

(Adjusted Air Rate) = 314.5 L/min

	Natural Gas Background (mol %)	Natural Gas (Stoich) (g/s)	Combustion Air (g/s)	Net Biomass (g/s)	Emission Factor (Biomass) (% dry fuel)	Biomass Element Conversion (%)	Net Natural Gas	Net Biomass	Total
CO2	0	0.003		1.412	178.227	99.695			
CO				0.002	0.295	0.259			
HC (as CH4)				0.000	0.030	0.046			
NOx (as NO2)				0.004	0.517	50.742			
SO2				1.24E-04	0.016	15.616			

O2 for Natural gas combustion (g/s)		0
Air for Natural gas combustion (g/s)		0
Air for Biomass combustion (g/s d.b.)		6.183
Air-Fuel Ratio (kg/kg, dry basis)		7.8
Stoich. Air for Biomass (g/s d.b.)		4.5
Stoich. Air-Fuel (kg/kg, dry basis)		5.7
Equivalence ratio for Biomass (d.b.)		0.727
Excess air for Biomass (% d.b.)		37
Volumetric exit gas density (kg/m^3 d.b.)		0.3955
Total volumetric exit gas flowrate (m^3/s w.b.)		0.0190
Exit gas velocity (m/s)		1.04
Reynolds Number		1,003
Approximate residence time (s)		3.85

Anticipated Gas Compositions from Measured Fuel Rate   **2b: Banagrass JC-PRP**

(including major species only, dry basis)

	Inlet Air			Exit Gas			Measured
	Mass Flow (g/s)	Mass Fraction (%)	Mol Fraction (%)	Mass Flow (g/s)	Mass Fraction (%)	Mol Fraction (%)	Mol Fraction (%)
O2	1.436	23.229	20.946	0.392	5.972	5.721	4.60
CO2	0.003	0.053	0.035	1.419	21.649	15.078	15.00
N2	4.743	76.718	79.019	4.745	72.380	79.201	80.31
Total	6.182	100.000	100.000	6.556	100.000	100.000	99.912
Mol. Wt.		28.854			30.653		

Table A3.a. Mass and element balance

3b: *Bagasse*

Measured Fuel Rate

(Unadjusted Air Rate)

	Mass Flowrate (g/s)	Mass Fractions (%)	Carbon Flowrate (g/s)	Hydrogen Flowrate (g/s)	Nitrogen Flowrate (g/s)	Sulfur Flowrate (g/s)	Oxygen Flowrate (g/s)
inputs							
Natural gas	0.000	0.0	0.000	0.000			
Dry air	8.575	89.0	0.001		6.578		1.995
Humidity in air	0.085	0.9		0.010			0.076
Moist biomass (as-fired)	0.980	10.2	0.408	0.050	0.001	0.0005	0.436
Moisture in biomass	0.078	0.8		0.009			0.070
Dry biomass	0.902	9.4	0.408	0.041	0.001	0.0005	0.366
Organic biomass	0.825	8.6		0.041	0.001	0.0005	0.366
Ash	0.076	0.8					
Total inputs	9.640	100.0	0.409	0.060	6.579	0.0005	2.507
Fraction of Total (%)	(100.00)		(4.24)	(0.62)	(68.25)	(0.005)	(26.00)
outputs							
Dry exit gas	9.031	93.7	0.538	1.19E-05	6.621		1.872
Water vapor from air humidity	0.085	0.9		0.010			0.076
Water vapor from biomass moisture	0.078	0.8		0.009			0.070
Water vapor from fuel hydrogen	0.369	3.8		0.041			0.328
Total water vapor	0.532	5.5		0.060			0.473
Unreacted carbon	0.000	0.0	0.000				
Vaporized inorganics	0.000	0.0					
Condensed phase inorganics	0.076	0.8					
Total inorganics	0.076	0.8					
Total condensed phase	0.076	0.8	0.000				
O2	0.434	4.5					0.434
CO2	1.972	20.5	0.538				1.434
CO	0.001	0.0	0.000				0.000
HC (as CH4)	4.73E-05	0.0	3.54E-05	1.19E-05			
NOx (as NO2)	0.005	0.1			0.001		0.003
SO2	4.91E-04	0.0				2.46E-04	2.45E-04
N2 (by difference)	6.619	68.7			6.619		
Total outputs	9.640	100.0	0.538	0.060	6.621	2.46E-04	2.344
Fraction of Total (%)	(100.00)		(5.59)	(0.62)	(68.68)	(0.003)	(24.32)
(Outputs - Inputs)	0.00E+00		1.30E-01	6.94E-18	4.14E-02	-2.05E-04	-1.62E-01
(Outputs/Inputs)	1.00000		1.31725	1.00000	1.00629	0.54509	0.93533

Table A3.b. Element Conversions, Emission Factors, and Stoichiometry from Measured Fuel Rate   *3b: Bagasse*

(Unadjusted Air Rate)   =   436.2 L/min

	Natural Gas Background (mol %)	Natural Gas (Stoich) (g/s)	Combustion Air (g/s)	Net Biomass (g/s)	Emission Factor (Biomass) (% dry fuel)	Biomass Element Conversion (%)	Net Natural Gas	Net Biomass	Total
CO2		0	0.005	1.967	218.216	131.758			
CO				0.001	0.058	0.055			
HC (as CH4)				0.000	0.005	0.009			
NOx (as NO2)				0.005	0.545	127.528			
SO2				4.91E-04	0.054	54.509			

O2 for Natural gas combustion (g/s)	0	
Air for Natural gas combustion (g/s)	0	
Air for Biomass combustion (g/s d.b.)		8.575
Air-Fuel Ratio (kg/kg, dry basis)		9.5
Stoich. Air for Biomass (g/s d.b.)		4.5
Stoich. Air-Fuel (kg/kg, dry basis)		5.0
Equivalence ratio for Biomass (d.b.)		0.526
Excess air for Biomass (% d.b.)		90
Volumetric exit gas density (kg/m^3 d.b.)		0.3959
Total volumetric exit gas flowrate (m^3/s w.b.)		0.0251
Exit gas velocity (m/s)		1.38
Reynolds Number		1,327
Approximate residence time (s)		2.91

Anticipated Gas Compositions from Measured Fuel Rate   *3b: Bagasse*

(including major species only, dry basis)

	Inlet Air				Exit Gas			Measured
	Mass Flow (g/s)	Mass Fraction (%)	Mol Fraction (%)		Mass Flow (g/s)	Mass Fraction (%)	Mol Fraction (%)	Mol Fraction (%)
O2	1.992	23.229	20.946		0.945	10.471	9.893	4.60
CO2	0.005	0.053	0.035		1.498	16.602	11.404	15.20
N2	6.578	76.718	79.019		6.579	72.927	78.702	80.15
Total	8.575	100.000	100.000		9.022	100.000	100.000	99.954
Mol. Wt.		28.854				30.232		

Table A3.c. Mass and element balance
Carbon Balance

3b: *Bagasse*

	Mass Flowrate (g/s)	Mass Fractions (%)	Carbon Flowrate (g/s)	Hydrogen Flowrate (g/s)	Nitrogen Flowrate (g/s)	Sulfur Flowrate (g/s)	Oxygen Flowrate (g/s)
inputs							
Natural gas	0.000	0.0	0.000	0.000			
Dry air	8.575	86.0	0.001		6.578		1.995
Humidity in air	0.085	0.9		0.010			0.076
Moist biomass (as-fired)	1.314	13.2	0.546	0.067	0.002	0.0006	0.585
Moisture in biomass	0.105	1.1		0.012			0.093
Dry biomass	1.209	12.1	0.546	0.055	0.002	0.0006	0.491
Organic biomass	1.107	11.1		0.055	0.002	0.0006	0.491
Ash	0.102	1.0					
Total inputs	9.974	100.0	0.548	0.077	6.580	0.0006	2.655
Fraction of Total (%)	(100.00)		(5.49)	(0.77)	(65.97)	(0.006)	(26.62)
outputs							
Dry exit gas	9.187	92.1	0.548	1.21E-05	6.735		1.904
Water vapor from air humidity	0.085	0.9		0.010			0.076
Water vapor from biomass moisture	0.105	1.1		0.012			0.093
Water vapor from fuel hydrogen	0.495	5.0		0.055			0.439
Total water vapor	0.685	6.9		0.077			0.608
Unreacted carbon	0.000	0.0	0.000				
Vaporized inorganics	0.000	0.0					
Condensed phase inorganics	0.102	1.0					
Total inorganics	0.102	1.0					
Total condensed phase	0.102	1.0	0.000				
O2	0.441	4.4					0.441
CO2	2.006	20.1	0.547				1.459
CO	0.001	0.0	0.000				0.000
HC (as CH4)	4.81E-05	0.0	3.60E-05	1.21E-05			
NOx (as NO2)	0.005	0.1			0.002		0.003
SO2	4.99E-04	5.01E-03				2.50E-04	2.49E-04
N2 (by difference)	6.733	67.5			6.733		
Total outputs	9.974	100.0	0.548	0.077	6.735	2.50E-04	2.512
Fraction of Total (%)	(100.00)		(5.49)	(0.77)	(67.52)	(0.003)	(25.19)
(Outputs - Inputs)	1.78E-15		2.22E-16	0.00E+00	1.55E-01	-3.55E-04	-1.43E-01
(Outputs/Inputs)	1.00000		1.00000	1.00000	1.02357	0.41349	0.94613

Table A3.d. Element Conversions, Emission Factors, and Stoichiometry from Carbon Balance   3b: Bagasse

	Natural Gas Background (mol %)	Natural Gas (Stoich) (g/s)	Air (g/s)	Net Biomass (g/s)	Emission Factor (Biomass) (% dry fuel)	Biomass Element Conversion (%)	Net Natural Gas	Net Biomass	Total
CO2		0	0.005	2.001	165.539	99.952			
CO				0.001	0.044	0.042			
HC (as CH4)				0.000	0.004	0.007			
NOx (as NO2)				0.005	0.413	96.739			
SO2				4.99E-04	0.041	41.349			

	Net Natural Gas	Net Biomass	Total
O2 for Natural gas combustion (g/s)	0		
Air for Natural gas combustion (g/s)	0		
Air for Biomass combustion (g/s d.b.)		8.575	
Biomass Air-Fuel Ratio (kg/kg, d.b.)		7.1	
Stoich. Air for Biomass (g/s d.b.)		6.0	
Stoich. Air-Fuel (kg/kg, dry basis)		5.0	
Equivalence ratio for Biomass (d.b.)		0.705	
Excess air for Biomass (% d.b.)		42	
Volumetric exit gas density (kg/m^3 d.b.)			0.3959
Total volumetric exit gas flowrate (m^3/s w.b.)			0.0261
Exit gas velocity (m/s)			1.43
Reynolds Number			1,383
Approximate residence time (s)			2.79

Anticipated Gas Compositions from Carbon Balance   3b: Bagasse
(including major species only, dry basis)

	Inlet Air			Exit Gas			Measured
	Mass Flow (g/s)	Mass Fraction (%)	Mol Fraction (%)	Mass Flow (g/s)	Mass Fraction (%)	Mol Fraction (%)	Mol Fraction (%)
O2	1.992	23.229	20.946	0.588	6.405	6.145	4.60
CO2	0.005	0.053	0.035	2.007	21.876	15.260	15.20
N2	6.578	76.718	79.019	6.580	71.719	78.595	80.15
Total	8.575	100.000	100.000	9.174	100.000	100.000	99.954
Mol. Wt.		28.854			30.699		

Table A3.e. Mass and element balance

3b: Bagasse

Measured Fuel Rate
(Adjusted Air Rate)

	Mass Flowrate (g/s)	Mass Fractions (%)	Carbon Flowrate (g/s)	Hydrogen Flowrate (g/s)	Nitrogen Flowrate (g/s)	Sulfur Flowrate (g/s)	Oxygen Flowrate (g/s)
inputs							
Natural gas	0.000	0.0	0.000	0.000			
Dry air	6.394	86.0	0.001		4.905		1.488
Humidity in air	0.063	0.9		0.007			0.056
Moist biomass (as-fired)	0.980	13.2	0.408	0.050	0.001	0.0005	0.436
Moisture in biomass	0.078	1.1		0.009			0.070
Dry biomass	0.902	12.1	0.408	0.041	0.001	0.0005	0.366
Organic biomass	0.825	11.1		0.041	0.001	0.0005	0.366
Ash	0.076	1.0					
Total inputs	7.438	100.0	0.408	0.057	4.907	0.0005	1.980
Fraction of Total (%)	(100.00)		(5.49)	(0.77)	(65.97)	(0.006)	(26.62)
outputs							
Dry exit gas	6.851	92.1	0.408	9.02E-06	5.022		1.420
Water vapor from air humidity	0.063	0.9		0.007			0.056
Water vapor from biomass moisture	0.078	1.1		0.009			0.070
Water vapor from fuel hydrogen	0.369	5.0		0.041			0.328
Total water vapor	0.511	6.9		0.057			0.454
Unreacted carbon	0.000	0.0	0.000				
Vaporized inorganics	0.000	0.0					
Condensed phase inorganics	0.076	1.0					
Total inorganics	0.076	1.0					
Total condensed phase	0.076	1.0	0.000				
O2	0.329	4.4					0.329
CO2	1.496	20.1	0.408				1.088
CO	0.000	0.0	0.000				0.000
HC (as CH4)	3.59E-05	0.0	2.69E-05	9.02E-06			
NOx (as NO2)	0.004	0.1			0.001		0.003
SO2	3.72E-04	0.0				1.86E-04	1.86E-04
N2 (by difference)	5.021	67.5			5.021		
Total outputs	7.438	100.0	0.408	0.057	5.022	1.86E-04	1.873
Fraction of Total (%)	(100.00)		(5.49)	(0.77)	(67.52)	(0.003)	(25.19)
(Outputs - Inputs)	8.88E-16		-5.55E-17	0.00E+00	1.16E-01	-2.64E-04	-1.07E-01
(Outputs/Inputs)	1.00000		1.00000	1.00000	1.02357	0.41349	0.94613

Table A3.f. Element Conversions, Emission Factors, and Stoichiometry from Measured Fuel Rate   *3b: Bagasse*

(Adjusted Air Rate)   =   325.3 L/min

	Natural Gas Background (mol %)	Natural Gas (Stoich) (g/s)	Combustion Air (g/s)	Net Biomass (g/s)	Emission Factor (Biomass) (% dry fuel)	Biomass Element Conversion (%)	Net Natural Gas	Net Biomass	Total
CO2		0	0.003	1.492	165.539	99.952			
CO				0.000	0.044	0.042			
HC (as CH4)				0.000	0.004	0.007			
NOx (as NO2)				0.004	0.413	96.739			
SO2				3.72E-04	0.041	41.349			

	Net Natural Gas	Net Biomass	Total
O2 for Natural gas combustion (g/s)	0		
Air for Natural gas combustion (g/s)	0		
Air for Biomass combustion (g/s d.b.)		6.394	
Air-Fuel Ratio (kg/kg, dry basis)		7.1	
Stoich. Air for Biomass (g/s d.b.)		4.5	
Stoich. Air-Fuel (kg/kg, dry basis)		5.0	
Equivalence ratio for Biomass (d.b.)		0.705	
Excess air for Biomass (% d.b.)		42	
Volumetric exit gas density (kg/m^3 d.b.)			0.3959
Total volumetric exit gas flowrate (m^3/s w.b.)			0.0195
Exit gas velocity (m/s)			1.07
Reynolds Number			1,031
Approximate residence time (s)			3.74

Anticipated Gas Compositions from Measured Fuel Rate   *3b: Bagasse*

(including major species only, dry basis)

	Inlet Air			Exit Gas			Measured
	Mass Flow (g/s)	Mass Fraction (%)	Mol Fraction (%)	Mass Flow (g/s)	Mass Fraction (%)	Mol Fraction (%)	Mol Fraction (%)
O2	1.485	23.229	20.946	0.438	6.405	6.145	4.60
CO2	0.003	0.053	0.035	1.497	21.876	15.260	15.20
N2	4.905	76.718	79.019	4.907	71.719	78.595	80.15
Total	6.394	100.000	100.000	6.841	100.000	100.000	99.954
Mol. Wt.		28.854			30.699		

Table A4.a. Mass and element balance   4a: Banagrass FC-P

Measured Fuel Rate
(Unadjusted Air Rate)

	Mass Flowrate (g/s)	Mass Fractions (%)	Carbon Flowrate (g/s)	Hydrogen Flowrate (g/s)	Nitrogen Flowrate (g/s)	Sulfur Flowrate (g/s)	Oxygen Flowrate (g/s)
inputs							
Natural gas	0.000	0.0	0.000	0.000			
Dry air	8.575	90.1	0.001		6.578		1.995
Humidity in air	0.085	0.9		0.010			0.076
Moist biomass (as-fired)	0.860	9.0	0.373	0.054	0.004	0.0005	0.404
Moisture in biomass	0.095	1.0		0.011			0.084
Dry biomass	0.765	8.0	0.373	0.043	0.004	0.0005	0.320
Organic biomass	0.742	7.8		0.043	0.004	0.0005	0.320
Ash	0.023	0.2					
Total inputs	9.520	100.0	0.374	0.063	6.582	0.0005	2.475
Fraction of Total (%)	(100.00)		(3.93)	(0.66)	(69.14)	(0.005)	(26.00)
outputs							
Dry exit gas	8.933	93.8	0.527	1.06E-05	6.569		1.837
Water vapor from air humidity	0.085	0.9		0.010			0.076
Water vapor from biomass moisture	0.095	1.0		0.011			0.084
Water vapor from fuel hydrogen	0.384	4.0		0.043			0.341
Total water vapor	0.563	5.9		0.063			0.500
Unreacted carbon	0.000	0.0	0.000				
Vaporized inorganics	0.000	0.0					
Condensed phase inorganics	0.023	0.2					
Total inorganics	0.023	0.2					
Total condensed phase	0.023	0.2	0.000				
O2	0.430	4.5					0.430
CO2	1.927	20.2	0.526				1.401
CO	0.003	0.0	0.001				0.002
HC (as CH4)	4.21E-05	0.0	3.16E-05	1.06E-05			
NOx (as NO2)	0.006	0.1			0.002		0.004
SO2	7.48E-05	0.0				3.74E-05	3.74E-05
N2 (by difference)	6.567	69.0			6.567		
Total outputs	9.520	100.0	0.527	0.063	6.569	3.74E-05	2.337
Fraction of Total (%)	(100.00)		(5.54)	(0.66)	(69.01)	(0.000)	(24.55)
(Outputs - Inputs)	0.00E+00		1.53E-01	0.00E+00	-1.26E-02	-4.22E-04	-1.38E-01
(Outputs/Inputs)	1.00000		1.41014	1.00000	0.99808	0.08151	0.94424

Table A4.b. Element Conversions, Emission Factors, and Stoichiometry from Measured Fuel Rate　　　　　　**4a: Banagrass FC-P**
(Unadjusted Air Rate)　　　　　=　　　　436.2 L/min

	Natural Gas Background (mol %)	Natural Gas (Stoich) (g/s)	Combustion Air (g/s)	Net Biomass (g/s)	Emission Factor (Biomass) (% dry fuel)	Biomass Element Conversion (%)	Net Natural Gas	Net Biomass	Total
CO2		0	0.005	1.922	251.156	140.777			
CO				0.003	0.416	0.366			
HC (as CH4)				0.000	0.006	0.008			
NOx (as NO2)				0.006	0.747	47.407			
SO2				7.48E-05	0.010	8.151			

O2 for Natural gas combustion (g/s)	0	
Air for Natural gas combustion (g/s)	0	
Air for Biomass combustion (g/s d.b.)	8.575	
Air-Fuel Ratio (kg/kg, dry basis)	11.2	
Stoich. Air for Biomass (g/s d.b.)	4.4	
Stoich. Air-Fuel (kg/kg, dry basis)	5.7	
Equivalence ratio for Biomass (d.b.)	0.509	
Excess air for Biomass (% d.b.)	97	
Volumetric exit gas density (kg/m^3 d.b.)		0.3955
Total volumetric exit gas flowrate (m^3/s w.b.)		0.0250
Exit gas velocity (m/s)		1.37
Reynolds Number		1,322
Approximate residence time (s)		2.92

Anticipated Gas Compositions from Measured Fuel Rate　　　　　　**4a: Banagrass FC-P**
(including major species only, dry basis)

	Inlet Air			Exit Gas			Measured
	Mass Flow (g/s)	Mass Fraction (%)	Mol Fraction (%)	Mass Flow (g/s)	Mass Fraction (%)	Mol Fraction (%)	Mol Fraction (%)
O2	1.992	23.229	20.946	0.978	10.954	10.305	4.60
CO2	0.005	0.053	0.035	1.370	15.342	10.494	15.00
N2	6.578	76.718	79.019	6.582	73.703	79.200	80.32
Total	8.575	100.000	100.000	8.930	100.000	100.000	99.917
Mol. Wt.		28.854			30.103	.	

Table A4.c. Mass and element balance 4a: Banagrass FC-P
Carbon Balance

	Mass Flowrate (g/s)	Mass Fractions (%)	Carbon Flowrate (g/s)	Hydrogen Flowrate (g/s)	Nitrogen Flowrate (g/s)	Sulfur Flowrate (g/s)	Oxygen Flowrate (g/s)
inputs							
Natural gas	0.000	0.0	0.000	0.000			
Dry air	8.575	86.7	0.001		6.578		1.995
Humidity in air	0.085	0.9		0.010			0.076
Moist biomass (as-fired)	1.235	12.5	0.535	0.077	0.005	0.0007	0.580
Moisture in biomass	0.136	1.4		0.015			0.121
Dry biomass	1.099	11.1	0.535	0.062	0.005	0.0007	0.460
Organic biomass	1.066	10.8		0.062	0.005	0.0007	0.460
Ash	0.034	0.3					
Total inputs	9.895	100.0	0.537	0.086	6.583	0.0007	2.651
Fraction of Total (%)	(100.00)		(5.42)	(0.87)	(66.53)	(0.007)	(26.79)
outputs							
Dry exit gas	9.089	91.9	0.537	1.08E-05	6.684		1.869
Water vapor from air humidity	0.085	0.9		0.010			0.076
Water vapor from biomass moisture	0.136	1.4		0.015			0.121
Water vapor from fuel hydrogen	0.551	5.6		0.062			0.489
Total water vapor	0.772	7.8		0.086			0.686
Unreacted carbon	0.000	0.0	0.000				
Vaporized inorganics	0.000	0.0					
Condensed phase inorganics	0.034	0.3					
Total inorganics	0.034	0.3					
Total condensed phase	0.034	0.3	0.000				
O2	0.437	4.4					0.437
CO2	1.961	19.8	0.535				1.426
CO	0.003	0.0	0.001				0.002
HC (as CH4)	4.29E-05	0.0	3.21E-05	1.08E-05			
NOx (as NO2)	0.006	0.1			0.002		0.004
SO2	7.61E-05	7.69E-04				3.81E-05	3.80E-05
N2 (by difference)	6.682	67.5			6.682		
Total outputs	9.895	100.0	0.537	0.086	6.684	3.81E-05	2.554
Fraction of Total (%)	(100.00)		(5.42)	(0.87)	(67.55)	(0.000)	(25.81)
(Outputs - Inputs)	-3.55E-15		-1.11E-16	-1.39E-17	1.01E-01	-6.22E-04	-9.68E-02
(Outputs/Inputs)	1.00000		1.00000	1.00000	1.01530	0.05774	0.96348

Table A4.d. Element Conversions, Emission Factors, and Stoichiometry from Carbon Balance   4a: Banagrass FC-P

	Natural Gas Background (mol %)	Natural Gas (Stoich) (g/s)	Air (g/s)	Net Biomass (g/s)	Emission Factor (Biomass) (% dry fuel)	Biomass Element Conversion (%)	Net Natural Gas	Net Biomass	Total
CO2		0	0.005	1.956	177.933	99.735			
CO				0.003	0.294	0.259			
HC (as CH4)				0.000	0.004	0.006			
NOx (as NO2)				0.006	0.529	33.584			
SO2				7.61E-05	0.007	5.774			

O2 for Natural gas combustion (g/s)	0	
Air for Natural gas combustion (g/s)	0	
Air for Biomass combustion (g/s d.b.)	8.575	
Biomass Air-Fuel Ratio (kg/kg, d.b.)	7.8	
Stoich. Air for Biomass (g/s d.b.)	6.3	
Stoich. Air-Fuel (kg/kg, dry basis)	5.7	
Equivalence ratio for Biomass (d.b.)	0.731	
Excess air for Biomass (% d.b.)	37	
Volumetric exit gas density (kg/m^3 d.b.)		0.3955
Total volumetric exit gas flowrate (m^3/s w.b.)		0.0263
Exit gas velocity (m/s)		1.44
Reynolds Number		1,391
Approximate residence time (s)		2.77

Anticipated Gas Compositions from Carbon Balance   4a: Banagrass FC-P
(including major species only, dry basis)

	Inlet Air				Exit Gas			Measured
	Mass Flow (g/s)	Mass Fraction (%)	Mol Fraction (%)		Mass Flow (g/s)	Mass Fraction (%)	Mol Fraction (%)	Mol Fraction (%)
O2	1.992	23.229	20.946		0.536	5.900	5.651	4.60
CO2	0.005	0.053	0.035		1.966	21.638	15.069	15.00
N2	6.578	76.718	79.019		6.583	72.462	79.280	80.32
Total	8.575	100.000	100.000		9.085	100.000	100.000	99.917
Mol. Wt.		28.854				30.649		

Table A4.e. Mass and element balance 4a: Banagrass FC-P

Measured Fuel Rate
(Adjusted Air Rate)

	Mass Flowrate (g/s)	Mass Fractions (%)	Carbon Flowrate (g/s)	Hydrogen Flowrate (g/s)	Nitrogen Flowrate (g/s)	Sulfur Flowrate (g/s)	Oxygen Flowrate (g/s)
inputs							
Natural gas	0.000	0.0	0.000	0.000			
Dry air	5.970	86.7	0.001		4.580		1.389
Humidity in air	0.059	0.9		0.007			0.053
Moist biomass (as-fired)	0.860	12.5	0.373	0.054	0.004	0.0005	0.404
Moisture in biomass	0.095	1.4		0.011			0.084
Dry biomass	0.765	11.1	0.373	0.043	0.004	0.0005	0.320
Organic biomass	0.742	10.8		0.043	0.004	0.0005	0.320
Ash	0.023	0.3					
Total inputs	6.889	100.0	0.374	0.060	4.584	0.0005	1.846
Fraction of Total (%)	(100.00)		(5.42)	(0.87)	(66.53)	(0.007)	(26.79)
outputs							
Dry exit gas	6.328	91.9	0.374	7.50E-06	4.654		1.301
Water vapor from air humidity	0.059	0.9		0.007			0.053
Water vapor from biomass moisture	0.095	1.4		0.011			0.084
Water vapor from fuel hydrogen	0.384	5.6		0.043			0.341
Total water vapor	0.537	7.8		0.060			0.477
Unreacted carbon	0.000	0.0	0.000				
Vaporized inorganics	0.000	0.0					
Condensed phase inorganics	0.023	0.3					
Total inorganics	0.023	0.3					
Total condensed phase	0.023	0.3	0.000				
O2	0.304	4.4					0.304
CO2	1.365	19.8	0.373				0.993
CO	0.002	0.0	0.001				0.001
HC (as CH4)	2.99E-05	0.0	2.24E-05	7.50E-06			
NOx (as NO2)	0.004	0.1			0.001		0.003
SO2	5.30E-05	0.0				2.65E-05	2.65E-05
N2 (by difference)	4.653	67.5			4.653		
Total outputs	6.889	100.0	0.374	0.060	4.654	2.65E-05	1.778
Fraction of Total (%)	(100.00)		(5.42)	(0.87)	(67.55)	(0.000)	(25.81)
(Outputs - Inputs)	0.00E+00		5.55E-17	0.00E+00	7.01E-02	-4.33E-04	-6.74E-02
(Outputs/Inputs)	1.00000		1.00000	1.00000	1.01530	0.05774	0.96348

Table A4.f. Element Conversions, Emission Factors, and Stoichiometry from Measured Fuel Rate   **4a: Banagrass FC-P**

(Adjusted Air Rate)   =   303.7 L/min

	Natural Gas Background (mol %)	Natural Gas (Stoich) (g/s)	Combustion Air (g/s)	Net Biomass (g/s)	Emission Factor (Biomass) (% dry fuel)	Biomass Element Conversion (%)	Net Natural Gas	Net Biomass	Total
CO2		0	0.003	1.362	177.933	99.735			
CO				0.002	0.294	0.259			
HC (as CH4)				0.000	0.004	0.006			
NOx (as NO2)				0.004	0.529	33.584			
SO2				5.30E-05	0.007	5.774			

	Net Natural Gas	Net Biomass	Total
O2 for Natural gas combustion (g/s)	0		
Air for Natural gas combustion (g/s)	0		
Air for Biomass combustion (g/s d.b.)		5.970	
Air-Fuel Ratio (kg/kg, dry basis)		7.8	
Stoich. Air for Biomass (g/s d.b.)		4.4	
Stoich. Air-Fuel (kg/kg, dry basis)		5.7	
Equivalence ratio for Biomass (d.b.)		0.731	
Excess air for Biomass (% d.b.)		37	
Volumetric exit gas density (kg/m^3 d.b.)			0.3955
Total volumetric exit gas flowrate (m^3/s w.b.)			0.0183
Exit gas velocity (m/s)			1.00
Reynolds Number			968
Approximate residence time (s)			3.98

Anticipated Gas Compositions from Measured Fuel Rate   **4a: Banagrass FC-P**

(including major species only, dry basis)

	Inlet Air			Exit Gas			Measured
	Mass Flow (g/s)	Mass Fraction (%)	Mol Fraction (%)	Mass Flow (g/s)	Mass Fraction (%)	Mol Fraction (%)	Mol Fraction (%)
O2	1.387	23.229	20.946	0.373	5.900	5.651	4.60
CO2	0.003	0.053	0.035	1.369	21.638	15.069	15.00
N2	4.580	76.718	79.019	4.584	72.462	79.280	80.32
Total	5.970	100.000	100.000	6.326	100.000	100.000	99.917
Mol. Wt.		28.854			30.649		

Table A5.a. Mass and element balance 5b: Banagrass FC-Un

Measured Fuel Rate
(Unadjusted Air Rate)

	Mass Flowrate (g/s)	Mass Fractions (%)	Carbon Flowrate (g/s)	Hydrogen Flowrate (g/s)	Nitrogen Flowrate (g/s)	Sulfur Flowrate (g/s)	Oxygen Flowrate (g/s)
inputs							
Natural gas	0.000	0.0	0.000	0.000			
Dry air	8.575	89.3	0.001		6.578		1.995
Humidity in air	0.085	0.9		0.010			0.076
Moist biomass (as-fired)	0.940	9.8	0.397	0.058	0.005	0.0008	0.442
Moisture in biomass	0.113	1.2		0.013			0.100
Dry biomass	0.827	8.6	0.397	0.045	0.005	0.0008	0.342
Organic biomass	0.795	8.3		0.045	0.005	0.0008	0.342
Ash	0.033	0.3					
Total inputs	9.600	100.0	0.398	0.068	6.583	0.0008	2.512
Fraction of Total (%)	(100.00)		(4.15)	(0.70)	(68.58)	(0.009)	(26.17)
outputs							
Dry exit gas	8.963	93.4	0.531	6.50E-05	6.587		1.845
Water vapor from air humidity	0.085	0.9		0.010			0.076
Water vapor from biomass moisture	0.113	1.2		0.013			0.100
Water vapor from fuel hydrogen	0.406	4.2		0.045			0.361
Total water vapor	0.604	6.3		0.068			0.536
Unreacted carbon	0.000	0.0	0.000				
Vaporized inorganics	0.000	0.0					
Condensed phase inorganics	0.033	0.3					
Total inorganics	0.033	0.3					
Total condensed phase	0.033	0.3	0.000				
O2	0.431	4.5					0.431
CO2	1.934	20.1	0.528				1.406
CO	0.007	0.1	0.003				0.004
HC (as CH4)	2.58E-04	0.0	1.93E-04	6.50E-05			
NOx (as NO2)	0.005	0.1			0.002		0.004
SO2	2.06E-04	0.0				1.03E-04	1.03E-04
N2 (by difference)	6.586	68.6			6.586		
Total outputs	9.600	100.0	0.531	0.068	6.587	1.03E-04	2.381
Fraction of Total (%)	(100.00)		(5.53)	(0.70)	(68.62)	(0.001)	(24.80)
(Outputs - Inputs)	0.00E+00		1.33E-01	0.00E+00	4.37E-03	-7.24E-04	-1.32E-01
(Outputs/Inputs)	1.00000		1.33349	1.00000	1.00066	0.12487	0.94766

Table A5.b. Element Conversions, Emission Factors, and Stoichiometry from Measured Fuel Rate   **5b: Banagrass FC-Un**
(Unadjusted Air Rate)   =   436.2 L/min

	Natural Gas Background (mol %)	Natural Gas (Stoich) (g/s)	Combustion Air (g/s)	Net Biomass (g/s)	Emission Factor (Biomass) (% dry fuel)	Biomass Element Conversion (%)	Net Natural Gas	Net Biomass	Total
CO2		0	0.005	1.929	233.187	132.640			
CO				0.007	0.857	0.766			
HC (as CH4)				0.000	0.031	0.049			
NOx (as NO2)				0.005	0.626	31.740			
SO2				2.06E-04	0.025	12.487			

O2 for Natural gas combustion (g/s)	0	
Air for Natural gas combustion (g/s)	0	
Air for Biomass combustion (g/s d.b.)	8.575	
Air-Fuel Ratio (kg/kg, dry basis)	10.4	
Stoich. Air for Biomass (g/s d.b.)	4.6	
Stoich. Air-Fuel (kg/kg, dry basis)	5.6	
Equivalence ratio for Biomass (d.b.)	0.541	
Excess air for Biomass (% d.b.)	85	
Volumetric exit gas density (kg/m^3 d.b.)		0.3954
Total volumetric exit gas flowrate (m^3/s w.b.)		0.0253
Exit gas velocity (m/s)		1.38
Reynolds Number		1,336
Approximate residence time (s)		2.89

Anticipated Gas Compositions from Measured Fuel Rate   **5b: Banagrass FC-Un**
(including major species only, dry basis)

	Inlet Air				Exit Gas			Measured
	Mass Flow (g/s)	Mass Fraction (%)	Mol Fraction (%)		Mass Flow (g/s)	Mass Fraction (%)	Mol Fraction (%)	Mol Fraction (%)
O2	1.992	23.229	20.946		0.915	10.215	9.636	4.60
CO2	0.005	0.053	0.035		1.459	16.287	11.171	15.00
N2	6.578	76.718	79.019		6.583	73.497	79.193	80.27
Total	8.575	100.000	100.000		8.957	100.000	100.000	99.869
Mol. Wt.		28.854				30.184	.	

Table A5.c. Mass and element balance   5b: *Banagrass FC-Un*
Carbon Balance

	Mass Flowrate (g/s)	Mass Fractions (%)	Carbon Flowrate (g/s)	Hydrogen Flowrate (g/s)	Nitrogen Flowrate (g/s)	Sulfur Flowrate (g/s)	Oxygen Flowrate (g/s)
inputs							
Natural gas	0.000	0.0	0.000	0.000			
Dry air	8.575	86.3	0.001		6.578		1.995
Humidity in air	0.085	0.9		0.010			0.076
Moist biomass (as-fired)	1.274	12.8	0.538	0.079	0.007	0.0011	0.599
Moisture in biomass	0.153	1.5		0.017			0.136
Dry biomass	1.121	11.3	0.538	0.062	0.007	0.0011	0.463
Organic biomass	1.077	10.8		0.062	0.007	0.0011	0.463
Ash	0.044	0.4					
Total inputs	9.933	100.0	0.539	0.088	6.585	0.0011	2.669
Fraction of Total (%)	(100.00)		(5.43)	(0.89)	(66.29)	(0.011)	(26.87)
outputs							
Dry exit gas	9.101	91.6	0.539	6.59E-05	6.689		1.873
Water vapor from air humidity	0.085	0.9		0.010			0.076
Water vapor from biomass moisture	0.153	1.5		0.017			0.136
Water vapor from fuel hydrogen	0.550	5.5		0.062			0.489
Total water vapor	0.788	7.9		0.088			0.700
Unreacted carbon	0.000	0.0	0.000				
Vaporized inorganics	0.000	0.0					
Condensed phase inorganics	0.044	0.4					
Total inorganics	0.044	0.4					
Total condensed phase	0.044	0.4	0.000				
O2	0.438	4.4					0.438
CO2	1.963	19.8	0.536				1.427
CO	0.007	0.1	0.003				0.004
HC (as CH4)	2.62E-04	0.0	1.96E-04	6.59E-05			
NOx (as NO2)	0.005	0.1			0.002		0.004
SO2	2.10E-04	2.11E-03				1.05E-04	1.05E-04
N2 (by difference)	6.687	67.3			6.687		
Total outputs	9.933	100.0	0.539	0.088	6.689	1.05E-04	2.573
Fraction of Total (%)	(100.00)		(5.43)	(0.89)	(67.34)	(0.001)	(25.90)
(Outputs - Inputs)	0.00E+00		0.00E+00	0.00E+00	1.04E-01	-1.02E-03	-9.63E-02
(Outputs/Inputs)	1.00000		1.00000	1.00000	1.01578	0.09356	0.96394

Table A5.d. Element Conversions, Emission Factors, and Stoichiometry from Carbon Balance   5b: Banagrass FC-Un

	Natural Gas Background (mol %)	Natural Gas (Stoich) (g/s)	Air (g/s)	Net Biomass (g/s)	Emission Factor (Biomass) (% dry fuel)	Biomass Element Conversion (%)	Net Natural Gas	Net Biomass	Total
CO2		0	0.005	1.959	174.732	99.390			
CO				0.007	0.642	0.574			
HC (as CH4)				0.000	0.023	0.037			
NOx (as NO2)				0.005	0.469	23.783			
SO2				2.10E-04	0.019	9.356			

	Net Natural Gas	Net Biomass	Total
O2 for Natural gas combustion (g/s)	0		
Air for Natural gas combustion (g/s)	0		
Air for Biomass combustion (g/s d.b.)		8.575	
Biomass Air-Fuel Ratio (kg/kg, d.b.)		7.6	
Stoich. Air for Biomass (g/s d.b.)		6.3	
Stoich. Air-Fuel (kg/kg, dry basis)		5.6	
Equivalence ratio for Biomass (d.b.)		0.733	
Excess air for Biomass (% d.b.)		36	
Volumetric exit gas density (kg/m^3 d.b.)			0.3954
Total volumetric exit gas flowrate (m^3/s w.b.)			0.0264
Exit gas velocity (m/s)			1.45
Reynolds Number			1,396
Approximate residence time (s)			2.76

Anticipated Gas Compositions from Carbon Balance   5b: Banagrass FC-Un
(including major species only, dry basis)

	Inlet Air				Exit Gas			Measured
	Mass Flow (g/s)	Mass Fraction (%)	Mol Fraction (%)		Mass Flow (g/s)	Mass Fraction (%)	Mol Fraction (%)	Mol Fraction (%)
O2	1.992	23.229	20.946		0.533	5.857	5.612	4.60
CO2	0.005	0.053	0.035		1.975	21.723	15.133	15.00
N2	6.578	76.718	79.019		6.585	72.419	79.255	80.27
Total	8.575	100.000	100.000		9.093	100.000	100.000	99.869
Mol. Wt.		28.854				30.658		

Table A5.e. Mass and element balance   5b: Banagrass FC-Un

Measured Fuel Rate
(Adjusted Air Rate)

	Mass Flowrate (g/s)	Mass Fractions (%)	Carbon Flowrate (g/s)	Hydrogen Flowrate (g/s)	Nitrogen Flowrate (g/s)	Sulfur Flowrate (g/s)	Oxygen Flowrate (g/s)
inputs							
Natural gas	0.000	0.0	0.000	0.000			
Dry air	6.328	86.3	0.001		4.854		1.472
Humidity in air	0.063	0.9		0.007			0.056
Moist biomass (as-fired)	0.940	12.8	0.397	0.058	0.005	0.0008	0.442
Moisture in biomass	0.113	1.5		0.013			0.100
Dry biomass	0.827	11.3	0.397	0.045	0.005	0.0008	0.342
Organic biomass	0.795	10.8		0.045	0.005	0.0008	0.342
Ash	0.033	0.4					
Total inputs	7.330	100.0	0.398	0.065	4.859	0.0008	1.970
Fraction of Total (%)	(100.00)		(5.43)	(0.89)	(66.29)	(0.011)	(26.87)
outputs							
Dry exit gas	6.716	91.6	0.398	4.87E-05	4.936		1.382
Water vapor from air humidity	0.063	0.9		0.007			0.056
Water vapor from biomass moisture	0.113	1.5		0.013			0.100
Water vapor from fuel hydrogen	0.406	5.5		0.045			0.361
Total water vapor	0.582	7.9		0.065			0.517
Unreacted carbon	0.000	0.0	0.000				
Vaporized inorganics	0.000	0.0					
Condensed phase inorganics	0.033	0.4					
Total inorganics	0.033	0.4					
Total condensed phase	0.033	0.4	0.000				
O2	0.323	4.4					0.323
CO2	1.449	19.8	0.395				1.053
CO	0.005	0.1	0.002				0.003
HC (as CH4)	1.94E-04	0.0	1.45E-04	4.87E-05			
NOx (as NO2)	0.004	0.1			0.001		0.003
SO2	1.55E-04	0.0				7.74E-05	7.72E-05
N2 (by difference)	4.935	67.3			4.935		
Total outputs	7.330	100.0	0.398	0.065	4.936	7.74E-05	1.899
Fraction of Total (%)	(100.00)		(5.43)	(0.89)	(67.34)	(0.001)	(25.90)
(Outputs - Inputs)	0.00E+00		4.44E-16	-1.39E-17	7.67E-02	-7.50E-04	-7.10E-02
(Outputs/Inputs)	1.00000		1.00000	1.00000	1.01578	0.09356	0.96394

Table A5.f. Element Conversions, Emission Factors, and Stoichiometry from Measured Fuel Rate   **5b: Banagrass FC-Un**

(Adjusted Air Rate)   =   321.9 L/min

	Natural Gas Background (mol %)	Natural Gas (Stoich) (g/s)	Combustion Air (g/s)	Net Biomass (g/s)	Emission Factor (Biomass) (% dry fuel)	Biomass Element Conversion (%)	Net Natural Gas	Net Biomass	Total
CO2		0	0.003	1.445	174.732	99.390			
CO				0.005	0.642	0.574			
HC (as CH4)				0.000	0.023	0.037			
NOx (as NO2)				0.004	0.469	23.783			
SO2				1.55E-04	0.019	9.356			

O2 for Natural gas combustion (g/s)	0	
Air for Natural gas combustion (g/s)	0	
Air for Biomass combustion (g/s d.b.)		6.328
Air-Fuel Ratio (kg/kg, dry basis)		7.6
Stoich. Air for Biomass (g/s d.b.)		4.6
Stoich. Air-Fuel (kg/kg, dry basis)		5.6
Equivalence ratio for Biomass (d.b.)		0.733
Excess air for Biomass (% d.b.)		36
Volumetric exit gas density (kg/m^3 d.b.)		0.3954
Total volumetric exit gas flowrate (m^3/s w.b.)		0.0195
Exit gas velocity (m/s)		1.07
Reynolds Number		1,030
Approximate residence time (s)		3.75

Anticipated Gas Compositions from Measured Fuel Rate   **5b: Banagrass FC-Un**

(including major species only, dry basis)

	Inlet Air				Exit Gas			Measured
	Mass Flow (g/s)	Mass Fraction (%)	Mol Fraction (%)		Mass Flow (g/s)	Mass Fraction (%)	Mol Fraction (%)	Mol Fraction (%)
O2	1.470	23.229	20.946		0.393	5.857	5.612	4.60
CO2	0.003	0.053	0.035		1.458	21.723	15.133	15.00
N2	4.854	76.718	79.019		4.859	72.419	79.255	80.27
Total	6.328	100.000	100.000		6.710	100.000	100.000	99.869
Mol. Wt.		28.854				30.658		

Table B1. XRF Results, FC-PRP Lower Probe Deposit

Atomic Number	Analyte	Reported as Oxide	%	Reported as Element	%
11	Sodium	Na2O*	<0.01	Na*	<0.01
12	Magnesium	MgO*	3.43	Mg*	2.07
13	Aluminum	Al2O3	<0.01	Al	<0.01
14	Silicon	SiO2	38.24	Si	17.88
15	Phosphorus	P2O5	3.62	P	1.58
16	Sulfur	SO3	3.03	S	1.21
17	Chlorine	Cl	3.58	Cl	3.58
19	Potassium	K2O	18.80	K	15.60
20	Calcium	CaO	18.92	Ca	13.53
21	Scandium	Sc2O3	<0.01	Sc	<0.01
22	Titanium	TiO2	0.32	Ti	0.19
23	Vanadium	V2O5	0.01	V	<0.01
24	Chromium	Cr2O3	<0.01	Cr	<0.01
25	Manganese	MnO	0.98	Mn	0.76
26	Iron	Fe2O3	2.20	Fe	1.54
27	Cobalt	CoO	0.01	Co	<0.01
28	Nickel	NiO	0.04	Ni	0.03
29	Copper	CuO	0.05	Cu	0.04
30	Zinc	ZnO	0.03	Zn	0.03
31	Gallium	GaO	<0.01	Ga	<0.01
32	Germanium	GeO2	<0.01	Ge	<0.01
33	Arsenic	As2O3	<0.01	As	<0.01
34	Selenium	SeO2	<0.01	Se	<0.01
35	Bromine	Br	0.03	Br	0.03
37	Rubidium	Rb2O	<0.01	Rb	<0.01
38	Strontium	SrO	0.05	Sr	0.04
39	Yttrium	Y2O3	<0.01	Y	<0.01
40	Zirconium	ZrO2	<0.01	Zr	<0.01
41	Niobium	Nb2O5	<0.01	Nb	<0.01
42	Molybdenum	MoO2	<0.01	Mo	<0.01
72	Hafnium	HfO2*	<0.01	Hf*	<0.01
74	Tungsten	WO3	<0.01	W	<0.01
77	Iridium	IrO2*	<0.01	Ir*	<0.01
80	Mercury	Hg2O*	<0.01	Hg*	<0.01
81	Thallium	Tl2O	<0.01	Tl	<0.01
82	Lead	PbO	0.01	Pb	0.01
83	Bismuth	BiO3	<0.01	Bi	<0.01
47	Silver	Ag2O	<0.01	Ag	<0.01
48	Cadmium	CdO	<0.01	Cd	<0.01
49	Indium	In2O3	<0.01	In	<0.01
50	Tin	SnO	<0.01	Sn	<0.01
51	Antimony	Sb2O3	<0.01	Sb	<0.01
52	Tellurium	TeO2	<0.01	Te	<0.01
53	Iodine	I	<0.01	I	<0.01
56	Barium	BaO	0.01	Ba	0.01
57	Lanthanum	La2O3	<0.01	La	<0.01
58	Cerium	Ce2O3	<0.01	Ce	<0.01
90	Thorium	ThO2	<0.01	Th	<0.01
92	Uranium	U2O3	<0.01	U	<0.01

*not generally considered reliable.

Table B2. XRF Results, JC-PRP Upper Probe Deposit

Atomic Number	Analyte	Reported as Oxide	%	Reported as Element	%
11	Sodium	Na2O*	<0.01	Na*	<0.01
12	Magnesium	MgO*	1.59	Mg*	0.96
13	Aluminum	Al2O3	<0.01	Al	<0.01
14	Silicon	SiO2	66.02	Si	30.86
15	Phosphorus	P2O5	1.15	P	0.50
16	Sulfur	SO3	1.68	S	0.67
17	Chlorine	Cl	0.49	Cl	0.49
19	Potassium	K2O	7.34	K	6.09
20	Calcium	CaO	15.91	Ca	11.37
21	Scandium	Sc2O3	<0.01	Sc	<0.01
22	Titanium	TiO2	0.18	Ti	0.11
23	Vanadium	V2O5	<0.01	V	<0.01
24	Chromium	Cr2O3	<0.01	Cr	<0.01
25	Manganese	MnO	0.62	Mn	0.48
26	Iron	Fe2O3	1.34	Fe	0.94
27	Cobalt	CoO	0.01	Co	0.01
28	Nickel	NiO	0.02	Ni	0.01
29	Copper	CuO	0.03	Cu	0.02
30	Zinc	ZnO	0.02	Zn	0.02
31	Gallium	GaO	<0.01	Ga	<0.01
32	Germanium	GeO2	<0.01	Ge	<0.01
33	Arsenic	As2O3	<0.01	As	<0.01
34	Selenium	SeO2	<0.01	Se	<0.01
35	Bromine	Br	0.02	Br	0.02
37	Rubidium	Rb2O	<0.01	Rb	<0.01
38	Strontium	SrO	0.10	Sr	0.09
39	Yttrium	Y2O3	<0.01	Y	<0.01
40	Zirconium	ZrO2	<0.01	Zr	<0.01
41	Niobium	Nb2O5	<0.01	Nb	<0.01
42	Molybdenum	MoO2	<0.01	Mo	<0.01
72	Hafnium	HfO2*	<0.01	Hf*	<0.01
74	Tungsten	WO3	<0.01	W	<0.01
77	Iridium	IrO2*	<0.01	Ir*	<0.01
80	Mercury	Hg2O*	<0.01	Hg*	<0.01
81	Thallium	Tl2O	<0.01	Tl	<0.01
82	Lead	PbO	<0.01	Pb	<0.01
83	Bismuth	BiO3	0.01	Bi	<0.01
47	Silver	Ag2O	<0.01	Ag	<0.01
48	Cadmium	CdO	<0.01	Cd	<0.01
49	Indium	In2O3	<0.01	In	<0.01
50	Tin	SnO	<0.01	Sn	<0.01
51	Antimony	Sb2O3	<0.01	Sb	<0.01
52	Tellurium	TeO2	<0.01	Te	<0.01
53	Iodine	I	<0.01	I	<0.01
56	Barium	BaO	0.02	Ba	0.02
57	Lanthanum	La2O3	<0.01	La	<0.01
58	Cerium	Ce2O3	<0.01	Ce	<0.01
90	Thorium	ThO2	<0.01	Th	<0.01
92	Uranium	U2O3	<0.01	U	<0.01

*not generally considered reliable.

Table B3. XRF Results, Bagasse Upper Probe Deposit

Atomic Number	Analyte	Reported as Oxide	%	Reported as Element	%
11	Sodium	Na2O*	1.69	Na*	1.26
12	Magnesium	MgO*	2.44	Mg*	1.47
13	Aluminum	Al2O3	10.98	Al	5.81
14	Silicon	SiO2	35.70	Si	16.69
15	Phosphorus	P2O5	1.11	P	0.48
16	Sulfur	SO3	0.51	S	0.21
17	Chlorine	Cl	<0.01	Cl	<0.01
19	Potassium	K2O	4.04	K	3.35
20	Calcium	CaO	2.61	Ca	1.86
21	Scandium	Sc2O3	<0.01	Sc	<0.01
22	Titanium	TiO2	5.12	Ti	3.07
23	Vanadium	V2O5	0.14	V	0.08
24	Chromium	Cr2O3	0.11	Cr	0.08
25	Manganese	MnO	1.45	Mn	1.12
26	Iron	Fe2O3	33.47	Fe	23.41
27	Cobalt	CoO	0.13	Co	0.10
28	Nickel	NiO	0.12	Ni	0.10
29	Copper	CuO	0.08	Cu	0.07
30	Zinc	ZnO	0.08	Zn	0.06
31	Gallium	GaO	<0.01	Ga	<0.01
32	Germanium	GeO2	<0.01	Ge	<0.01
33	Arsenic	As2O3	<0.01	As	<0.01
34	Selenium	SeO2	<0.01	Se	<0.01
35	Bromine	Br	<0.01	Br	<0.01
37	Rubidium	Rb2O	0.02	Rb	0.01
38	Strontium	SrO	0.04	Sr	0.04
39	Yttrium	Y2O3	0.01	Y	<0.01
40	Zirconium	ZrO2	0.07	Zr	0.05
41	Niobium	Nb2O5	<0.01	Nb	<0.01
42	Molybdenum	MoO2	<0.01	Mo	<0.01
72	Hafnium	HfO2*	<0.01	Hf*	<0.01
74	Tungsten	WO3	<0.01	W	<0.01
77	Iridium	IrO2*	<0.01	Ir*	<0.01
80	Mercury	Hg2O*	<0.01	Hg*	<0.01
81	Thallium	Tl2O	<0.01	Tl	<0.01
82	Lead	PbO	<0.01	Pb	<0.01
83	Bismuth	BiO3	<0.01	Bi	<0.01
47	Silver	Ag2O	<0.01	Ag	<0.01
48	Cadmium	CdO	<0.01	Cd	<0.01
49	Indium	In2O3	<0.01	In	<0.01
50	Tin	SnO	<0.01	Sn	<0.01
51	Antimony	Sb2O3	<0.01	Sb	<0.01
52	Tellurium	TeO2	<0.01	Te	<0.01
53	Iodine	I	<0.01	I	<0.01
56	Barium	BaO	0.02	Ba	0.02
57	Lanthanum	La2O3	<0.01	La	<0.01
58	Cerium	Ce2O3	0.01	Ce	0.01
90	Thorium	ThO2	<0.01	Th	<0.01
92	Uranium	U2O3	<0.01	U	<0.01

*not generally considered reliable.

Table B4. XRF Results, FC-P Upper Probe Deposit

Atomic Number	Analyte	Reported as Oxide	%	Reported as Element	%
11	Sodium	Na2O*	<0.01	Na*	<0.01
12	Magnesium	MgO*	4.08	Mg*	2.46
13	Aluminum	Al2O3	<0.01	Al	<0.01
14	Silicon	SiO2	41.26	Si	19.29
15	Phosphorus	P2O5	2.85	P	1.25
16	Sulfur	SO3	2.60	S	1.04
17	Chlorine	Cl	3.68	Cl	3.68
19	Potassium	K2O	17.84	K	14.81
20	Calcium	CaO	11.13	Ca	7.96
21	Scandium	Sc2O3	<0.01	Sc	<0.01
22	Titanium	TiO2	0.86	Ti	0.52
23	Vanadium	V2O5	0.02	V	0.01
24	Chromium	Cr2O3	0.02	Cr	0.01
25	Manganese	MnO	0.95	Mn	0.74
26	Iron	Fe2O3	5.31	Fe	3.72
27	Cobalt	CoO	0.02	Co	0.02
28	Nickel	NiO	0.04	Ni	0.03
29	Copper	CuO	0.05	Cu	0.04
30	Zinc	ZnO	0.05	Zn	0.04
31	Gallium	GaO	<0.01	Ga	<0.01
32	Germanium	GeO2	<0.01	Ge	<0.01
33	Arsenic	As2O3	<0.01	As	<0.01
34	Selenium	SeO2	<0.01	Se	<0.01
35	Bromine	Br	0.09	Br	0.09
37	Rubidium	Rb2O	0.02	Rb	0.02
38	Strontium	SrO	0.11	Sr	0.09
39	Yttrium	Y2O3	<0.01	Y	<0.01
40	Zirconium	ZrO2	<0.01	Zr	<0.01
41	Niobium	Nb2O5	<0.01	Nb	<0.01
42	Molybdenum	MoO2	<0.01	Mo	<0.01
72	Hafnium	HfO2*	<0.01	Hf*	<0.01
74	Tungsten	WO3	<0.01	W	<0.01
77	Iridium	IrO2*	<0.01	Ir*	<0.01
80	Mercury	Hg2O*	<0.01	Hg*	<0.01
81	Thallium	Tl2O	<0.01	Tl	<0.01
82	Lead	PbO	0.01	Pb	<0.01
83	Bismuth	BiO3	0.02	Bi	0.02
47	Silver	Ag2O	<0.01	Ag	<0.01
48	Cadmium	CdO	<0.01	Cd	<0.01
49	Indium	In2O3	<0.01	In	<0.01
50	Tin	SnO	<0.01	Sn	<0.01
51	Antimony	Sb2O3	<0.01	Sb	<0.01
52	Tellurium	TeO2	<0.01	Te	<0.01
53	Iodine	I	<0.01	I	<0.01
56	Barium	BaO	0.05	Ba	0.05
57	Lanthanum	La2O3	<0.01	La	<0.01
58	Cerium	Ce2O3	<0.01	Ce	<0.01
90	Thorium	ThO2	<0.01	Th	<0.01
92	Uranium	U2O3	<0.01	U	<0.01

*not generally considered reliable.

Table B5. XRF Results, FC-Untreated Lower Probe Deposit

Atomic Number	Analyte	Reported as Oxide	%	Reported as Element	%
11	Sodium	Na2O*	0.14	Na*	0.10
12	Magnesium	MgO*	2.88	Mg*	1.73
13	Aluminum	Al2O3	<0.01	Al	<0.01
14	Silicon	SiO2	24.45	Si	11.43
15	Phosphorus	P2O5	2.96	P	1.29
16	Sulfur	SO3	1.93	S	0.77
17	Chlorine	Cl	6.71	Cl	6.71
19	Potassium	K2O	28.89	K	23.97
20	Calcium	CaO	12.95	Ca	9.26
21	Scandium	Sc2O3	<0.01	Sc	<0.01
22	Titanium	TiO2	0.48	Ti	0.29
23	Vanadium	V2O5	0.02	V	<0.01
24	Chromium	Cr2O3	0.06	Cr	0.04
25	Manganese	MnO	1.33	Mn	1.03
26	Iron	Fe2O3	3.45	Fe	2.41
27	Cobalt	CoO	0.01	Co	<0.01
28	Nickel	NiO	0.07	Ni	0.05
29	Copper	CuO	0.06	Cu	0.05
30	Zinc	ZnO	0.07	Zn	0.06
31	Gallium	GaO	<0.01	Ga	<0.01
32	Germanium	GeO2	<0.01	Ge	<0.01
33	Arsenic	As2O3	<0.01	As	<0.01
34	Selenium	SeO2	<0.01	Se	<0.01
35	Bromine	Br	0.14	Br	0.14
37	Rubidium	Rb2O	0.03	Rb	0.03
38	Strontium	SrO	0.10	Sr	0.09
39	Yttrium	Y2O3	<0.01	Y	<0.01
40	Zirconium	ZrO2	<0.01	Zr	<0.01
41	Niobium	Nb2O5	<0.01	Nb	<0.01
42	Molybdenum	MoO2	<0.01	Mo	<0.01
72	Hafnium	HfO2*	<0.01	Hf*	<0.01
74	Tungsten	WO3	<0.01	W	<0.01
77	Iridium	IrO2*	<0.01	Ir*	<0.01
80	Mercury	Hg2O*	<0.01	Hg*	<0.01
81	Thallium	Tl2O	<0.01	Tl	<0.01
82	Lead	PbO	<0.01	Pb	<0.01
83	Bismuth	BiO3	0.03	Bi	0.03
47	Silver	Ag2O	<0.01	Ag	<0.01
48	Cadmium	CdO	<0.01	Cd	<0.01
49	Indium	In2O3	<0.01	In	<0.01
50	Tin	SnO	<0.01	Sn	<0.01
51	Antimony	Sb2O3	<0.01	Sb	<0.01
52	Tellurium	TeO2	<0.01	Te	<0.01
53	Iodine	I	<0.01	I	<0.01
56	Barium	BaO	0.03	Ba	0.02
57	Lanthanum	La2O3	<0.01	La	<0.01
58	Cerium	Ce2O3	<0.01	Ce	<0.01
90	Thorium	ThO2	<0.01	Th	<0.01
92	Uranium	U2O3	<0.01	U	<0.01

*not generally considered reliable.

Table B6. XRF Results, FC-Untreated Upper Probe Deposit

Atomic Number	Analyte	Reported as Oxide	%	Reported as Element	%
11	Sodium	Na2O*	<0.01	Na*	<0.01
12	Magnesium	MgO*	4.28	Mg*	2.58
13	Aluminum	Al2O3	<0.01	Al	<0.01
14	Silicon	SiO2	30.67	Si	14.34
15	Phosphorus	P2O5	3.13	P	1.37
16	Sulfur	SO3	2.47	S	0.99
17	Chlorine	Cl	5.02	Cl	5.02
19	Potassium	K2O	25.18	K	20.90
20	Calcium	CaO	10.77	Ca	7.70
21	Scandium	Sc2O3	<0.01	Sc	<0.01
22	Titanium	TiO2	0.22	Ti	0.13
23	Vanadium	V2O5	0.01	V	<0.01
24	Chromium	Cr2O3	<0.01	Cr	<0.01
25	Manganese	MnO	0.97	Mn	0.75
26	Iron	Fe2O3	1.72	Fe	1.20
27	Cobalt	CoO	<0.01	Co	<0.01
28	Nickel	NiO	0.04	Ni	0.03
29	Copper	CuO	0.05	Cu	0.04
30	Zinc	ZnO	0.04	Zn	0.03
31	Gallium	GaO	<0.01	Ga	<0.01
32	Germanium	GeO2	<0.01	Ge	<0.01
33	Arsenic	As2O3	<0.01	As	<0.01
34	Selenium	SeO2	<0.01	Se	<0.01
35	Bromine	Br	0.13	Br	0.13
37	Rubidium	Rb2O	0.03	Rb	0.03
38	Strontium	SrO	0.10	Sr	0.09
39	Yttrium	Y2O3	<0.01	Y	<0.01
40	Zirconium	ZrO2	<0.01	Zr	<0.01
41	Niobium	Nb2O5	<0.01	Nb	<0.01
42	Molybdenum	MoO2	<0.01	Mo	<0.01
72	Hafnium	HfO2*	<0.01	Hf*	<0.01
74	Tungsten	WO3	<0.01	W	<0.01
77	Iridium	IrO2*	<0.01	Ir*	<0.01
80	Mercury	Hg2O*	<0.01	Hg*	<0.01
81	Thallium	Tl2O	<0.01	Tl	<0.01
82	Lead	PbO	0.01	Pb	<0.01
83	Bismuth	BiO3	0.02	Bi	0.02
47	Silver	Ag2O	<0.01	Ag	<0.01
48	Cadmium	CdO	<0.01	Cd	<0.01
49	Indium	In2O3	<0.01	In	<0.01
50	Tin	SnO	<0.01	Sn	<0.01
51	Antimony	Sb2O3	<0.01	Sb	<0.01
52	Tellurium	TeO2	<0.01	Te	<0.01
53	Iodine	I	<0.01	I	<0.01
56	Barium	BaO	0.04	Ba	0.04
57	Lanthanum	La2O3	<0.01	La	<0.01
58	Cerium	Ce2O3	<0.01	Ce	<0.01
90	Thorium	ThO2	<0.01	Th	<0.01
92	Uranium	U2O3	<0.01	U	<0.01

*not generally considered reliable.

Table B7. XRF Results, FC-PRP Flyash

Atomic Number	Analyte	Reported as Oxide	%	Reported as Element	%
11	Sodium	Na2O*	<0.01	Na*	<0.01
12	Magnesium	MgO*	1.67	Mg*	1.01
13	Aluminum	Al2O3	<0.01	Al	<0.01
14	Silicon	SiO2	24.10	Si	11.27
15	Phosphorus	P2O5	1.53	P	0.67
16	Sulfur	SO3	0.36	S	0.14
17	Chlorine	Cl	0.07	Cl	0.07
19	Potassium	K2O	6.20	K	5.15
20	Calcium	CaO	9.31	Ca	6.65
21	Scandium	Sc2O3	<0.01	Sc	<0.01
22	Titanium	TiO2	0.15	Ti	0.09
23	Vanadium	V2O5	<0.01	V	<0.01
24	Chromium	Cr2O3	0.02	Cr	0.01
25	Manganese	MnO	0.38	Mn	0.30
26	Iron	Fe2O3	0.51	Fe	0.36
27	Cobalt	CoO	<0.01	Co	<0.01
28	Nickel	NiO	0.01	Ni	<0.01
29	Copper	CuO	0.02	Cu	0.02
30	Zinc	ZnO	<0.01	Zn	<0.01
31	Gallium	GaO	<0.01	Ga	<0.01
32	Germanium	GeO2	<0.01	Ge	<0.01
33	Arsenic	As2O3	<0.01	As	<0.01
34	Selenium	SeO2	<0.01	Se	<0.01
35	Bromine	Br	<0.01	Br	<0.01
37	Rubidium	Rb2O	<0.01	Rb	<0.01
38	Strontium	SrO	0.01	Sr	0.01
39	Yttrium	Y2O3	<0.01	Y	<0.01
40	Zirconium	ZrO2	<0.01	Zr	<0.01
41	Niobium	Nb2O5	<0.01	Nb	<0.01
42	Molybdenum	MoO2	<0.01	Mo	<0.01
72	Hafnium	HfO2*	<0.01	Hf*	<0.01
74	Tungsten	WO3	<0.01	W	<0.01
77	Iridium	IrO2*	<0.01	Ir*	<0.01
80	Mercury	Hg2O*	<0.01	Hg*	<0.01
81	Thallium	Tl2O	<0.01	Tl	<0.01
82	Lead	PbO	<0.01	Pb	<0.01
83	Bismuth	BiO3	<0.01	Bi	<0.01
47	Silver	Ag2O	<0.01	Ag	<0.01
48	Cadmium	CdO	<0.01	Cd	<0.01
49	Indium	In2O3	<0.01	In	<0.01
50	Tin	SnO	<0.01	Sn	<0.01
51	Antimony	Sb2O3	<0.01	Sb	<0.01
52	Tellurium	TeO2	<0.01	Te	<0.01
53	Iodine	I	<0.01	I	<0.01
56	Barium	BaO	<0.01	Ba	<0.01
57	Lanthanum	La2O3	<0.01	La	<0.01
58	Cerium	Ce2O3	<0.01	Ce	<0.01
90	Thorium	ThO2	<0.01	Th	<0.01
92	Uranium	U2O3	<0.01	U	<0.01

*not generally considered reliable.

Table B8. XRF Results, JC-PRP Flyash

Atomic Number	Analyte	Reported as Oxide	%	Reported as Element	%
11	Sodium	Na2O*	0.22	Na*	0.16
12	Magnesium	MgO*	0.97	Mg*	0.59
13	Aluminum	Al2O3	<0.01	Al	<0.01
14	Silicon	SiO2	39.80	Si	18.61
15	Phosphorus	P2O5	0.70	P	0.31
16	Sulfur	SO3	0.38	S	0.15
17	Chlorine	Cl	0.07	Cl	0.07
19	Potassium	K2O	4.57	K	3.80
20	Calcium	CaO	10.85	Ca	7.75
21	Scandium	Sc2O3	<0.01	Sc	<0.01
22	Titanium	TiO2	0.08	Ti	0.05
23	Vanadium	V2O5	<0.01	V	<0.01
24	Chromium	Cr2O3	<0.01	Cr	<0.01
25	Manganese	MnO	0.45	Mn	0.35
26	Iron	Fe2O3	0.63	Fe	0.44
27	Cobalt	CoO	<0.01	Co	<0.01
28	Nickel	NiO	0.01	Ni	<0.01
29	Copper	CuO	0.04	Cu	0.03
30	Zinc	ZnO	0.02	Zn	0.01
31	Gallium	GaO	<0.01	Ga	<0.01
32	Germanium	GeO2	<0.01	Ge	<0.01
33	Arsenic	As2O3	<0.01	As	<0.01
34	Selenium	SeO2	<0.01	Se	<0.01
35	Bromine	Br	<0.01	Br	<0.01
37	Rubidium	Rb2O	<0.01	Rb	<0.01
38	Strontium	SrO	0.11	Sr	0.09
39	Yttrium	Y2O3	<0.01	Y	<0.01
40	Zirconium	ZrO2	<0.01	Zr	<0.01
41	Niobium	Nb2O5	<0.01	Nb	<0.01
42	Molybdenum	MoO2	<0.01	Mo	<0.01
72	Hafnium	HfO2*	<0.01	Hf*	<0.01
74	Tungsten	WO3	<0.01	W	<0.01
77	Iridium	IrO2*	<0.01	Ir*	<0.01
80	Mercury	Hg2O*	<0.01	Hg*	<0.01
81	Thallium	Tl2O	<0.01	Tl	<0.01
82	Lead	PbO	<0.01	Pb	<0.01
83	Bismuth	BiO3	<0.01	Bi	<0.01
47	Silver	Ag2O	<0.01	Ag	<0.01
48	Cadmium	CdO	<0.01	Cd	<0.01
49	Indium	In2O3	<0.01	In	<0.01
50	Tin	SnO	<0.01	Sn	<0.01
51	Antimony	Sb2O3	<0.01	Sb	<0.01
52	Tellurium	TeO2	<0.01	Te	<0.01
53	Iodine	I	<0.01	I	<0.01
56	Barium	BaO	0.03	Ba	0.03
57	Lanthanum	La2O3	<0.01	La	<0.01
58	Cerium	Ce2O3	<0.01	Ce	<0.01
90	Thorium	ThO2	<0.01	Th	<0.01
92	Uranium	U2O3	<0.01	U	<0.01

*not generally considered reliable.

Table B9. XRF Results, Bagasse Flyash

Atomic Number	Analyte	Reported as Oxide	%	Reported as Element	%
11	Sodium	Na2O*	1.48	Na*	1.10
12	Magnesium	MgO*	2.16	Mg*	1.31
13	Aluminum	Al2O3	11.96	Al	6.33
14	Silicon	SiO2	45.22	Si	21.14
15	Phosphorus	P2O5	0.88	P	0.38
16	Sulfur	SO3	0.18	S	0.07
17	Chlorine	Cl	0.01	Cl	0.01
19	Potassium	K2O	2.75	K	2.28
20	Calcium	CaO	2.92	Ca	2.08
21	Scandium	Sc2O3	<0.01	Sc	<0.01
22	Titanium	TiO2	3.85	Ti	2.31
23	Vanadium	V2O5	0.10	V	0.05
24	Chromium	Cr2O3	0.09	Cr	0.06
25	Manganese	MnO	1.10	Mn	0.86
26	Iron	Fe2O3	25.90	Fe	18.11
27	Cobalt	CoO	0.11	Co	0.09
28	Nickel	NiO	0.10	Ni	0.08
29	Copper	CuO	0.06	Cu	0.05
30	Zinc	ZnO	0.04	Zn	0.03
31	Gallium	GaO	<0.01	Ga	<0.01
32	Germanium	GeO2	<0.01	Ge	<0.01
33	Arsenic	As2O3	<0.01	As	<0.01
34	Selenium	SeO2	<0.01	Se	<0.01
35	Bromine	Br	<0.01	Br	<0.01
37	Rubidium	Rb2O	<0.01	Rb	<0.01
38	Strontium	SrO	0.04	Sr	0.03
39	Yttrium	Y2O3	<0.01	Y	<0.01
40	Zirconium	ZrO2	0.08	Zr	0.06
41	Niobium	Nb2O5	<0.01	Nb	<0.01
42	Molybdenum	MoO2	<0.01	Mo	<0.01
72	Hafnium	HfO2*	0.01	Hf*	0.01
74	Tungsten	WO3	<0.01	W	<0.01
77	Iridium	IrO2*	<0.01	Ir*	<0.01
80	Mercury	Hg2O*	<0.01	Hg*	<0.01
81	Thallium	Tl2O	<0.01	Tl	<0.01
82	Lead	PbO	<0.01	Pb	<0.01
83	Bismuth	BiO3	<0.01	Bi	<0.01
47	Silver	Ag2O	<0.01	Ag	<0.01
48	Cadmium	CdO	<0.01	Cd	<0.01
49	Indium	In2O3	<0.01	In	<0.01
50	Tin	SnO	<0.01	Sn	<0.01
51	Antimony	Sb2O3	<0.01	Sb	<0.01
52	Tellurium	TeO2	<0.01	Te	<0.01
53	Iodine	I	<0.01	I	<0.01
56	Barium	BaO	0.08	Ba	0.07
57	Lanthanum	La2O3	0.01	La	<0.01
58	Cerium	Ce2O3	0.05	Ce	0.04
90	Thorium	ThO2	<0.01	Th	<0.01
92	Uranium	U2O3	<0.01	U	<0.01

*not generally considered reliable.

Table B10. XRF Results, FC-P Flyash

Atomic Number	Analyte	Reported as Oxide	%	Reported as Element	%
11	Sodium	Na2O*	<0.01	Na*	<0.01
12	Magnesium	MgO*	3.74	Mg*	2.26
13	Aluminum	Al2O3	<0.01	Al	<0.01
14	Silicon	SiO2	42.96	Si	20.09
15	Phosphorus	P2O5	2.78	P	1.21
16	Sulfur	SO3	0.98	S	0.39
17	Chlorine	Cl	0.45	Cl	0.45
19	Potassium	K2O	15.86	K	13.16
20	Calcium	CaO	12.36	Ca	8.83
21	Scandium	Sc2O3	<0.01	Sc	<0.01
22	Titanium	TiO2	0.25	Ti	0.15
23	Vanadium	V2O5	0.01	V	<0.01
24	Chromium	Cr2O3	0.01	Cr	<0.01
25	Manganese	MnO	0.90	Mn	0.70
26	Iron	Fe2O3	1.69	Fe	1.18
27	Cobalt	CoO	0.01	Co	<0.01
28	Nickel	NiO	0.03	Ni	0.02
29	Copper	CuO	0.05	Cu	0.04
30	Zinc	ZnO	0.03	Zn	0.02
31	Gallium	GaO	<0.01	Ga	<0.01
32	Germanium	GeO2	<0.01	Ge	<0.01
33	Arsenic	As2O3	<0.01	As	<0.01
34	Selenium	SeO2	<0.01	Se	<0.01
35	Bromine	Br	0.01	Br	0.01
37	Rubidium	Rb2O	0.02	Rb	0.02
38	Strontium	SrO	0.12	Sr	0.10
39	Yttrium	Y2O3	<0.01	Y	<0.01
40	Zirconium	ZrO2	<0.01	Zr	<0.01
41	Niobium	Nb2O5	<0.01	Nb	<0.01
42	Molybdenum	MoO2	<0.01	Mo	<0.01
72	Hafnium	HfO2*	<0.01	Hf*	<0.01
74	Tungsten	WO3	<0.01	W	<0.01
77	Iridium	IrO2*	<0.01	Ir*	<0.01
80	Mercury	Hg2O*	<0.01	Hg*	<0.01
81	Thallium	Tl2O	<0.01	Tl	<0.01
82	Lead	PbO	<0.01	Pb	<0.01
83	Bismuth	BiO3	0.01	Bi	0.01
47	Silver	Ag2O	<0.01	Ag	<0.01
48	Cadmium	CdO	<0.01	Cd	<0.01
49	Indium	In2O3	<0.01	In	<0.01
50	Tin	SnO	<0.01	Sn	<0.01
51	Antimony	Sb2O3	<0.01	Sb	<0.01
52	Tellurium	TeO2	<0.01	Te	<0.01
53	Iodine	I	<0.01	I	<0.01
56	Barium	BaO	0.06	Ba	0.05
57	Lanthanum	La2O3	<0.01	La	<0.01
58	Cerium	Ce2O3	<0.01	Ce	<0.01
90	Thorium	ThO2	<0.01	Th	<0.01
92	Uranium	U2O3	<0.01	U	<0.01

*not generally considered reliable.

Table B11. XRF Results, FC-Untreated Flyash

Atomic Number	Analyte	Reported as Oxide	%	Reported as Element	%
11	Sodium	Na2O*	0.11	Na*	0.08
12	Magnesium	MgO*	4.84	Mg*	2.92
13	Aluminum	Al2O3	<0.01	Al	<0.01
14	Silicon	SiO2	35.98	Si	16.82
15	Phosphorus	P2O5	3.28	P	1.43
16	Sulfur	SO3	0.95	S	0.38
17	Chlorine	Cl	0.55	Cl	0.55
19	Potassium	K2O	21.45	K	17.80
20	Calcium	CaO	11.98	Ca	8.56
21	Scandium	Sc2O3	<0.01	Sc	<0.01
22	Titanium	TiO2	0.22	Ti	0.13
23	Vanadium	V2O5	<0.01	V	<0.01
24	Chromium	Cr2O3	<0.01	Cr	<0.01
25	Manganese	MnO	1.02	Mn	0.79
26	Iron	Fe2O3	1.46	Fe	1.02
27	Cobalt	CoO	0.01	Co	0.01
28	Nickel	NiO	0.04	Ni	0.03
29	Copper	CuO	0.05	Cu	0.04
30	Zinc	ZnO	0.03	Zn	0.02
31	Gallium	GaO	<0.01	Ga	<0.01
32	Germanium	GeO2	<0.01	Ge	<0.01
33	Arsenic	As2O3	<0.01	As	<0.01
34	Selenium	SeO2	<0.01	Se	<0.01
35	Bromine	Br	0.01	Br	0.01
37	Rubidium	Rb2O	0.02	Rb	0.02
38	Strontium	SrO	0.12	Sr	0.10
39	Yttrium	Y2O3	<0.01	Y	<0.01
40	Zirconium	ZrO2	<0.01	Zr	<0.01
41	Niobium	Nb2O5	<0.01	Nb	<0.01
42	Molybdenum	MoO2	<0.01	Mo	<0.01
72	Hafnium	HfO2*	<0.01	Hf*	<0.01
74	Tungsten	WO3	<0.01	W	<0.01
77	Iridium	IrO2*	<0.01	Ir*	<0.01
80	Mercury	Hg2O*	<0.01	Hg*	<0.01
81	Thallium	Tl2O	<0.01	Tl	<0.01
82	Lead	PbO	<0.01	Pb	<0.01
83	Bismuth	BiO3	0.02	Bi	0.01
47	Silver	Ag2O	<0.01	Ag	<0.01
48	Cadmium	CdO	<0.01	Cd	<0.01
49	Indium	In2O3	<0.01	In	<0.01
50	Tin	SnO	<0.01	Sn	<0.01
51	Antimony	Sb2O3	<0.01	Sb	<0.01
52	Tellurium	TeO2	<0.01	Te	<0.01
53	Iodine	I	<0.01	I	<0.01
56	Barium	BaO	0.06	Ba	0.05
57	Lanthanum	La2O3	<0.01	La	<0.01
58	Cerium	Ce2O3	<0.01	Ce	<0.01
90	Thorium	ThO2	<0.01	Th	<0.01
92	Uranium	U2O3	<0.01	U	<0.01

*not generally considered reliable.

Table B12. XRF Results, Bagasse Gas Filter

Atomic Number	Analyte	Reported as Oxide	%	Reported as Element	%
11	Sodium	Na2O*	2.38	Na*	1.77
12	Magnesium	MgO*	1.54	Mg*	0.93
13	Aluminum	Al2O3	11.77	Al	6.23
14	Silicon	SiO2	44.54	Si	20.82
15	Phosphorus	P2O5	1.52	P	0.66
16	Sulfur	SO3	0.52	S	0.21
17	Chlorine	Cl	0.62	Cl	0.62
19	Potassium	K2O	5.74	K	4.77
20	Calcium	CaO	2.09	Ca	1.50
21	Scandium	Sc2O3	<0.01	Sc	<0.01
22	Titanium	TiO2	4.40	Ti	2.64
23	Vanadium	V2O5	0.09	V	0.05
24	Chromium	Cr2O3	0.05	Cr	0.03
25	Manganese	MnO	0.77	Mn	0.60
26	Iron	Fe2O3	21.23	Fe	14.85
27	Cobalt	CoO	0.09	Co	0.07
28	Nickel	NiO	0.07	Ni	0.06
29	Copper	CuO	0.07	Cu	0.06
30	Zinc	ZnO	0.17	Zn	0.13
31	Gallium	GaO	<0.01	Ga	<0.01
32	Germanium	GeO2	<0.01	Ge	<0.01
33	Arsenic	As2O3	<0.01	As	<0.01
34	Selenium	SeO2	<0.01	Se	<0.01
35	Bromine	Br	<0.01	Br	<0.01
37	Rubidium	Rb2O	<0.01	Rb	<0.01
38	Strontium	SrO	<0.01	Sr	<0.01
39	Yttrium	Y2O3	<0.01	Y	<0.01
40	Zirconium	ZrO2	0.02	Zr	0.01
41	Niobium	Nb2O5	<0.01	Nb	<0.01
42	Molybdenum	MoO2	<0.01	Mo	<0.01
72	Hafnium	HfO2*	<0.01	Hf*	<0.01
74	Tungsten	WO3	<0.01	W	<0.01
77	Iridium	IrO2*	<0.01	Ir*	<0.01
80	Mercury	Hg2O*	<0.01	Hg*	<0.01
81	Thallium	Tl2O	<0.01	Tl	<0.01
82	Lead	PbO	<0.01	Pb	<0.01
83	Bismuth	BiO3	0.01	Bi	0.01
47	Silver	Ag2O	<0.01	Ag	<0.01
48	Cadmium	CdO	<0.01	Cd	<0.01
49	Indium	In2O3	<0.01	In	<0.01
50	Tin	SnO	<0.01	Sn	<0.01
51	Antimony	Sb2O3	<0.01	Sb	<0.01
52	Tellurium	TeO2	<0.01	Te	<0.01
53	Iodine	I	<0.01	I	<0.01
56	Barium	BaO	<0.01	Ba	<0.01
57	Lanthanum	La2O3	<0.01	La	<0.01
58	Cerium	Ce2O3	<0.01	Ce	<0.01
90	Thorium	ThO2	<0.01	Th	<0.01
92	Uranium	U2O3	<0.01	U	<0.01

*not generally considered reliable.

Table B13. XRF Results, FC-P Gas Filter

Atomic Number	Analyte	Reported as Oxide	%	Reported as Element	%
11	Sodium	Na2O*	<0.01	Na*	<0.01
12	Magnesium	MgO*	<0.01	Mg*	<0.01
13	Aluminum	Al2O3	<0.01	Al	<0.01
14	Silicon	SiO2	4.13	Si	1.93
15	Phosphorus	P2O5	0.94	P	0.41
16	Sulfur	SO3	4.45	S	1.78
17	Chlorine	Cl	30.01	Cl	30.01
19	Potassium	K2O	68.13	K	56.54
20	Calcium	CaO	1.56	Ca	1.12
21	Scandium	Sc2O3	0.05	Sc	0.03
22	Titanium	TiO2	0.22	Ti	0.13
23	Vanadium	V2O5	<0.01	V	<0.01
24	Chromium	Cr2O3	<0.01	Cr	<0.01
25	Manganese	MnO	0.15	Mn	0.12
26	Iron	Fe2O3	1.21	Fe	0.85
27	Cobalt	CoO	<0.01	Co	<0.01
28	Nickel	NiO	0.02	Ni	0.02
29	Copper	CuO	0.07	Cu	0.06
30	Zinc	ZnO	0.11	Zn	0.09
31	Gallium	GaO	<0.01	Ga	<0.01
32	Germanium	GeO2	<0.01	Ge	<0.01
33	Arsenic	As2O3	0.02	As	0.01
34	Selenium	SeO2	<0.01	Se	<0.01
35	Bromine	Br	0.35	Br	0.35
37	Rubidium	Rb2O	0.06	Rb	0.05
38	Strontium	SrO	<0.01	Sr	<0.01
39	Yttrium	Y2O3	<0.01	Y	<0.01
40	Zirconium	ZrO2	<0.01	Zr	<0.01
41	Niobium	Nb2O5	<0.01	Nb	<0.01
42	Molybdenum	MoO2	<0.01	Mo	<0.01
72	Hafnium	HfO2*	<0.01	Hf*	<0.01
74	Tungsten	WO3	<0.01	W	<0.01
77	Iridium	IrO2*	<0.01	Ir*	<0.01
80	Mercury	Hg2O*	<0.01	Hg*	<0.01
81	Thallium	Tl2O	<0.01	Tl	<0.01
82	Lead	PbO	0.02	Pb	0.02
83	Bismuth	BiO3	0.05	Bi	0.04
47	Silver	Ag2O	<0.01	Ag	<0.01
48	Cadmium	CdO	<0.01	Cd	<0.01
49	Indium	In2O3	<0.01	In	<0.01
50	Tin	SnO	<0.01	Sn	<0.01
51	Antimony	Sb2O3	<0.01	Sb	<0.01
52	Tellurium	TeO2	<0.01	Te	<0.01
53	Iodine	I	<0.01	I	<0.01
56	Barium	BaO	<0.01	Ba	<0.01
57	Lanthanum	La2O3	<0.01	La	<0.01
58	Cerium	Ce2O3	<0.01	Ce	<0.01
90	Thorium	ThO2	<0.01	Th	<0.01
92	Uranium	U2O3	<0.01	U	<0.01

*not generally considered reliable.

Table B14. XRF Results, FC-Untreated Gas Filter

Atomic Number	Analyte	Reported as Oxide	%	Reported as Element	%
11	Sodium	Na2O*	0.69	Na*	0.51
12	Magnesium	MgO*	<0.01	Mg*	<0.01
13	Aluminum	Al2O3	<0.01	Al	<0.01
14	Silicon	SiO2	1.80	Si	0.84
15	Phosphorus	P2O5	0.79	P	0.34
16	Sulfur	SO3	5.25	S	2.10
17	Chlorine	Cl	30.99	Cl	30.99
19	Potassium	K2O	70.54	K	58.54
20	Calcium	CaO	0.69	Ca	0.49
21	Scandium	Sc2O3	0.03	Sc	0.02
22	Titanium	TiO2	0.02	Ti	0.01
23	Vanadium	V2O5	<0.01	V	<0.01
24	Chromium	Cr2O3	<0.01	Cr	<0.01
25	Manganese	MnO	0.09	Mn	0.07
26	Iron	Fe2O3	0.28	Fe	0.20
27	Cobalt	CoO	<0.01	Co	<0.01
28	Nickel	NiO	0.01	Ni	0.01
29	Copper	CuO	0.06	Cu	0.05
30	Zinc	ZnO	0.09	Zn	0.07
31	Gallium	GaO	<0.01	Ga	<0.01
32	Germanium	GeO2	<0.01	Ge	<0.01
33	Arsenic	As2O3	<0.01	As	<0.01
34	Selenium	SeO2	<0.01	Se	<0.01
35	Bromine	Br	0.44	Br	0.44
37	Rubidium	Rb2O	0.08	Rb	0.07
38	Strontium	SrO	<0.01	Sr	<0.01
39	Yttrium	Y2O3	<0.01	Y	<0.01
40	Zirconium	ZrO2	<0.01	Zr	<0.01
41	Niobium	Nb2O5	<0.01	Nb	<0.01
42	Molybdenum	MoO2	<0.01	Mo	<0.01
72	Hafnium	HfO2*	<0.01	Hf*	<0.01
74	Tungsten	WO3	0.01	W	<0.01
77	Iridium	IrO2*	<0.01	Ir*	<0.01
80	Mercury	Hg2O*	<0.01	Hg*	<0.01
81	Thallium	Tl2O	<0.01	Tl	<0.01
82	Lead	PbO	0.02	Pb	0.02
83	Bismuth	BiO3	0.06	Bi	0.05
47	Silver	Ag2O	<0.01	Ag	<0.01
48	Cadmium	CdO	<0.01	Cd	<0.01
49	Indium	In2O3	<0.01	In	<0.01
50	Tin	SnO	<0.01	Sn	<0.01
51	Antimony	Sb2O3	<0.01	Sb	<0.01
52	Tellurium	TeO2	<0.01	Te	<0.01
53	Iodine	I	<0.01	I	<0.01
56	Barium	BaO	<0.01	Ba	<0.01
57	Lanthanum	La2O3	<0.01	La	<0.01
58	Cerium	Ce2O3	0.01	Ce	<0.01
90	Thorium	ThO2	<0.01	Th	<0.01
92	Uranium	U2O3	<0.01	U	<0.01

*not generally considered reliable.

Gasification Characteristics of High Alkali Biomass Subjected to Mechanical Dewatering and Leaching Processes

Scott Turn
Charles Kinoshita
Darren Ishimura
Jiachun Zhou

January, 1997

Abstract

Four banagrass fuels and bagasse obtained from an operating sugar factory were gasified in a benchscale fluidized bed at a nominal equivalence ratio of 0.3, reactor temperature of 800° C, and atmospheric pressure. The gasifier output stream was characterized for permanent gas species, ammonia, condensable hydrocarbon species, char content and composition, and gas phase inorganic concentration. The primary objective of the tests was to determine how the alkali species present in the fuel was partitioned between gas and solid phases of the output stream, with particular interest focused on gas phase concentrations of alkali species.

Bagasse ash was characterized by high silica, iron and aluminum concentrations whereas banagrass ash was composed primarily of silica, calcium and potassium. Banagrass was treated in a previous study to determine the degree to which inorganic constituents, with focus on alkali metals, were removed by mechanical dewatering and leaching processes. Fresh banagrass was subjected to two particle size reduction methods, a coarse preparation using a forage chopper (FC) and fine preparation using a Jeffco cutter (JC). The fuel in these two particle sizes were subjected to an initial dewatering press followed by water leaching, a final dewatering press, and ambient air drying. These treatments were identified as JC-PRP and FC-PRP. A third treatment consisted of forage chopped material subjected to a single dewatering press and ambient air drying, FC-P. The final treatment, FC-UP, entailed ambient air drying of the unpressed forage cut banagrass. In order of increasing severity, and decreasing alkali content, the banagrass treatments were ranked FC-UP, FC-P, FC-PRP, and JC-PRP. Bagasse was included as a test material because of its common use as a trouble-free boiler fuel.

Gas phase potassium concentrations were ~0.8 ppmw for bagasse and the two more severe banagrass fuel treatments, JC-PRP and FC-PRP. FC-P and FC-UP banagrass treatments contained higher concentrations of K and greater concentrations were found in the gas phase, 4 and 53 ppmw, respectively. All fuels yielded product gas Na levels in the range of 2 to 15 ppmw with no apparent correlation to Na concentration in the fuel. Ca was present in the product gas of all fuels in the range of 1 to 3 ppmw. Measured gas phase concentrations of total alkali (Na+K) and Ca were in excess of recognized combustion turbine tolerances for gaseous fuels. Si and Fe were found in the product gas at concentration of 0.5 to 5 ppmw for all fuels. Gas phase concentrations of P were determined to be in the range of 6 to 25 ppmw. Of all the inorganic species, chlorine was present in greatest concentrations in the product gas varying from 60 to 2100 ppmw and displayed a linear dependence on fuel Cl concentration. The data indicate that gas cleaning will be required before producer gas can be used in a combustion turbine application.

About 50% of the Ca and K present in bagasse was retained in the bed material. For banagrass fuels, more than 80% of K input remained in the bed material and calcium was retained at levels similar to those of bagasse. Approximately 20% of the magnesium and 30 to 60% of sodium were also retained in the bed. Examination of individual beads using a scanning electron microscope equipped with an energy dispersive x-ray spectrometer showed that fuel derived inorganic material was dispersed over the bead surfaces.

Introduction

Alkali metals in concert with other inorganic elements present in solid fuels can cause deleterious effects in thermal energy conversion systems. In the case of biomass, the alkali of primary concern is potassium, a plant macro-nutrient present at levels generally less than 5% of dry matter. Other principal inorganic elements present in biomass are silica, calcium and chlorine, with relative proportions depending on plant species and the part of the plant from which the fuel originates. Fuel materials may also acquire substantial amounts of inorganic elements as part of handling and processing activities. This composite inorganic fuel fraction can directly affect the performance of energy conversion facilities.

Depending on the relative proportions of the ash constituents, the temperature regime, whether the environment is oxidizing or reducing, and the particular type of conversion facility, the effects of the inorganic fraction are manifested in varied forms. High temperature combustion environments can cause sintering and slagging of ash in boilers and produce inorganic vapor and particulate matter deposits on downstream heat exchange surfaces (Baxter, 1993; Baxter et al., 1993, Jenkins et al., 1994; Miles et al., 1995, Salmenoja et al., 1996). Fluidized bed combustors and gasifiers may develop bed agglomerates leading to loss of fluidization. Alkali vapor in producer gas is a potential problem for integrated gasifier combined cycle power systems. When used in combustion turbines, alkalis result in increased rates of hot corrosion on turbine working surfaces. All of these lead to increased facility maintenance costs and reduced equipment availability and operating time.

Suggested methods for controlling the effects of inorganic fuel components include: (1) removal of these elements prior to fuel utilization (Jenkins et al., 1996), (2) addition of limestone or dolomite in fluidized bed applications to increase the calcium content of the inorganic fraction and thereby produce a eutectic with a higher melting point, (3) use of a gettering bed to remove alkali vapors from gasifier or combustor product streams prior to expansion through a gas turbine, and (4) novel design of thermal energy conversion facilities to avoid conditions which result in problematic operations.

Previous work (Turn et al., 1996) studied the removal of inorganic fuel constituents from banagrass (*Pennisetum purpureum*) using mechanical dewatering and leaching methods. This effort resulted in fuels which contained varying levels of inorganic elements. Material was processed in sufficient quantity to permit subsequent testing in laboratory scale thermal conversion test equipment. The focus of the current work was to examine the behavior of each of the treated fuels under fluidized bed gasification conditions and determine in what proportions inorganic elements contained in the fuel were partitioned between solid and gas output streams and the amount retained in the reactor attached to the bed material.

Past research efforts have sought to address agglomeration problems in fluidized bed gasifiers (Padban et al., 1995). Ergudenler and Ghaly (1993a) studying wheat straw gasification in a fluidized, alumina-sand bed observed a well defined agglomeration temperature at 920° C, a higher temperature than the 800 to 850° C normally experienced in gasification applications. Similar experiments conducted using silica sand as a bed material (Ergudenler and Ghaly, 1993b) found that agglomeration occurred at 800° C followed by fusing if the temperature increased to 850° C. The reaction of the silica sand with potassium compounds present in the fuel was cited as the cause.

Using chemical equilibrium calculations and experiments, Mojtahedi et al. (1989, 1990) studied the fate of sodium and potassium in pressurized fluidized-bed gasification and combustion of peat. Gas phase alkali released under gasification and combustion test conditions were found to be in excess of concentrations deemed acceptable for gaseous fuels in combustion turbine applications, about 0.1 ppmw (Scandrett and Clift, 1984). Gas phase concentrations were higher under

gasification conditions than those observed during combustion. Experimentally determined values were found to be considerably lower than predicted by equilibrium calculations. At equilibrium, KCl and NaCl were predicted to be the predominant alkali gas species under gasification conditions and volatile K and Na were found to increase with increasing fuel Cl content.

Materials and Methods

Gasification tests were performed on five herbaceous fuels to determine the partitioning of the fuel inorganic fraction between the gas and solid product streams.

Fuels

Previous work (Turn et al., 1996) described fuel treatment methods used in a laboratory scale experiment to determine the practicality of removing alkali elements from biomass fuels as a method of improving fuel quality. Freshly harvested banagrass, a fast-growing tropical grass, was used in the study. The fuel treatments are summarized in Table 1. Bagasse was included in the study to serve as a benchmark fuel known to exhibit desirable fuel properties in steam boiler applications (Kinoshita, 1991). Each fuel was hammermilled to pass through a 3.2 mm screen.

Table 1. Summary of banagrass treatment processing steps.

Banagrass Treatment	Size Reduction	Initial Dewatering	Water Rinse with Secondary Dewatering Press
FC-UP	Forage Chopper		
FC-P	Forage Chopper	x	
FC-PRP	Forage Chopper	x	x
JC-PRP	Jeffco Cutter	x	x

Experimental

Each of the fuels was tested in a benchscale fluidized-bed gasification system. The system is shown schematically in Figure 1 and a detailed drawing of the reactor is presented in Figure 2. The reactor is constructed of 310 stainless steel pipe, with a bed diameter of 89 mm and a freeboard diameter of 152 mm. The reactor is externally heated by four, 4 kW heaters (Model 274A, Thermcraft, Inc., Winston-Salem, NC) as shown in Figure 2. Pressure taps, thermocouples and probe access ports are located along the height of the reactor. Fuel was fed to the reactor from a sealed fuel hopper via a variable speed metering screw. Air, used as the fluidizing agent for the tests, was metered into the windbox below the distributor by a mass flow controller (Model 5851E, Brooks Instruments, Hatfield, PA). The bed material consisted of beads with diameters in the range of 0.21 to 0.42 mm (+40–70M)(Norton-Alcoa, Fort Smith, AR). Flow exits the reactor, passes through a heated sintered stainless steel filter (Model C-20-18-2PF, Pall Process Filtration Corporation, Cortland, NY), 50 mm in diameter and 0.46 m in length with a pore size of 3 µm, and is flared in a swirl combustor. All electronic signals are processed using two, 32 channel multiplexer amplifiers (Model SCXI-1100, National Instruments, Austin, TX) and a 12 bit, analog to digital converter board (Model AT-MIO-16E-2, National Instruments, Austin, TX) in an IBM PC-750 personal computer.

Figure 1. Schematic of benchscale gasifier test facility.

Figure 2. Benchscale fluidized bed reactor.

Each of the five fuels was tested individually over a 3 week period. In preparation for each test, fresh bed material and fuel were weighed and placed in the reactor and the fuel hopper, respectively. All tests were performed at 800 °C and the bed was preheated using the external heaters with air flowing through the reactor until a stable temperature profile was obtained. To begin the test, the feeder was turned on and air flow to the reactor adjusted to produce the desired equivalence ratio. These conditions were maintained throughout the test. Quantitative sampling, as described below, was begun when the system had attained a steady temperature distribution and relatively constant gas composition as determined by on-line gas analyzers. Steady conditions were normally achieved about one hour after the commencement of fuel feeding. After the sampling period and prior to shutdown, the bed temperature was increased in a controlled manner in an effort to induce bed agglomeration. Pressure drop across the bed was monitored as an indicator. At the conclusion of a test, fuel and air flow to the reactor and system heaters were shut down simultaneously. After the system had cooled, remaining fuel was removed from the feed hopper, char was recovered from the main filter, and bed material was removed from the reactor. Each was sampled and weighed.

Sampling and Analytical Methods

The fuel used in each of the gasifier tests was sampled and subjected to ultimate (C, H, O, N, S and Cl), proximate (volatile, fixed carbon and ash), heating value, and elemental ash (Si, Al, Ti, Fe, Ca, Mg, Na, K, P, S, Cl, and CO_2) analyses (Hazen Research, Inc., Golden, CO). The process stream from the gasifer was quantitatively sampled to determine the alkali content of the gas and solid phases, permanent gas species and concentrations, condensable light oil and tar species and concentrations, and concentrations of ammonia and oxides of nitrogen. A description of the sampling and analytical methods for each component follows.

The extraction point for the alkali sampling system was located just below the freeboard as shown in Figures 1 and 2. The stream was removed non-isokinetically through a 13 mm diameter probe and passed through a sintered stainless-steel candle filter 38 mm in diameter and 152 mm in length with a 2 μm pore size (Mott Metals, Farmington, CT). The reactor temperature at the extraction point was 725 °C and the probe, sample line and filter were maintained at the same temperature by heat tracing. All components were fabricated from stainless steel. Temperatures at the probe, and within the filter assembly were monitored by thermocouples mounted in the reactor wall and filter housing, respectively. Upon exiting the filter assembly, the gas stream passed through a heat exchanger constructed from a 0.46 m length of 13 mm diameter tubing encased in a cooling water jacket. Gas temperature at the exit of the heat exchanger was monitored by a thermocouple mounted in the gas stream. The cooled flow (near-ambient temperature) was directed through a series of four impingers, each containing 100 ml of deionized water. The impinger set was submerged in an ice water bath. Gas exiting the impinger train passed through a coalescing filter (Hepa-Cap 36, Whatman Inc., Haverhill, MA), rotameter and dry test meter. Flow rates through the sampling system were maintained in the range of 2.5 to 3.5 L min^{-1}, resulting in total dry gas sample volumes of 400 to 500 L.

At the conclusion of each test, the tubing in the heat exchange section of the sampling system was rinsed with acetone and deionized water to remove all condensed substances, and liquids were recovered from each of the impingers. All samples were stored in separate sealed containers. Each of the five liquid samples were analyzed for the inorganic elements, Al, Ca, Cl, Fe, Mg, P, K, Si, Na, S and Ti (Hazen Research, Inc., Golden, CO).

The following day, after the sampling components had cooled, the alkali sampling probe and filter were removed from the gasifier and disassembled. Char was collected, weighed, and sent for ultimate and elemental ash analyses. The probe, filter element, and tubing within the heat exchanger were replaced after each test.

A sample stream for permanent gas analysis was extracted from the process directly after the main filter housing. The gas stream was passed through a water cooled heat exchanger followed by a condenser trap cooled with dry ice, two impingers in an ice bath, each containing 100 ml of methanol, an additional dry ice condenser trap, and a coalescing filter. Grab samples of the cool, clean, dry gas were collected and analyzed off-line for the permanent gases H_2, N_2, CO, CH_4, CO_2, and C_2H_m using a gas chromatograph (GC) (AutoSystem, Perkin-Elmer, Norwalk, CT) equipped with a 1.5 m by 3 mm packed column (Carboxen 1000, Supelco, Bellefonte, PA) and thermal conductivity detector. A three-point GC calibration was performed using a certified standard gas prior to each test. A gas stream was also directed to a three channel, on-line, nondispersive infrared gas analyzer (Model URAS 10E, Applied Automation/Hartmann & Braun, Bartlesville, OK) equipped to analyze CO, CO_2 and CH_4, and a continuous-flow, thermal-conductivity detector (Model CALDOS 5G, Applied Automation/Hartmann & Braun, Bartlesville, OK) which was indicative of gas H_2 concentration. An additional gas stream was directed to a chemiluminescent analyzer for the detection of oxides of nitrogen as NO (Model 10-AR, Thermo Environmental Instruments, Franklin, MA). The on-line analyzers were calibrated prior to each test using certified zero and span gases. Calibration was reconfirmed after each test using the same calibration gases.

A sample stream was extracted from the exit of the main filter to obtain a sample of condensable light oil and tar species. In a manner similar to the gas conditioning system described above, the sample stream was passed through a water cooled heat exchanger, a twin-chamber dry-ice condenser trap and two ice-bath-cooled methanol impingers followed by a coalescing filter, rotameter, and dry gas test meter. Elapsed times of approximately 30 to 40 minutes and total dry gas volumes of 70 L were typical of each tar sampling period. At the conclusion of each sampling period, the sampling train was cleaned with acetone. This rinsate, condensate collected in the dry ice traps, and the methanol from the impingers were combined into a single tar solution sample. Total sample volume was recorded and a subsample retained for analysis. Tar analysis was performed on a GC (AutoSystem, Perkin-Elmer, Norwalk, CT) equipped with a 60 m by 0.53 mm capillary column (Model Rtx-5, Restek Corporation) and flame ionization detector. Details of the GC calibration and analysis have been described elsewhere (Kinoshita et al., 1994).

A separate sampling system was employed to determine the ammonia concentration of the process gas stream. The gas sample was extracted at the exit of the main filter and passed through a water cooled heat exchanger, a series of four impingers containing 150 ml of 0.1 M sulfuric acid solution followed by a coalescing filter, rotameter and dry gas test meter. Elapsed times of 30 minutes and total dry gas volumes of approximately 70 L were typical of each ammonia sampling period. At the conclusion of the sampling period, the volume of the trapping solution from each impinger was measured and the samples stored refrigerated in individual containers until analyzed. The ammonia concentration of each impinger sample was determined using a calibrated ion-selective electrode (Model 290A, Orion Research, Boston, MA). Details of the ion-selective electrode calibration and analysis of the impinger solutions have been described elsewhere (Ishimura, et al., 1994).

Bulk, post-test bed material samples from each of the five fuel tests and one of fresh, unused bed material were subjected to geologic assay for the elements Ca, C, Cl (water soluble), Mg, P (as P_2O_5), K, Na, and S (Hazen Research, Inc., Golden, CO). In addition, fresh bed material was analyzed for Al, Fe, Si, and Ti, which, according to the manufacturer, were its primary constituents along with oxygen. Bed material samples were also examined using a scanning electron microscope (SEM) (Zeiss 962) equipped with an energy dispersive x-ray fluorescence analysis system (Oxford Instruments) operated by the Analytical Electron Microscope Laboratory at the University of Hawaii. This technique was used to obtain semi-quantitative elemental analyses of the surface of individual beads from the bed material samples for 11 inorganic ash elements (Ca, Cl, Mg, P , K, Na, S, Al, Fe, Si, and Ti) and oxygen. Each spectra was collected from the full screen at a SEM magnification of 1000X at a rate of ~3000 counts per second over a

period of 200 seconds. Ten beads, randomly chosen from each test, were examined and a mean concentration and standard deviation were computed for each element.

Results and Discussion

Fuel Properties

Properties of bagasse obtained from the Waialua Sugar Co., Inc. on Oahu and four banagrass treatments are presented in Table 2. The progression from left to right is the order in which gasification tests were performed and one of increasing fuel and ash alkali concentrations. Fuel and ash chlorine content exhibits a similar trend. Ash content of the banagrass fuels shows no distinct trend, but when compared against the Waialua bagasse, banagrass has a markedly lower ash content. Ash content of bagasse is known to vary from factory to factory, and at any given factory over time, depending on local weather and field harvest conditions (Payne, 1991), and the ash content of this particular sample is not indicative of the industry as a whole. The ash chemistry of the bagasse sample is also different from banagrass, with large concentrations of aluminum and iron due to soil incorporation which occurs when sugarcane is harvested. Earlier analysis of JC-PRP fuel samples obtained prior to air drying possessed markedly lower ash concentrations of aluminum and iron (Turn et al., 1996), indicating possible soil contamination of either the fuel lot or the fuel sample used for the analysis reported here.

Test Conditions

A summary of test operating conditions and results is presented in Table 3. All tests were conducted at a fuel feed rate of roughly 1.1 kg hr^{-1}, equivalence ratio of approximately 0.3, and nominal reactor temperature of 800 °C. H_2 content is consistently about 10% of the dry product gas. CO and CH_4 concentrations show similar trends across the test sequence, decreasing from bagasse to FC-P, then increasing for the FC-UP test, with values ranging from 11 to 16% and 3 to 4% respectively. CO_2 exhibits less distinct trends with concentrations varying from 16 to 18%. On-line measurements of the major species were in close agreement with off-line determinations made using GC. Dry, inert-free gas yields, calculated based on closure of the molecular nitrogen balance, ranged from 0.8 to 1.1 Nm^3 kg^{-1} dry fuel. Measurements of tar concentration in the gas ranged from 12 to 19 g Nm^{-3} of dry gas or 25 to 35 g kg^{-1} dry biomass. Tar and ammonia measurements were not made for the FC-UP test due to equipment problems. Ammonia levels in the gas stream increased from 900 ppmv when bagasse was tested to 1700 ppmv for the FC-P fuel test. Figure 3 plots dry gas ammonia concentration versus fuel nitrogen content. Regression shows the relationship to be linear (r^2=1). Bed temperatures were increased near the conclusion of two of the tests to determine if bed agglomeration would occur. For the other three tests, insufficient fuel remained in the feed hopper to continue operating beyond the sampling periods. Maximum bed temperatures attained during these periods are shown in Table 3. Bed differential pressure was monitored, but behavior characteristic of agglomeration was not evident for any of the fuels. This was later confirmed when the bed material was removed and examined.

Table 2. Summary of fuel analyses for bagasse and banagrass fuel treatments.

Fuel	Bagasse	Banagrass			
		JC-PRP	FC-PRP	FC-P	FC-UP
Moisture Content, as Fired (% wet basis)	6.4	11.36	7.07	7.07	8.4
Proximate Analysis (% dry basis)					
Ash	5.83	3.75	3	4.07	4.47
Volatiles	79.25	80.55	81.52	79.45	78.2
Fixed Carbon	14.92	15.7	15.48	16.48	17.33
HHV (MJ/kg)	17.9	18.5	18.7	18.5	18.3
Ultimate Analysis (% dry basis)					
C	46.27	47.04	47.39	46.93	47.10
H	5.27	5.11	5.24	5.09	5.29
O (by difference)	42.41	43.81	43.76	43.01	41.93
N	0.12	0.22	0.36	0.44	0.44
S	0.05	0.04	0.14	0.14	0.16
Cl	0.05	0.03	0.11	0.32	0.61
Ash	5.83	3.75	3.00	4.07	4.47
Ash Analysis (% dry basis)					
SiO_2	42.93	61.56	57.11	47.87	37.73
Al_2O_3	23.77	8.2	0.81	0.96	0.93
TiO_2	2.54	0.82	0.02	0.1	0.07
Fe_2O_3	16.86	3.58	1.08	1.03	1.16
CaO	2.19	8.66	9.97	8.48	6.05
MgO	2.07	2.07	4.12	5.19	5.16
Na_2O	0.57	0.74	0.82	0.79	0.9
K_2O	3.22	5.52	15	23.9	33.8
P_2O_5	1.3	1.6	3.18	3.55	3.61
SO_3	0.6	1.55	1.42	2.16	1.65
Cl	<0.01	0.09	2.24	5.75	11.2
CO_2	0.4	0.91	0.5	0.26	0.3
Other (by difference)	3.55	4.70	3.73	-0.04	-2.56

Table 3. Summary of test operating conditions and results.

Feedstock	Bagasse	Banagrass JC-PRP	FC-PRP	FC-P	FC-UP
Feedstock Fed (wet kg)	4.9371	4.2182	3.8754	4.6066	4.5514
Total Run Time (hr)	4.50	4.00	3.48	4.17	3.48
Feedrate (wet kg hr^{-1})	1.10	1.05	1.11	1.11	1.31
Moisture Content (% wet basis)	6.4	11.4	7.1	7.1	8.4
Feedrate (dry kg hr^{-1})	1.03	0.93	1.03	1.03	1.20
Oxygen Flowrate (L min^{-1})	4.4	5.2	4.7	5.2	5.1
Nitrogen Flowrate (L min^{-1})	16.5	19.6	17.7	19.6	19.2
Equivalence Ratio	0.27	0.33	0.27	0.30	0.26
Bed Temperature (°C)	800	800	800	800	800
Dry Gas Composition (volume %)					
H_2	10.8	10.8	10.0	9.6	10.9
N_2	50.8	52.2	56.3	57.0	53.8
CO	16.0	13.5	12.6	11.3	13.0
CH_4	4.3	4.0	3.7	3.2	3.9
CO_2	15.9	17.6	15.4	16.9	15.5
C_2H_2	0.00	0.00	0.23	0.56	1.05
C_2H_4	1.94	1.66	1.64	1.24	1.64
C_2H_6	0.28	0.27	0.13	0.10	0.15
Gas Molecular Weight (kg kmole^{-1})	27.2	27.5	27.4	27.8	27.2
Dry Inert Free Gas Yield (m^3 kg^{-1})	0.93	1.15	0.80	0.86	0.83
Total Dry Gas Yield (m^3 kg^{-1})	1.90	2.41	1.82	2.01	1.79
Oil & Tar in Dry Gas (g Nm^{-3})	14.8	12.8	19.5	15.0	*
Oil & Tar Yield (g kg^{-1} dry biomass)	28.1	30.8	35.4	30.2	*
Ammonia in dry Product Gas (ppmv)	930	1170	1510	1710	*
NO Concentration (ppmv)	27	23	30	21	22
Main Filter Char (g)	266	130.4	125	171.3	154.7
Alkali Filter Char (g)	53.6	42.7	43.6	62.1	74
Alkali Sampling Temperature (°C)	725	723	720	726	730
Maximum Bed Temperature (°C)	875	800	810	910	800

* Data not available.

Figure 3. Gas ammonia concentration versus fuel nitrogen concentration.

Char Analysis

Table 3 contains the weight of char collected in the main filter for each of the fuels. Elemental composition of each of the main filter char samples is presented in Table 4. Carbon content of the bagasse main filter char sample is 34%, with the banagrass fuels producing higher values ranging from 47 to 57%. In all cases, ash accounts for much of the remainder, with the combined fractions of hydrogen, oxygen, nitrogen, sulfur, and chlorine accounting for 1 to 5% of the total. Differences in carbon content may be due in part to the higher ash content of bagasse, the slightly lower fluidizing gas flow rate used during the bagasse test and the processing methods employed in sugar extraction. SiO_2 is the primary component of all of the main filter ash samples accounting for 60 to 70% of the char from the banagrass fuels and 40% in the case of bagasse. The high alumina and iron oxide content of bagasse fuel ash is also found in the ash of the main filter char, representing 24% and 18% of the total, respectively. Concentrations of these two components in ash of the main filter char from the banagrass treatments are very similar to the fuel compositions. This indicates that the JC-PRP fuel analysis which exhibited higher iron and aluminum concentrations was characteristic of the fuel lot rather than the fuel sample. Of the alkali compounds, K_2O accounts for 2 to 6% of the main filter char's ash component, while Na_2O is present at less than 0.5% concentration. For bagasse, the alkali concentrations in the main filter ash are less than 0.5% (absolute) different from those of the fuel samples. This is true of Na_2O in the banagrass treatments as well. A large reduction in K_2O concentrations is evident between fuel and main filter ash for the banagrass tests indicating that K was depleted in the solid material elutriating from the reactor. For banagrass fuels, a similar trend is evident for Cl.

Table 4. Summary of main filter char analyses.

| Fuel | Waialua Sugar Co. Bagasse | \|--------------------Banagrass--------------------\| | | | |
		JC-PRP	FC-PRP	FC-P	FC-UP
Ultimate Analysis (% dry basis)					
C	33.69	47.10	52.00	51.43	57.07
H	0.59	0.95	0.82	0.81	0.85
O (by difference)	0.71	2.71	2.82	1.82	0.12
N	0.11	0.44	0.60	0.63	0.75
S	0.07	0.07	0.09	0.11	0.12
Cl	0.14	0.29	0.66	1.77	2.62
Ash	64.69	48.44	43.01	43.43	38.47
Ash Analysis (% dry basis)					
SiO_2	42.81	67.75	73.46	69.91	63.15
Al_2O_3	24.34	6.23	3.09	2.46	2.5
TiO_2	2.93	1.29	0.75	0.58	0.58
Fe_2O_3	17.58	5.6	2.51	2.5	3.32
CaO	1.94	8.19	8.61	9.29	9.27
MgO	1.64	2.09	3.79	5.31	7.38
Na_2O	0.63	0.36	0.27	0.32	0.25
K_2O	3.08	2.32	2.14	2.86	5.88
P_2O_5	1.21	0.76	2.45	3.16	4.04
SO_3	0.3	0.45	0.76	0.76	0.94
Cl	0.02	0.12	0.75	0.99	3.63
CO_2	0.05	0.24	0.3	0.18	0.2
Other (by difference)	3.47	4.60	1.12	1.68	-1.14

Weights of char recovered from the alkali sampling system filter are presented in Table 3. Results of ultimate and elemental ash analyses are shown in Table 5. Differences in ultimate analyses between the char recovered from the main filter and the alkali filter are generally small. The exception to this is the carbon, oxygen and ash contents of the bagasse and JC-PRP tests. A higher carbon content in the alkali filter char compared to the main filter char (8.5% absolute) in the bagasse test is offset by a lower ash content. For the JC-PRP test, the lower ash content (9.9% absolute) of the alkali filter char is accounted for by higher carbon and oxygen concentrations. These differences may be due to differences in fuel particle morphologies resulting from the comminution methods employed. The latter three tests utilized a sampling probe 32 mm shorter than the first two tests. This resulted, by design, in the sample being withdrawn from a location 13 mm from the wall rather than the centerline of the reactor as in the first two tests. The change was made in an attempt to reduce the amount of particulate present in the sample stream, and may have resulted in the extraction of a smaller size fraction of more completely reacted particles, accounting for the lower carbon content of the alkali char in the latter three tests.

Ash content and ash compositions of the fuel, main filter char and alkali filter char samples are graphically presented in Figures 4 through 8. In general, ash compositions of the main filter char

and alkali sampling system are similar. The composition of ash from fuel and the two char samples from the bagasse test is almost identical. The depletion of K_2O and Cl in the char samples of the FC-PRP, FC-P and FC-UP banagrass fuels is readily apparent. Na_2O and SO_3, present in much lower quantities in these fuels, are also depleted. The Cl content of the alkali filter ash is roughly 30% of that found in the main filter ash. This may be due to the decrease in temperature to 350 °C of the product stream at the main filter which permits the condensation of Cl compounds onto particulate, resulting in a higher Cl concentration. Enrichment of Al, Si, Fe, or Ti in the ash from the two char samples may be due to contamination of the char with dust from the bed material. This is particularly noticeable for the three latter banagrass fuels which have low fuel concentrations of these elements.

Table 5. Summary of alkali filter char analyses.

Fuel	Waialua Sugar Co.	|----------------Banagrass----------------|		
	Bagasse	JC-PRP	FC-PRP	FC-P	FC-UP
Ultimate Analysis (% dry basis)					
C	42.19	54.74	51.95	51.17	56.88
H	0.39	0.56	0.50	0.42	0.50
O (by difference)	0.76	5.68	2.75	2.91	2.33
N	0.30	0.45	0.52	0.54	0.68
S	0.07	0.06	0.07	0.10	0.13
Cl	0.04	0.04	0.11	0.30	0.65
Ash	56.25	38.47	44.10	44.56	38.83
Ash Analysis (% dry basis)					
SiO_2	44.6	73.06	75.33	73.19	69.51
Al_2O_3	23.06	2.35	2.85	1.34	1.16
TiO_2	2.96	0.48	0.62	0.24	0.24
Fe_2O_3	17.08	2.98	2.46	2.86	4.09
CaO	2.17	7.2	6.55	6.55	9.76
MgO	1.7	1.75	2.96	4.08	5.54
Na_2O	0.49	0.24	0.18	0.16	0.21
K_2O	2.69	1.73	1.63	2.48	4.38
P_2O_5	1.14	0.62	2.04	2.36	3.17
SO_3	0.48	0.49	0.67	0.64	0.95
Cl	0.01	0.05	0.26	0.31	1.11
CO_2	0.06	0.32	0.23	0.22	0.17
Other (by difference)	3.56	8.73	4.22	5.57	-0.29

Figure 4. Ash content and composition of fuel and main and alkali filter chars for the bagasse gasification test.

Figure 5. Ash content and composition for fuel and main and alkali filter chars for JC-PRP gasification test.

Figure 6. Ash content and composition of fuel and main and alkali filter chars for FC-PRP gasification test.

Figure 7. Ash content and composition for fuel and main and alkali filter chars for FC-P gasification test.

Figure 8. Ash content and composition for fuel and main and alkali filter chars for FC-UP gasification test.

Gas Phase Inorganics

Gas phase concentrations of ash elements are presented in Table 6 and graphically in Figure 9. Chlorine is present in the greatest concentrations, increasing monotonically from 60 to 2100 ppmw with increasing fuel chlorine concentration as shown in Figure 10. Potassium is present in the gas phase at levels of roughly 1 ppmw for fuels with K concentrations in the 0.15 to 0.4% range – bagasse, JC-PRP and FC-PRP. Higher fuel K concentrations, FC-P (0.8% K) and FC-UP (1.3% K), produced gas phase K concentrations of 4 and 53 ppmw, respectively. Sodium is present in all the fuels at levels of 0.02 to 0.03% and gas phase concentrations are grouped in the 2 to 15 ppmw range. At equilibrium, Mojtahedi (1989) predicted higher alkali volatilization rates for greater fuel chlorine concentrations. The potassium data confirm this behavior although the increasing fuel K concentration is more likely the cause. Sodium data does not exhibit a similar trend. Total alkali concentrations (Na+K) exceed recognized limits for gaseous fuels used in combustion turbines, 0.1 ppmw (Scandrett and Clift, 1984). In all cases, gas phase chlorine concentrations greatly exceed those required if chlorides are the primary forms of alkali evolution as predicted by equilibrium calculations (Mojtahedi, 1990), indicating the presence of additional forms of Cl, possibly as HCl. Phosphorous is consistently present in the 7 to 25 ppmw range, with higher levels corresponding to fuels containing greater P concentrations; FC-PRP, FC-P, and FC-UP. Ca, Fe, and Si are present in the product gas streams from all fuels at concentrations in the range of 0.5 to 5 ppmw with no apparent relationship to fuel concentration.

Table 6. Measured concentrations of inorganic elements in gas output streams.

Fuel	Waialua Sugar Co. Bagasse	Banagrass			
		JC-PRP	FC-PRP	FC-P	FC-UP
Gas concentration (ppmw)					
Si	0.80	1.40	5.40	4.02	1.89
Al	0.00	0.00	0.00	6.10	11.14
Ti	0.00	0.00	7.53	7.93	0.17
Fe	1.69	4.03	1.60	0.38	3.17
Ca	1.98	1.20	2.02	3.14	2.38
Mg	0.71	0.00	0.00	0.00	0.00
Na	11.55	2.40	8.41	14.81	8.32
K	0.73	0.84	0.84	4.21	53.36
P	6.77	6.64	20.59	24.83	15.88
S	0.00	0.00	0.00	0.00	0.00
Cl	60.66	98.49	164.75	804.48	2119.01

Figure 9. Gas phase concentrations of inorganic elements in producer gas by fuel.

Figure 10. Gas phase chlorine concentration versus fuel chlorine content.

Bed Material

The manufacturer provided the following analysis as being typical of the bed material: aluminum oxide, 16 to 30%; alumina silicate, 60 to 70%; silicon dioxide, <10%; iron oxide, 4 to 11%; titanium oxide, 3 to 5%. Analyses of bulk samples of bed material from each of the tests and a sample of fresh, unused bed material are presented in Table 7. Individual beads and fuel derived material present in the sample were homogenized and the resulting composite was subjected to analysis. In addition to the elements specified by the manufacturer, the fresh bed material contains measurable, albeit trace, quantities of calcium, magnesium, phosphorus, potassium, sodium, and sulfur. The 5.2% silica content of the bed material (see Table 7 footnote) is not consistent with the silica content of the bed material reported by the manufacturer, which at a minimum would be roughly 8%. The reason for this inconsistency is unclear. For all of the fuels, the elements Ca, C, Mg, K, and Na were present at greater concentrations in the post-test bed material than in the fresh bed material. Ca, C, Mg and Na concentrations do not vary appreciably across the fuel treatments. Potassium concentration in the bed material tracks increasing fuel potassium content, indicating that the bed is an important repository for alkali. It is uncertain whether sequestering of potassium in the bed would have continued over a longer duration test, or if instead, a retention capacity would have been reached, beyond which additional input would have exited the bed in volatile or solid form. The former could affect the useful life of bed material as excessive potassium levels may result in bed agglomeration, whereas the latter would necessitate more aggressive downstream gas conditioning if potassium were in volatile form. Results for phosphorous in the test bed material samples are generally lower than the fresh bed material. Fresh

Table 7. Summary of elemental analyses of bulk samples of fresh, unused bed material and bed material recovered from the reactor after each fuel test.

	Waialua Sugar Co. Bagasse	JC-PRP	FC-PRP	FC-P	FC-UP	Fresh* Unused Material
Selected Elements (% mass)						
Ca	0.223	0.25	0.224	0.246	0.232	0.191
C	0.07	0.17	0.03	0.03	0.03	<0.01
Cl	<0.01	<0.01	<0.01	<0.01	0.02	<0.01
Mg	0.026	0.023	0.023	0.029	0.033	0.019
P as P_2O_5	0.033	0.043	0.029	0.032	0.058	0.05
K	0.12	0.144	0.194	0.433	0.617	0.084
Na	0.039	0.037	0.034	0.035	0.037	0.032
S	0.003	0.005	0.006	0.006	0.007	0.006

* Fresh unused bed material also contains 30.2% Al, 4.28% Fe, 5.22% Si, and 1.7% Ti.

bed material which was simply heated to 800°C in the reactor was found to have a lower P_2O_5 content (0.019%) than the fresh unheated bed material (0.05%) suggesting that phosphorus present in the fresh beads is volatilized when heated. Sulfur is present in all samples in the range of 30 to 70 ppmw, and in two of the five post-test samples, concentrations are lower than the fresh bed material making these data suspect. Chlorine was not found in any of the samples with the exception of the bed material from the FC-UP test in which it was present at a level only slightly higher than the detection limit. This is consistent with the higher fuel chlorine concentration of the FC-UP fuel.

The analyses presented in Table 7 were performed on bulk, homogenized, bed material samples, however, inorganic species originating from the fuel and retained in the bed would be expected to be found deposited on the surface of the individual beads. Thus the original mass of the bead is large compared to the surface deposit, and dominates the analysis. To provide validation for the bulk analyses, a scanning electron microscope equipped with an energy dispersive x-ray fluorescence analysis system (XRF) was used to obtain semi-quantitative elemental analyses for the surface of individual beads from the bed material samples. Ten beads, randomly chosen from each test, were examined; the mean concentration and standard deviation for the 11 inorganic ash elements and oxygen, are in Table 8. Detection limits for the XRF are generally 0.1%, and low sample concentrations are indicated in the table; Na (all tests), S (all tests), Mg (all tests except FC-P and FC-UP), Cl (all tests except FC-UP), and K (JC-PRP and fresh, unused bed material). Of the trace elements contributed by the fuel, P, K, and Ca are present on the bead surfaces in concentrations which are clearly greater than the fresh, unused beads. Phosphorus data are contrary to those determined in the bulk analyses (Table 7) where levels in the fuel test bed material samples were lower than the concentration in fresh beads. Surface concentrations of aluminum and titanium are lower for all of the fuel test materials compared to the fresh beads as a result of ash deposited on the bead surfaces. Silicon is present in substantial amounts in both the fresh beads and the fuel ash. Surface concentrations of the fuel test beads are greater than fresh bead levels as a result of ash surface deposits enriched in silicon. Iron concentration on the surface of the beads from the bagasse test is nearly 2% greater than the fresh beads. Beads from the bagasse test displayed an obvious reddish brown hue resembling the color of agricultural soils in Hawaii. Beads from three of the four banagrass fuel tests also exhibit higher iron surface concentrations. In total, the XRF surface analyses of individual unused and fuel test beads substantiate the results obtained from bulk sample analyses.

Table 8. Summary of semi-quantitative elemental analyses of bed material surfaces by SEM/XRF.

Mass %	Waialua Sugar Co. Bagasse Mean	S.D.	JC-PRP Mean	S.D.	FC-PRP Mean	S.D.	FC-P Mean	S.D.	FC-UP Mean	S.D.	Fresh Unused Bed Material Mean	S.D.
				---Banagrass---								
O	44.30	2.38	44.25	3.41	45.56	3.50	45.11	2.77	43.06	1.67	44.37	2.51
Na	*		*		*		*		*		*	
Mg	*		*		*		0.27	0.10	0.38	0.17	*	
Al	21.91	3.27	23.46	3.47	23.79	2.13	23.67	3.80	24.18	2.59	25.93	2.60
Si	6.86	0.87	6.48	1.00	6.02	0.67	6.26	1.15	6.21	0.88	5.89	0.66
P	0.28	0.04	0.22	0.03	0.37	0.05	0.60	0.09	0.66	0.14	0.16	0.03
S	*		*		*		*		*		*	
Cl	*		*		*		*		0.14	0.09	*	
K	0.23	0.14	*		0.15	0.09	0.39	0.34	1.51	0.62	*	
Ca	0.75	0.16	1.95	0.53	1.57	0.38	1.94	0.36	1.86	0.63	0.14	0.05
Ti	8.54	2.36	8.45	2.86	8.26	2.24	7.54	3.00	6.66	2.14	8.89	2.11
Fe	13.92	4.15	12.32	3.23	12.01	3.27	12.19	4.36	11.04	3.02	11.82	1.65

Figure 11. Bead surface element maps for fresh, unused bed material (1000x).

Mg

Fe

Al

Ti

Figure 11. (continued)

Figure 12. Bead surface element maps from FC-UP test (1000x).

Figure 12. (continued)

Secondary and backscattered electron images and element maps (K, Si, Ca, P, Mg, Fe, Al and Ti) of single bead surfaces of fresh, unused material and from the FC-UP test are presented in Figures 17 and 18. Light areas indicate the presence of the particular element and gray scale intensity is proportional to concentration. In each case, the backscattered electron image coincides with the presence of iron and titanium, the two elements with highest atomic number. Aluminum and silicon share similar distributions because they are present as alumina silicate in the fresh bed material, although silicon is also present as silicon dioxide. These four elements (Fe, Ti, Al, Si), along with oxygen, are the main components of the fresh bed material and are most apparent. Potassium, calcium, phosphorus and magnesium are uniformly distributed over the surface of the unused bead. The spacial occurence of these elements on the bead from the FC-UP test displays similarity to the silicon and aluminum distributions suggesting that the alumina silicate and silicon dioxide surfaces of the fresh beads more readily bond with inorganic fuel compounds. Several areas of high concentration for the minor elements are evident. Most obvious is the 3 μm diameter white spot located mid-height on the left hand side of the K, Ca, P, and Mg maps. The secondary electron image does not show a readily apparent or unique structure at this location but composition suggests a fuel derived ash particle bonded to the bead surface. SEM/XRF analysis of beads from the other fuel tests revealed similar patterns of element dispersal over their surfaces. Due to low surface concentrations of the minor elements in the bed material (see Table 8), discernable differences among the fuels were not apparent.

Element Balances

Element balances (output elemental mass as a percentage of the elemental mass present in the fuel) for C, N, and 11 inorganic ash species are presented in Table 9. Figures 11 through 15 show the bed material, main filter ash, alkali filter ash and gas phase contributions to the element balances for each of the fuels. Gas phase contributions have been calculated based on measured concentrations and gas yield. Post-test bed material values have been corrected by the fresh, unused bed material analyses for the elements Ca, Mg, K, and Na. Bed material values for C and Cl were included in the balance computations but were not corrected as they were not present in the fresh beads in concentrations above the detection limit. Elements whose balances are far in excess of 100% in Table 9 have not been included in the figures so as to preserve relative scale.

Carbon balances are generally good, ranging from 80% to slightly in excess of 100%. Carbon present in the condensable, light-hydrocarbon and tar species is included in the gas phase percentages shown in the figures. In all cases, the gas phase accounts for the bulk of the carbon in the output stream, with the char streams contributing roughly 5%.

Nitrogen balance closure decreases with increasing nitrogen content, varying from 90% for bagasse (0.12% fuel N) to 50% for the FC-PRP and FC-P banagrass treatments (0.36% and 0.46% fuel N, respectively). As noted earlier, ammonia measurements were not made for the FC-UP test, and as a result, only 9% of fuel N was accounted for in the output streams. The main filter and alkali filter solids contain 5 to 7% and 1 to 3% of fuel nitrogen, respectively, for all fuels. Ammonia is the largest identified nitrogen output, decreasing from 80 to 40% of fuel N with increasing fuel N content. NO concentrations on the order of 20 ppmv account for milligram quantities of N, not affecting the balance substantially. Molecular nitrogen, not measured in the product gas, is believed to be the major part of the unquantified shortfall, with a lesser quantity of HCN also formed (Ishimura et al., 1994; Leppälahti, 1993).

Table 9. Balances for major fuel elements, output as percentage of input.

Fuel	Waialua Sugar Co. Bagasse	Banagrass		
		JC-PRP	FC-PRP	FC-P	FC-UP
Total Ash, output as % of input	78.4	66.6	82.7	87.3	89.4
Element balance, output as % of input					
C	93.0	109.7	78.6	85.2	78.1
N	92.6	82.4	51.3	52.0	9.1
Si	75.3	63.5	87.6	86.7	81.9
Al	76.2	37.6	252.4	138.3	115.1
Ti	86.7	77.7	2845.9	360.0	319.3
Fe	78.0	81.4	157.6	148.0	147.5
Ca	143.5	119.8	97.3	111.2	124.7
Mg	80.6	78.0	73.3	74.4	86.3
Na	151.1	93.2	59.9	64.0	58.0
K	120.2	115.2	90.1	107.4	109.9
P	73.6	32.8	59.9	57.6	65.6
S	9.7	7.8	2.8	4.2	5.7
Cl	42.7	124.3	52.7	80.9	90.8

Figure 13. Elemental distribution in the gasifier output streams as percentage of input mass, bagasse test.

Figure 14. Elemental distribution in the gasifier output streams as percentage of input mass, JC-PRP test.

Figure 15. Elemental distribution in the gasifier output streams as percentage of input mass, FC-PRP test.

Figure 16. Elemental distribution in the gasifier output streams as percentage of input mass, FC-P test.
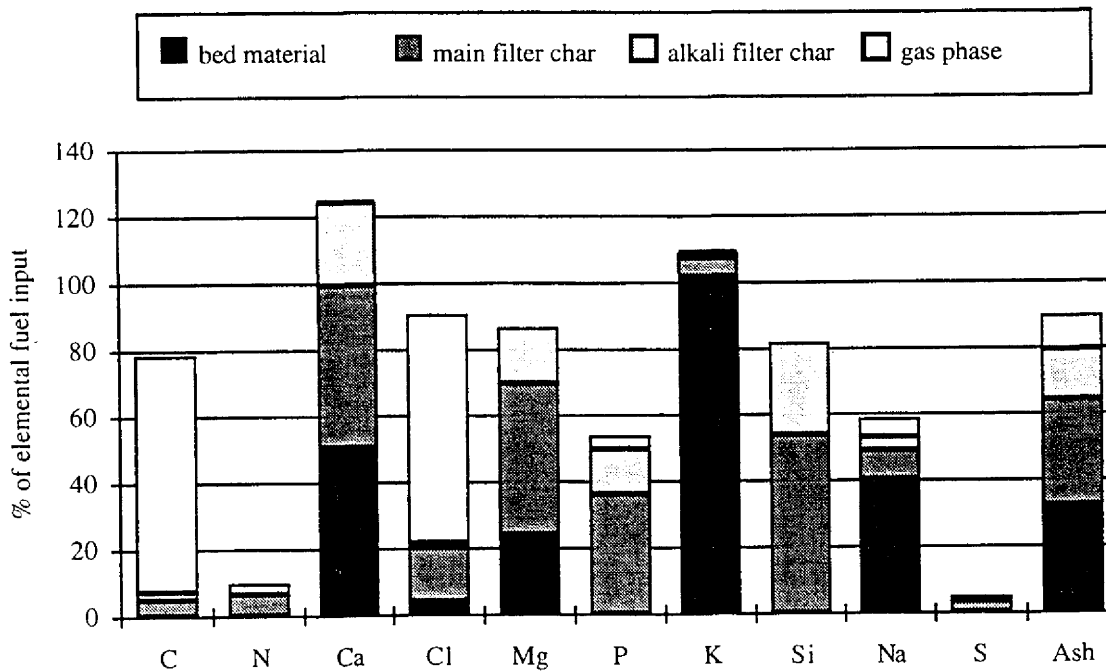

Figure 17. Elemental distribution in the gasifier output streams as percentage of input mass, FC-UP test.

Contamination of the char samples with bed material is evidenced by the excess quantities of Al, Fe, and Ti in the FC-PRP, FC-P, and FC-UP treatments. It is believed that dust originating from, and present in, the fresh bed material used for each test was the source, since no beads were found in the char removed from the filters. The total mass input of each of these elements in the latter three banagrass fuels is <1.5 g, and for Ti, <100 mg, thus, even small amounts of extraneous material could have a large impact on the element balances. Si is also a component of the bed material but its fuel input is in the range of 30 to 50 g and contamination is not readily apparent. Si balances ranged from 60 to 90% with no correction for possible contamination. Bagasse and JC-PRP fuel analyses indicate the presence of soil which contains all of these elements and masks small amounts of contaminants.

Calcium and potassium were present in the fresh, unused bed material at 0.1% and 0.2% by weight, respectively. Balances for both elements were generally in excess of 100% indicating that the bed material may have affected the analyses. Nonetheless, the balances range from 100 to 140% for Ca and 90% to 120% for potassium and show that most of the potassium and roughly half of the calcium is retained in the bed with char containing most of the remainder.

Closure of the magnesium balances for all tests ranged from 70 to 85%. Sodium balances for all of the fuels tested varied from 60 to 150% with no apparent relationship to fuel Na concentration or total fuel Na input mass. Balances for phosphorus ranged from 60 to 70% with the exception of the JC-PRP test for which only 30% of the total input was recovered. Phosphorus balances did not include material retained in the bed and would be expected to improve with this addition. Although XRF analysis identified P as being present on the surface of the fuel test beads at concentrations higher than the unused beads, the bulk analyses were inconclusive. Chlorine balances were highly variable, from 43% for bagasse to 124% for the JC-PRP test. Chlorine balances of 80 and 90% were computed for the two fuels (FC-P and FC-UP) which contained higher chlorine concentrations (>0.3%). Sulfur, present in the fuels in concentrations less than 0.2% was recovered with a balance of less than 10%. Total ash balances were computed by summing contributions from the char samples and masses of individual inorganic species measured in the gas and bed material analyses. Values ranged from 67% for the JC-PRP test, to 90% for FC-UP.

The elemental balances for inorganic species are generally acceptable considering the small elemental masses present in the fuel. Balances from Table 9 are plotted against element fuel concentrations in Figure 16. A convergence toward 100% is evident with increasing fuel concentration. Balances could be expected to improve with the use of bed material which did not have elements in common with the fuels. This would simplify the identification and quantification of the inorganic fuel species, although the results would be less relevant to industrial applications. Balances may have also been affected by attrition of the bed material, although the extent to which it occurred was not quantified. Attrited material would be expected to be removed by filtration, with little impact on gas phase concentrations. Although choice of a different bed material may have improved inorganic elemental balances by contributing to greater analytical clarity, this would likely have resulted in a different disposition of the inorganic fraction among the output streams as bed material composition is known to influence inorganic retention (Ergudenler and Ghaly, 1993a, 1993b).
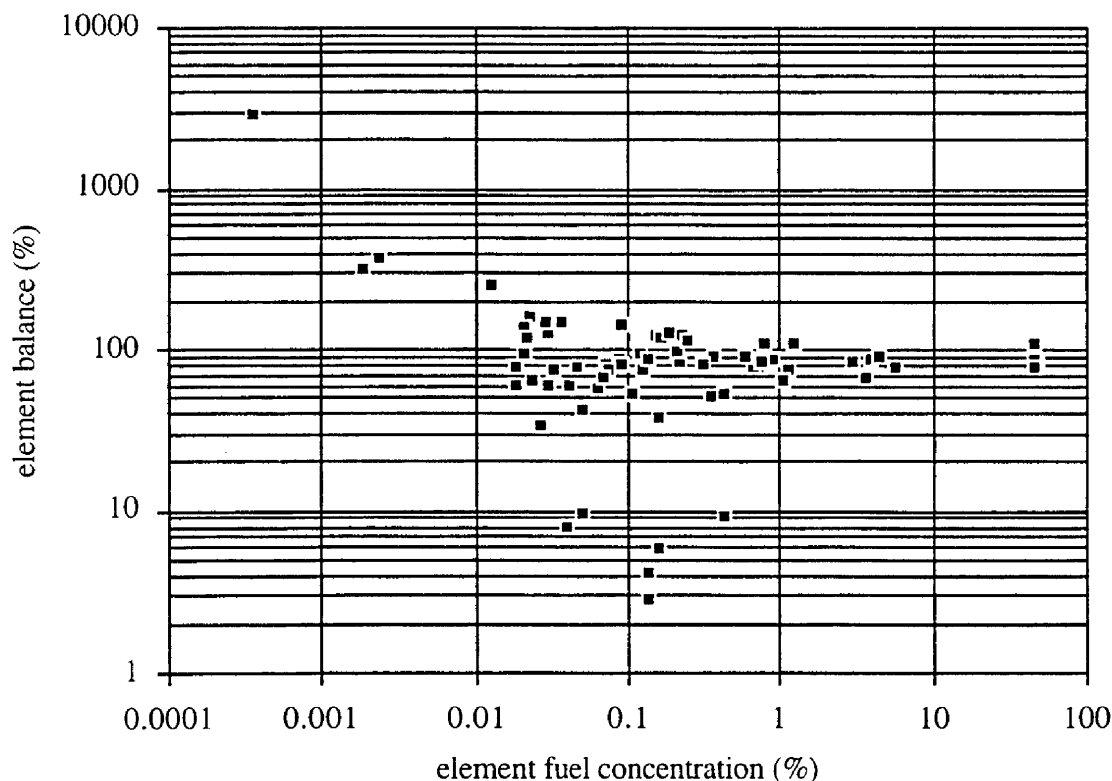
Figure 18. Correlation of element balances with fuel concentrations.

Comparison with Other Studies

The Institute of Gas Technology (Onischak et al., 1995) measured gas phase alkali concentration of the product stream from the Renugas® process. Bagasse used as fuel and the bed material in the fluidized bed reactor were of similar composition as those of the current study. In addition, bed material particles were of the same size class. At operating pressures of ~20 bar, Na and K concentrations were 6.6 and 0.55 ppmw, respectively. These compare well with the values determined for bagasse in the current work, 11.6 ppmw Na and 0.73 ppmw K, taking into consideration that increased operating pressure should result in lower gas phase concentrations.

Mojtahedi et al. (1990) reported results of experimental peat gasification. Concentration of Na in the fuel was 0.03%, comparable to the fuels used in the present work. Potassium fuel concentration was 0.04%, roughly one third of the value for bagasse. Na and K gas concentrations ranged from 2.5 to 5 ppmw and 1 to 1.6 ppmw, respectively, over a gasifier operating pressure range of 5 to 9.5 bar and maximum reactor temperature of 860° C. Although direct comparison with the present work is difficult due to differences in fuel and operating conditions, measured values of gas phase alkali concentrations are of comparable magnitude. Mojtahedi et al. (1989) also found experimental values of gas phase alkali concentration to be consistently below that predicted by equilibrium calculation. This would appear to be true for all fuels used in the present effort. Fuel concentrations of potassium and chlorine are much greater

and gasifier operating pressure is lower than conditions used in Mojtahedi's equilibrium calculations, but measured gas phase concentrations are comparable.

Mojtahedi et al. (1990) reported an alkali balance (combined potassium and sodium) of 105% in a pressurized fluidized bed gasification test of peat. Alkali was distributed between the cyclone catch (97%), post cyclone particulate (6.7%) and vapor (1.2%). Unlike the current work, none was found in the bottom ash or bed material. The type of bed material and its composition was not reported.

Summary and Conclusions

Bagasse and four treated banagrass fuels, each with unique ash chemistry, were tested in a benchscale fluidized bed gasification reactor. Input fuel, solid and gas phases of the output process stream, and post-test bed material were sampled and analyzed. Mass balances were computed for the elements C, N, Al, Ca, Cl, Fe, Mg, P, K, Si, Na, S, and Ti, and total ash.

Measured gas phase concentrations of Na and K for all fuels ranged from 2 to 15 ppmw and 0.7 to 53 ppmw, respectively, with greater fuel potassium concentrations resulting in higher gas concentrations. Bagasse and the JC-PRP and FC-PRP treatments for banagrass, those fuels subjected to more severe leaching processes, exhibited consistently lower gas phase concentrations of potassium, ~0.8 ppmw. All fuels produced total gas phase alkali (Na+K) concentrations in excess of 0.1 ppmw, the maximum allowable limit for combustion turbine applications. Ca, Cl, Si, and P were found in the gas stream at concentration levels in excess of 1 ppmw. Chlorine gas phase concentration exhibited a linear dependence on fuel chlorine content. All of these elements have been identified in fire side deposits in conventional steam boiler power plants and may be expected to contribute to operating difficulties in integrated gasifier combined cycle systems as well. Future work in the removal of gas phase inorganics should be pursued.

For all fuels, calcium is partitioned approximately equally between the post-test bed material and the char recovered from the filters. More than 80% of the potassium present in the banagrass fuels was retained in the bed. Bagasse test results showed 40% retention of potassium in the bed with most of the balance present in the char. Approximately 20% of the magnesium and 30 to 60% of sodium were also retained in the bed. SEM/XRF analysis found Ca, K, Mg, and P adhered to the bead surfaces in a dispersed form. Retention of inorganic species will affect the useful life expectancy of bed material in commercial applications and may contribute to bed agglomeration. Additional tests are required to better understand the long-term implications of inorganic accumulation in the bed.

Closure of element balances based on analyses of fuel input, gas and solid outputs, and post-test bed material varied widely for different species and for the same species among the fuels. The test using bagasse as fuel produced the most consistent set of balances, with closures in the range of 70 to 120% for the elements present in the fuel at levels in excess of 0.1% of dry matter, C, N, Si, Al, Ti, Fe, Mg, and P. Carbon and nitrogen balances were slightly greater than 90%. The ash composition of the char in the exit stream of the reactor was very similar to that of the parent bagasse and most of each elemental mass was recovered in the char, indicating that bagasse ash under gasification conditions is relatively stable. The exception to this was chlorine which was consistently found predominantly in the product gas for all fuels tested.

References

Baxter, L.L., T.R. Miles, T.R. Miles, Jr., B.M. Jenkins, G.H. Richards and L.L. Oden. 1993. Transformations and deposition of inorganic material in biomass boilers. In M.G. Carvalho (ed.) Second International Conference on Combustion Technologies for a Clean Environment. pp. 9-15. Commission of the European Communities. Lisbon, Portugal.

Baxter, L.L. 1993. Ash deposition during biomass and coal combustion: a mechanistic approach. Biomass and Bioenergy. (4)2, pp. 85-102.

Ergudenler A., and A.E. Ghaly. 1993a. Agglomeration of alumina sand in a fluidized bed straw gasifier at elevated temperatures. Bioresource Technology, 43, pp. 259-268.

Ergudenler A., and A.E. Ghaly. 1993b. Agglomeration of silica sand in a fluidized bed gasifier operating on wheat straw. Biomass and Bioenergy, 4(2), pp. 135-147.

Ishimura, D.M., S.M. Masutani, C.M. Kinoshita and Y. Wang. 1994. Investigation of nitrogenous compound formation in biomass gasification. in J. Farrell, S. Sargent, D. Swanson and R. Nelson (eds.) Bioenergy '94, Proceedings of the 6th National Bioenergy Conference. Reno, NV.

Jenkins, B.M., L.L. Baxter, T.R. Miles, T.R. Miles, Jr., L.L. Oden, R.W. Bryers and E. Winther. 1994. Composition of ash deposits in biomass fueled boilers: results of full-scale experiments and laboratory simulations. Paper No. 946007. Presented at the 1994 International Summer Meeting Sponsored by ASAE, Kansas City, Kansas, June 19-24, 1994.

Jenkins, B.M., R.R. Bakker and J.B. Wei. 1996. On the properties of washed straw. Biomass and Bioenergy. 10(4) pp. 177-200.

Kinoshita, C.M. 1991. Cogeneration in the Hawaiian sugar industry. Bioresource Technology, 35, pp. 231-237.

Kinoshita, C.M., Y. Wang and J. Zhou. 1994. Tar formation under different biomass gasification conditions. Journal of Analytical and Applied Pyrolysis. 29, pp 169-181.

Leppälahti, J. 1993. Formation and behavior of nitrogen compounds in an IGCC process. Bioresource Technology 46, pp. 65-70.

Miles, T.R., T.R. Miles, Jr., L.L. Baxter, R.W. Bryers, B.M. Jenkins and L.L. Oden. 1995. Alkali deposits found in biomass power plants, a preliminary investigation of their extent and nature. Summary report for the National Renewable Energy Laboratory. NREL Subcontract TZ-2-11226-1.

Mojtahedi, W., E. Kurkela and M. Nieminen. 1990. Release of sodium and potassium in the PFB gasification of peat. Journal of the Institute of Energy, 63, pp. 95-100.

Mojtahedi, W. and R. Backman. 1989. The fate of sodium and potassium in the pressurised fluidised-bed combustion and gasification of peat. Journal of the Institute of Energy, 62, pp. 189-196.

Onischak, M. R.H. Carty, R.A. Knight. 1995. Hot gas cleanup for operation of a gas turbine with a fluidized bed air blown biomass gasifier, Filter performance short duration tests. Volume III – PDU operations and analytical results, Topical Report – Task 2.9, National Renewable Energy Laboratory Contract Number XAZ-3-12092-01-106794. pp. 41. Westinghouse Electric Corporation.

Padban, N., S. Kiuru and A.L. Hallgren. 1995. Bed material agglomeration in PFB biomass gasification. Preprints of papers presented at the 210th ACS National Meeting. Volume 40, No. 3. Chicago Illinois, August 20-25, 1995.

Payne, J.H. 1991. Cogeneration in the Cane Sugar Industry, pp. 62. Elsevier, New York.

Salmenoja, K., K. Makela, M. Hupa, and R. Backman. 1996. Superheater corrosion in environments containing potassium and chlorine. Journal of the Institute of Energy, 69, pp. 155-162.

Scandrett, L.A. and R. Clift. 1984. The thermodynamics of alkali removal from coal derived gases. Journal of the Institute of Energy, 57, pp. 391-397.

Turn, S.Q., C.M. Kinoshita, and D.M. Ishimura. Removal of inorganic constituents of biomass feedstocks by mechanical dewatering and leaching. Biomass and Bioenergy, (in press).

REPORT DOCUMENTATION PAGE

The public reporting burden for this collection of information is estimated to average 1 hour per response, including the time for reviewing instructions, searching existing data sources, gathering and maintaining the data needed, and completing and reviewing the collection of information. Send comments regarding this burden estimate or any other aspect of this collection of information, including suggestions for reducing the burden, to Department of Defense, Washington Headquarters Services, Directorate for Information Operations and Reports (0704-0188), 1215 Jefferson Davis Highway, Suite 1204, Arlington, VA 22202-4302. Respondents should be aware that notwithstanding any other provision of law, no person shall be subject to any penalty for failing to comply with a collection of information if it does not display a currently valid OMB control number.
PLEASE DO NOT RETURN YOUR FORM TO THE ABOVE ADDRESS.

1. REPORT DATE *(DD-MM-YYYY)*	2. REPORT TYPE	3. DATES COVERED *(From - To)*

4. TITLE AND SUBTITLE

5a. CONTRACT NUMBER

5b. GRANT NUMBER

5c. PROGRAM ELEMENT NUMBER

6. AUTHOR(S)

5d. PROJECT NUMBER

5e. TASK NUMBER

5f. WORK UNIT NUMBER

7. PERFORMING ORGANIZATION NAME(S) AND ADDRESS(ES)

8. PERFORMING ORGANIZATION REPORT NUMBER

9. SPONSORING/MONITORING AGENCY NAME(S) AND ADDRESS(ES)

10. SPONSOR/MONITOR'S ACRONYM(S)

11. SPONSOR/MONITOR'S REPORT NUMBER(S)

12. DISTRIBUTION/AVAILABILITY STATEMENT

13. SUPPLEMENTARY NOTES

14. ABSTRACT

15. SUBJECT TERMS

16. SECURITY CLASSIFICATION OF:			17. LIMITATION OF ABSTRACT	18. NUMBER OF PAGES	19a. NAME OF RESPONSIBLE PERSON
a. REPORT	b. ABSTRACT	c. THIS PAGE			
					19b. TELEPHONE NUMBER *(Include area code)*